EPSC2018

SB4 abstracts

EPSC Abstracts
Vol. 12, EPSC2018-81, 2018
European Planetary Science Congress 2018

Ideal method for asteroid compositional analysis - mid-infrared spectral work with DRIFTs for HERA mission

Agnes Skulteti (1), **Akos Kereszturi** (2)
(1) Geographical Institute, CSFK, MTA (2) Konkoly Observatory, CSFK, MTA, (skulteti.agnes@csfk.mta.hu)

Abstract

Earth laboratory based analysis of meteorite powder supports the interpretation of asteroid spectra, especially in the case of nearby recording by spacecrafts. The HERA (formerly named AIM) mission of ESA targets Didymos asteroid and planned to use a middle infrared detectors for the analysis of mineralogy and granular plus thermal properties of the regolith. Diffuse reflectance infrared fourier transform spectroscopy (DRIFTs) is a newly used technology for meteorite powder analysis. In the mid-infrared (2.5-25 μm) region it allows the analysis of the main meteorite minerals (e.g. olivines, pyroxenes and plagioclase feldspar) and meteorite groups as analogues of asteroids. However in order to we can get reliable estimation for the grain size, chemical composition, physical state and temperature dependence of the measured meteorite samples we should suitably know the spectral effects of these parameters.

1. Introduction

Analysis of different meteorite minerals is important in order to get information about surface characteristics of asteroids (Table 1). DRIFTs is an infrared sampling method, using a complex process, which covers absorption, transmission, reflection and diffusion, and mainly used to analyze powders and solid samples [4] for qualitative analysis, but it also provides quantitative information by the absorption bands. The most prominent absorption bands in the spectra of meteorites are expected from the most common minerals: olivine, pyroxene and plagioclase feldspar [11]. The change in spectral parameters of bands (e.g. peak position, band shape, FWHM) provide information about grain size, chemical composition (like Fe^{2+}, Mg/(Fe+Mg), H_2O), physical state and target temperature of the meteorite in the laboratory and of the asteroid by the mission. Below effects of these parameters are discusses.

2.1 Grain size effect

The properties of infrared spectrum significantly depend on grain size, with increasing grain size the reflectance decreases, effect weaker absorption bands and the apparent loss of spectral detail [3, 11]. The grain size must be smaller than the wavelength of the incident IR radiation (middle IR region <5-10 μm). Samples with smaller average particle sizes (<10 μm) give better spectra with reduced peak widths compared to samples with large average particle sizes (>90 μm) [4].

2.2 Chemical composition and physical state

The number, wavelength position and strength of bands change in complex ways, partly with changing of the chemical composition [8]. In case of The amount of Fe^{2+} and the rate of Mg/(Mg+Fe) significantly influences the spectral parameters of mafic silicates (olivine and pyroxene) [2, 6]. At plagioclase feldspar the amount of anorthite (An) endmember also cause similar effects [9]. The occurrence of H_2O both in hydrated and anhydrous minerals (without structurally bedded water) (such as olivine, pyroxene) is important, because contaminating water can slightly distort the spectral features [11]. The overall spectrum of crystalline material (physical state) show sharper bands than those of the amorphous [7]. In shocked samples (with deformed crystalline lattice) the band strengths are reduced with increasing shock pressures [5].

2.3 Temperature effect

Along with the increasing temperature the bands get broader and weaker, some bands are lost and others are shifted in wavenumber. These effects are due to diffusion of the infrared beam on the sample, which decreases with increasing temperature and the signal-to-noise ratio accordingly decreases [1]. The

variations in temperature produce a number of significant spectral effects on the wavelength positions, shapes, and intensities of the absorption bands, the reflectance spectra of several mafic silicates vary with temperature [10].

2. Summary and Conclusions

DRIFTs is a newly used technology for meteorite powder analysis. In the mid-infrared (2.5-25 μm) region it allows the analysis of the main meteorite minerals and meteorite groups as analogues of asteroids. The DRIFTs spectra are mainly influenced by grain size, chemical composition, physical state of the sample and the recording temperature. Samples with smaller particle sizes give better spectra with reduced peak widths compared to samples with large average particle sizes. The chemical composition, so the occurrence of H_2O and in case of mafic silicates the amount of Fe^{2+} and the rate of Mg/(Mg+Fe) can cause the distortion of spectral features and the appearing and disappearing of some bands. The spectrum of crystalline material will have much sharper bands than the spectrum of amorphous material. With the increasing temperature the bands get broader and weaker, some bands are lost, and all the bands are shifted to longer wavelengths.

First results of the authors' measurements on meteorite samples with DRIFT detector will be presented at the meeting.

Acknowledgements

NEOMETLAB ESA (4000123143) and GINOP-2.3.2-15-2016-00003 projects.

References

[1] Armaroli, T., Bécue, T., Gautier, S.: Diffuse Reflection Infrared Spectroscopy (DRIFTS): Application to the in situ Analysis of Catalysts, Oil & Gas Science and Technology – Rev.IFP, Vol. 59, pp. 215–237, 2004. [2] Chihara, H., Koike, C., Tsuchiyama, A., Tachibana, S., Sakamoto, D.: Compositional dependence of infrared absorption spectra of crystalline silicates I. Mg–Fe pyroxenes, Astronomy & Astrophysics, Vol. 391, pp. 267-273, 2002. [3] Cloutis E.A., Mann, P., Izawa, M.R.M., Nathues, A., Reddy, V., Hiesinger, H., Le Corre, L., Palomba, E.: The 2.5-5.1 μm reflectance spectra of HED meteorites and their constituent minerals: Implications for Dawn, Icarus, Vol. 225, pp. 581-601, 2013. [4] Fuller, M.P., Griffith, P.R.: Diffuse reflectance measurements by infrared Fourier transform spectrometry, Anal. Chem., Vol. 50, pp. 1960–1910, 1978. [5] Johnson, J.R., Hörz, F., Christensen, P., Lucey, P.G.: Thermal infrared spectroscopy of experimentally shocked anorthosite and pyroxenite, Lunar Planet. Sci.,Vol. 32. pp. 1195, 2001. [6] Koike, C., Shibai, H., Tsuchiyama, A.: Extinction of olivine and pyroxene in the mid- and far-infrared, MNRAS, Vol. 264, pp. 654-658, 1993. [7] Koike, C., Tsuchiyama, A., Shibai, H., Suto, H., Tanabé, T., Chihara, H., Sogawa, H., Mouri, H., Okada, K..: Absorption spectra of Mg-rich Mg-Fe and Ca pyroxenes in the mid- and far-infrared regions, Astronomy and Astrophysics, Vol. 363, pp. 1115-1122, 2000. [8] Milam, K.A., McSween Jr., H.Y., Christensen, P.R.: Plagioclase compositions derived from thermal emission spectra of compositionally complex mixtures: Implications for martian feldspar mineralogy, J. Geophys. Res., Vol. 112, E10005, 2007. [9] Nash, D.B., Salisbury, J.W.: Infrared reflectance spectra (2.2–15 μm) of plagioclase feldspars. Geophys. Res. Lett., Vol. 18, pp. 1151–1154, 1991. [10] Roush, T.L., Singer, R.B.: Gaussian analysis of temperature effects on the reflectance spectra of mafic minerals in the 1-um region, J. Geophys. Res., Vol. 91, pp. 10301–10308, 1986. [11] Salisbury, J.W., D'Aria, D.M., Jarosewich, E.: Midinfrared (2.5-13.5 μm) Reflectance Spectra of Powdered Stony Meteorites, Icarus, Vol. 92, pp. 280-297, 1991. [12] Sullivan, R.J., Thomas, P.C., Murchie, S.L., Robinson, M.S.: Asteroid Geology from Galileoand NEAR Shoemaker Data. In: Bottke JR. W.F., Cellino, A., Paolicchi, P., Binzel, R.P. (eds.): Asteroids III. The University of Arizona Press, 2002.

Table 1: Examples of mineral observations in laboratory based meteorite powder and telescopic based asteroid data [12]

Name of mineral	IR spectral band position	Meteorite example	Asteroid example
Pyroxene	1, 2 μm	L, LL, H chondrites	Eros
Olivine	1 μm	L, LL, H chondrites	Eros

EPSC Abstracts
Vol. 12, EPSC2018-91, 2018
European Planetary Science Congress 2018

The Brazil nut effect under reduced gravity

Ingo von Borstel (1), Fabian Schulz (1), H. Katsuragi (2) and Jürgen Blum (1)
(1) Institut für Geophysik und extraterrestrische Physik, TU Braunschweig, Germany (i.vonborstel@tu-bs.de)
(2) Department of Earth and Environment Sciences, Nagoya University, Japan

Abstract

We present laboratory experiments of a vertically vibrated granular medium consisting of 1mm diameter glass beads with embedded 8mm diameter intruder glass beads. We carried out laboratory experiments for an effective gravity range between 0.25g and 2.0g. We use these to refine the empirical relation between the shaking and the gravity dependence of the effect as suggested by [6].

1. Introduction

The Brazil nut effect has been suggested to play a role in explaining the size seggregation on solar system bodies like Itokawa [5]. Initial experiments by [2] show a dependency of the Brazil Nut effect with the ambient gravity but do not allow to constrain well the functional dependence. These new experiments are performed in the laboratory using a linear motor, allowing covering a broader effective gravity range for the experiments, ranging from 0.25g to 2.0g . These measurements also allow a detailed assessment of the influence of different excitation accelerations. We use the data of the derived rise velocities to compare with and to look into the validity of models (e.g. Knight et al, or Grossman [1, 4])

2. Experiment

We use a linear stage which allows us to impose arbitrary movement onto the experiment container. The experiment container is 10cm in diameter and 10cm in height. We use lime glass beads with 1mm and intruders of 8mm diameter. The top of the container is observed by a camera to assess when the intruders moved from the bottom of the container to the top

3. Analysis

Yamada and Katsuragi [3,6] defined a dimension-less shaking parameter S and showed that it suited the description of vibration systems well:

$$S = \Gamma \cdot \frac{A_0}{d} = \frac{\left(2\pi \cdot A_0 f\right)^2}{gd} \qquad (1)$$

With the amplitude A_0, frequency of shaking f, ambient gravity g and the particle diameter d. We will use this dimension-less view on the brazil nut to derive its more dependence on experiment dimensions and gravity.

4. Summary and Conclusions

Fitting relation for the g dependence in this dimensionless form which suggests a dependence less than linear in g but more than square-root.

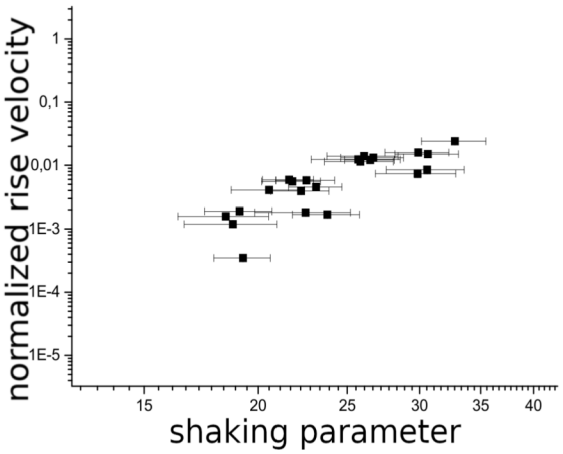

Figure 1: Relation between the shaking parameter and the observed rise velocity

We will disucss our findings with respect to the surface of small bodies like Itokawa , where the measured rise time will allow to estimate the exposure of the asteroid to impact-induced vibrations.

Acknowledgements

I.v.B is funded by the DLR through grant 50WM1536.

References

[1] E.L. Grossman, Phys. Rev. E 56, 3290 (1997)

[2] C. Güttler, I. Von Borstel, R. Schräpler and J. Blum, Phys. Rev. E 87 (2013)

[3] H. Katsuragi, Sci. Rep. 5, 17279 (2015)

[4] J.B. Knight, E.E. Ehrichs, V. Y. Kuperman, J.K. Flint, H.M. Jaeger and S.R. Nagel, Phys. Rev. E 54, 5726 (1996)

[5] S. Matsumura, D.C. Richardson, P. Michel, S.R. Schwartz, R.-L. Ballouz, MNRAS, Volume 443, Issue 4, pp 3368–3380 (2014),

[6] T.M. Yamada and H. Katsuragi, Planet. Space Sci., 100, 79 (2014)

EPSC Abstracts
Vol. 12, EPSC2018-108, 2018
European Planetary Science Congress 2018

Understanding iron meteorites and early Solar System metallic cores of asteroid parent bodies

Nancy L. Chabot
Johns Hopkins Applied Physics Laboratory, 11100 Johns Hopkins Rd, Laurel, MD, 20723, USA
(Nancy.Chabot@jhuapl.edu)

Abstract

Iron meteorites provide unique opportunities to investigate the central metallic cores of asteroid-sized bodies in the early Solar System. This work investigates the chemical variability present in asteroidal cores as represented in our iron meteorite collections, with implications for the parent bodies.

1. Introduction

Recent work [1] has identified isotopic signatures in iron meteorites that suggest that they formed in two distinct reservoirs in the early Solar System: one with similarities to carbonaceous chondrites (CC-type) and the other with similarities to other meteorites (NC-type, non-carbonaceous). The two reservoirs have been proposed to be separated by Jupiter, thus representing inner and outer Solar System formation regions [1]. An important follow-on question to this observation is whether there are chemical differences between asteroidal cores that formed in the inner and outer Solar System. This work explores this question through using iron meteorite measurements and experimental partitioning data to understand the chemical compositions of asteroidal cores in the early Solar System.

2. Iron meteorite trends revealed on a Co vs. Ni diagram

A Co vs. Ni diagram can provide a framework to understand iron meteorite compositions. As shown in Fig.1, many iron meteorite groups plot roughly along a trend consistent with the Ni/Co CI ratio. For irons along the CI Ni/Co line, higher absolute concentrations of Co and Ni may be produced by more oxidized core formation conditions on the parent asteroidal body. As a body becomes more oxidized, the amount of FeO rather than Fe increases, resulting in less Fe in the metallic core; consequently, the core concentrations of Ni and Co are higher, as Ni and Co continue to partition dominantly into the core. As seen on Fig. 1, the large majority of CC-type irons have higher Co and Ni values, suggesting more oxidized parent bodies than the NC-type irons, and hence more oxidized parent bodies in the outer Solar System than the inner Solar System.

Additionally, in this work, it is postulated that irons with low Ni/Co ratios may be due to the formation of schreibersite in these irons, which are avoided during the analysis of the metal of the irons [2]. Schreibersite can have a substantial amount of Ni [3], resulting in lower Ni/Co ratios in the remaining metal phase. It is also postulated that irons with high Ni/Co ratios may be due to the formation of troilite. Slight differences in the solid metal-liquid metal partitioning values for Ni and Co [4] result in the formation of troilite at the Fe-Ni-S cotectic producing enrichments in Ni in the metal while the Co concentration in the metal is relatively constant.

3. Iron meteorite experiments to determine bulk core compositions

To determine the bulk composition of an asteroidal core as sampled by iron meteorites, it is necessary to model the fractional crystallization trends of each iron meteorite group. The S content of the asteroidal core can have a large effect on the partitioning behavior of elements and was recently parameterized in [4]. Using these parameterizations, the bulk core compositions for the IIAB, IIIAB, IVB, IVA, and IID iron meteorite groups were modeled [5] and are discussed briefly in the conclusions below.

Summary and Conclusions

Overall, there is strong evidence that the majority of CC-type irons sampled more oxidized parent bodies than NC-type irons, based on the separation observed on a Co vs. Ni diagram. This suggests that the parent asteroids of iron meteorites in the outer Solar System were more oxidized than the parent asteroids that formed iron meteorites in the inner Solar System.

Modeling of the bulk compositions of iron meteorite parent bodies cores shows largely chondritic bulk compositions, with varying levels of volatility depletions that are not correlated with classification as NC or CC-type. The modeled bulk compositions also show evidence for enrichment in refractory siderophile elements in some cores of both NC and CC-types.

Acknowledgements

NASA Emerging Worlds grant NNX15AJ27G.

References

[1] Kruijer, T. S., et al. Age of Jupiter inferred from the distinct genetics and formation times of meteorites. PNAS 114, 6712–6716, 2017.

[2] Wasson, J. T. Formation of the Treysa quintet and the main-group pallasites by impact-generated processes in the IIIAB asteroid. Meteorit Planet Sci 51, 773–784, 2016.

[3] Doan, A. S. and Goldstein, J. I. The formation of phosphides in iron meteorites. In: Meteorite Research. vol 12. Springer, 1969.

[4] Chabot, N. L. et al. Experimental determination of partitioning in the Fe-Ni system for applications to modeling meteoritic metals. Meteorit Planet Sci 52, 1133–1145, 2017.

[5] Chabot, N. L. Composition of metallic cores in the early Solar System. 49th LPSC, #1532, 2018.

[6] Goldstein, J. I., Scott, E. R. D. & Chabot, N. L. Iron meteorites: Crystallization, thermal history, parent bodies, and origin. Chemie der Erde - Geochemistry 69, 293–325, 2009.

[7] Budde, G. et al. Molybdenum isotopic evidence for the origin of chondrules and a distinct genetic heritage of carbonaceous and non-carbonaceous meteorites. Earth and Planetary Science Letters 454, 293–303, 2016.

[8] Poole, G. M. et al. Nucleosynthetic molybdenum isotope anomalies in iron meteorites – new evidence for thermal processing of solar nebula material. Earth and Planetary Science Letters 473, 215–226, 2017.

[9] Worsham, E. A., Bermingham, K. R. and Walker, R. J. Characterizing cosmochemical materials with genetic affinities to the Earth: Genetic and chronological diversity within the IAB iron meteorite complex. Earth and Planetary Science Letters 467, 157–166, 2017.

[10] Bermingham, K. R., Worsham, E. A. and Walker, R. J. New insights into Mo and Ru isotope variation in the nebula and terrestrial planet accretionary genetics. Earth and Planetary Science Letters 487, 221–229, 2018.

[11] Hilton, C. D. et al. Genetics, age, and crystallization sequence of the South Byron trio and the potential relation to the Milton pallasite. 49th LPSC, #1186, 2018.

[12] Wasson, J. T. and Choe, W.-H. The IIG iron meteorites: Probable formation in the IIAB core. Geochimica et Cosmochimica Acta 73, 4879–4890, 2009.

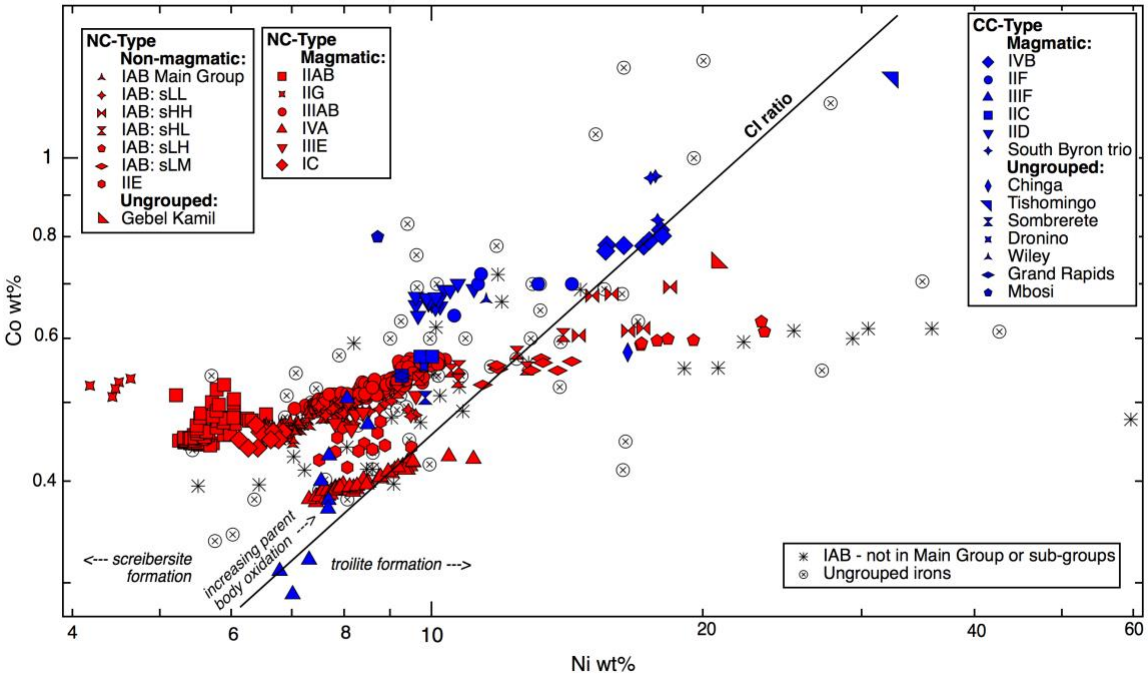

Figure 1: Co vs. Ni diagram provides a framework to evaluate processes that have influenced the chemistry of iron meteorites. Iron meteorite data from numerous studies, largely from the UCLA Wasson group, as listed in [6]. NC and CC classifications from: [1], [7–11]. IIG shown as NC based on association with the IIAB parent body [12].

EPSC Abstracts
Vol. 12, EPSC2018-118, 2018
European Planetary Science Congress 2018

Earth's missing co-orbitals

Apostolos Christou (1), Aldo dell'Oro (2) , Galin Borisov (1,3), Stefano Bagnulo (1), Alberto Cellino (4)
(1) Armagh Observatory and Planetarium, Armagh, UK, (2) Osservatorio di Arcetri, Florence, Italy, (3) Institute of Astronomy and National Astronomical Observatory, Sofia, Bulgaria, (4) Osservatorio di Torino, Torino, Italy

Abstract

Some, but not all, of the planets in our solar system are accompanied by Trojan asteroids, objects confined by solar and planetary gravity to orbit the Sun 60° ahead or behind the planet [1]. They most likely represent material from the formation and early evolution of the planets, put in "safe storage" well away from planetary gravitational wells.

Numerous objects are known to exist in a temporary 1:1 orbital resonance with the Earth[1], yet no *stable* Trojan companions have so far been found; observational searches from the ground [3, 4] and, more recently, *in situ* by the OSIRIS-REx spacecraft [5] have so far not born fruit. For the ground-based searches, this is because detection of objects in Earth-like orbits is hampered by the low solar elongation [6]. Indeed, the temporary Earth Trojan, 2010 TK_7, found by the WISE satellite [7] has a significant orbital eccentricity, rendering it easier to detect. Therefore, the existence of permanent Trojan companions to our planet remains an open question.

Searches to-date for objects permanently locked to the Earth may, however, have been too limited in scope. Because of the low Earth-Sun mass ratio and the particular dynamics of asteroids in Earth's orbital vicinity, not only Trojan but also "horseshoe" orbits - where the asteroid is not restricted to move near L4 and L5 but only to avoid the location of the planet itself - are theoretically stable for at least a Gyr [8, 9]. Interestingly, the current observational census of near-Earth asteroids shows a relative deficit of objects at a=1 au (Fig. 1). The dip in the plotted distribution corresponds to 70-80 "missing" asteroids and is significant at the 6-σ level. This feature is reproduced by population completeness models [10] and is due to the very long Earth re-approach times (100s of yr) for the asteroids vs the relatively short (10s of yr) timespan of NEA surveying to-date. Most of these objects will have a semimajor axis within one Earth Hill sphere radius (∼0.01 au) of 1 au so they are likely to be trapped in different modes of the 1:1 resonance. Regardless of their dynamical status, they are self-evidently unobservable with current instrumentation. In this presentation, I will discuss what these missing coorbitals might be and how best to find them.

[1]The so-called "coorbital" asteroids [2]

1. Figures

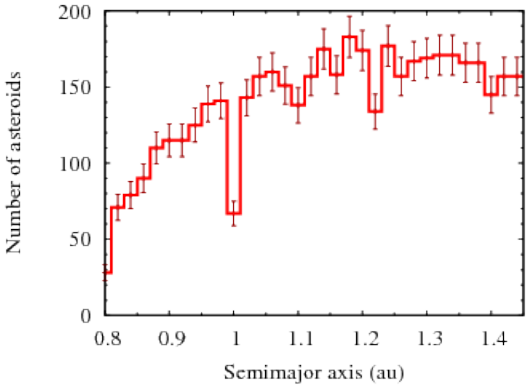

Figure 1: Number of NEAs as a function of semimajor axis plotted with a bin size of 0.02 au. Data was downloaded from the *NEODyS-2* online service (https://newton.dm.unipi.it/neodys/) on 21st November 2017. The error bars represent 1-σ Poisson statistics. Note the dip at a=1 au representing a ∼50% deficit of discovered objects relative to asteroids in neighbouring orbits.

Acknowledgements

Astronomical research at the Armagh Observatory and Planetarium is funded by the Northern Ireland Department for Communities (DfC). We acknowledge funding support from the UK Science and Technology Facilities Council (STFC; Grant ST/R000573/1).

References

[1] Murray, C.D. and Dermott, S.F.: Solar System Dynamics, Cambridge University Press, 1999.

[2] Namouni, F., Christou, A.A., Murray, C.D.: Coorbital dynamics at large eccentricity and inclination, Ph. Rev. Lett., Vol. 83, 2506-2509, 1999.

[3] Whiteley, R.J., Tholen, D.J.: A CCD Search for Lagrangian Asteroids of the Earth-Sun System, Icarus, Vol. 420, pp. 154-167, 1998.

[4] Connors, M., et al.: Initial results of a survey of Earth's L4 point for possible Earth Trojan asteroids, Bulletin of the American Astronomical Society, Vol. 32, p. 1019, 2018.

[5] Cambioni, S. et al.: An upper limit on Earth's Trojan asteroid population from OSIRIS-REx, 49th Lunar and Planetary Science Conference, 19-23 March 2018, The Woodlands, Texas, 2018.

[6] Todd, M., et al: An optimal Earth Trojan asteroid search strategy, MNRAS, Vol. 420, pp. L28-L32, 2012.

[7] Connors, M., Wiegert, P., Veillet, Ch.: Earth's Trojan asteroid, Nature, Vol. 475, 481-483.

[8] Ćuk, M, A., Hamilton, D. P., and Holman, M. J.: Long-term stability of horseshoe orbits, MNRAS, Vol. 26, pp. 3051-3056, 2012.

[9] Marzari, F., Scholl, H.: Long term stability of Earth Trojans, CeMDA, Vol. 117, 91-100, 2013.

[10] Tricarico, P.: The near-Earth asteroid population from two decades of observations, Icarus, Vol. 284, pp. 416-423, 2017.

EPSC Abstracts
Vol. 12, EPSC2018-130, 2018
European Planetary Science Congress 2018

Magma ascent in planetesimals: control by grain size

Tim Lichtenberg (1), Tobias Keller (2), Richard F. Katz (3), Gregor J. Golabek (4), Taras V. Gerya (1)
(1) Institute of Geophysics, ETH Zürich, Switzerland (tim.lichtenberg@phys.ethz.ch), (2) Department of Geophysics, Stanford University, United States, (3) Department of Earth Sciences, University of Oxford, United Kingdom, (4) Bayerisches Geoinstitut, University of Bayreuth, Germany

Abstract

Rocky planetesimals in the early solar system melted internally and evolved chemically due to radiogenic heating from ^{26}Al. Here we quantify the parametric controls on magma genesis and transport using a coupled petrological and fluid mechanical model of reactive two-phase flow. We find the mean grain size of silicate minerals to be a key control on magma ascent. For grain sizes larger than $\sim$1 mm, melt segregation produces distinct radial structure and chemical stratification. This stratification is most pronounced for bodies formed at around 1 Myr after Ca,Al-rich inclusions. These findings suggest a link between the time and orbital location of planetesimal formation and their subsequent structural and chemical evolution.

According to our models, the evolution of partially molten planetesimal interiors falls into two categories. In the *global magma ocean* scenario, the whole interior of a planetesimal experiences nearly complete melting, resulting in turbulent convection and core-mantle differentiation by the rainfall mechanism. In the *magma sill* scenario, segregating melts gradually deplete the deep interior of the radiogenic heat source. In this case, magma may form melt-rich sills beneath a cool and stable lid, while core formation would proceed by percolation.

Our findings [1] suggest that grain sizes prevalent during the internal-heating stage governed magma ascent in planetesimals. Regardless of whether evolution progresses toward a global magma ocean or segregated magma sills, our models predict that temperature inversions due to rapid ^{26}Al redistribution are limited to bodies formed earlier than $\sim$1 Myr after CAIs. We find that if grain size was smaller than $\sim$1 mm during peak internal melting, only elevated solid-melt density contrasts (such as found for enstatite chondrite compositions) would allow substantial melt segregation to occur.

Melt segregation regimes

We define the non-dimensional *melt segregation number* to quantify the propensity of a planetesimal to undergo substantial melt segregation,

$$R_{\mathrm{seg}} = \log_{10}\left(\frac{k_\phi \Delta\rho g_0 c_{\mathrm{p}} \Delta T_0}{R_{\mathrm{P}} \mu H_{0,^{26}\mathrm{Al}}}\right) , \qquad (1)$$

with rock permeability, k_ϕ, solid-melt density contrast, $\Delta\rho$, planetesimal surface gravity, g_0, specific heat of silicates, c_{p}, temperature difference between planetesimal accretion temperature and silicate solidus, ΔT_0, planetesimals radius, R_{P}, silicate melt viscosity, μ, and the decay power of ^{26}Al, $H_{0,^{26}\mathrm{Al}}$.

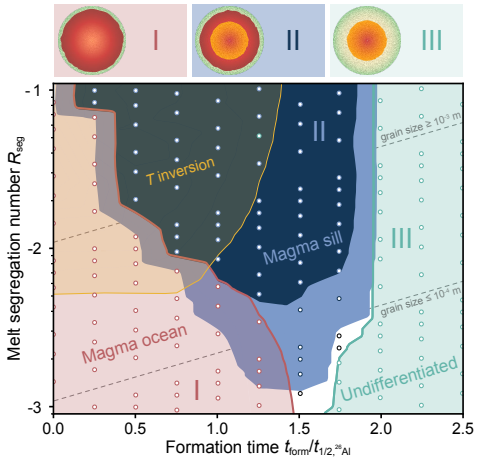

Figure 1: Melt segregation regimes and potential temperature inversions during planetesimal evolution [1].

References

[1] Lichtenberg, T., Keller, T., Katz, R. F., Golabek, G. J., and Gerya, T. V., arXiv:1802.02157.

EPSC Abstracts
Vol. 12, EPSC2018-131, 2018
European Planetary Science Congress 2018

Evaluating the extent of aqueous alteration among the fine-grained micrometeorite flux

Martin Suttle[1,2,3] (mds10@ic.ac.uk), Luigi Folco[1], Matt Genge[2,3] and Sara Russell[3]
(1) Dipartimento di Scienze della Terra, Università di Pisa, 56126 Pisa, Italy
(2) Department of Earth Science and Engineering, Imperial College London, South Kensington, London, SW7 2AZ, UK
(3) Department of Earth Science, The Natural History Museum, Cromwell Rd, London SW7 5BD, UK

Abstract
The degree of aqueous alteration affecting the fine-grained micrometeorite population is investigated using criteria originally developed for CM chondrites [1]. We analyse >50 micrometeorites derived from the Transantarctic Mountain (TAM) and Cap Prud'homme collections, revealing that most unmelted fine-grained particles are intensely altered, with petrographic grades equivalent to <CM2.3.

By analysing a large population of micrometeorites, spanning a range of different collection sites (and, therefore, different terrestrial accumulation windows) as well as including a range of particle sizes ([50-800μm] providing a more representative sample of the micrometeorite flux) we demonstrate that a significant fraction of the cosmic dust reaching Earth over the last 1Ma is derived from intensely altered C-type asteroids.

This implies that the young Veritas family and Beagle sub-cluster of the Themis family, that reside in the outer main asteroid belt – and which are currently considered the most probable source bodies of the fine-grained micrometeorite flux [2] – are intensely altered, water-rich, phyllosilicate-bearing bodies.

1. Introduction
The alteration of primary minerals and amorphous condensates by liquid water is a fundamental process of the early solar system and has been thoroughly investigated within the hydrated carbonaceous chondrite group.
The CM chondrites show significant variability in their degree of aqueous alteration. This has been extensively investigated using textural features [3], elemental ratios [1], modal mineralogy [4], spectroscopy [5] and isotopic signatures [6]. Almost all CM chondrites now have a petrographic grade that quantifies the degree of aqueous alteration in that sample. This numerical classification ranges between CM2.0 to CM2.7 (and theoretically up to an entirely unaltered CM3.0). In this scale, lower subtypes represent meteorites which are more intensely altered by fluid interaction.

2. Evidence of alteration
Textural evidence of aqueous alteration in fine-grained micrometeorites include: hydrated CAIs, sulphates, pseudomorphic chondrules and complex intergrown and cross-cut assemblages of phyllosilicate (Fig.1.). In many instances, extensive alteration has resulted in the near-complete replacement of anhydrous components with secondary minerals. Geochemical evidence of alteration includes decreasing Fe/Mg ratios, a loss of sulfides and metal and progressively higher abundances of oxides such as magnetite and ferrihydrite.

3. Assigning petrographic grades
In the classification scheme of Rubin et al., [1], 8 criteria are used to evaluate petrographic grade. We use an adapted version of this method, with the following metrics: (1) the percentage of metallic FeNi [varying between <0.02%-1% by vol], (2) the degree of replacement affecting anhydrous silicates [0-100%], (3) The abundance of large phyllosilicate clumps [varying between 2-40%vol] and (4) the elemental FeO/SiO_2 ratio of phyllosilicate [varying between 1.0-3.3].
These criteria are suitable for the analysis of micrometeorites, because they focus on major mineralogy and/or their heat-resistant phases. Conversely, the remaining metrics consider accessory phases, such as sulfides or carbonates that are rarely preserved in micrometeorites, owing to atmospheric entry heating.

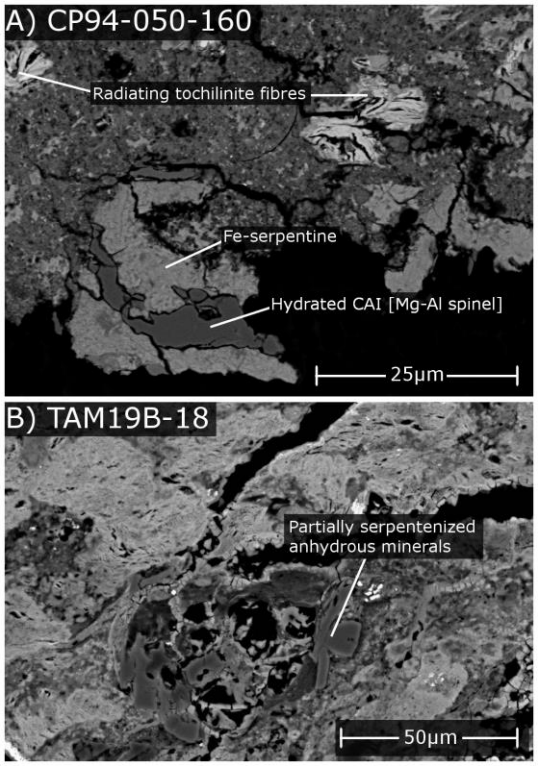

Figure.1. Alteration textures in fine-grained micrometeorites, attesting to significant interaction with liquid water.

4. Results

4.1 Cap Prud'homme micrometeorites

We analysed 30 particles from the Cap Prud'homme population (<100µm in size). The modal petrographic grade is CM2.2, representing 43% of the particles studied. Seven particles (23%) are classified as CM2.1 and 7 particles also have CM2.3 grades. However, completely altered CM2.0 particles are not recognised.

4.2. TAM micrometeorites

Among the TAM particles (250-800µm) unaltered chondrules are not recognised, while anhydrous mafic silicates commonly have skeletal morphologies and thick phyllosilicate overgrowths. Although we have analysed only 7 of these particles to date. Further analysis of the TAM micrometeorites will continue, and an updated set of statistics provided at the congress.

5. Summary and Conclusions

A large population of CM-like fine-grained micrometeorites, representing >4mm^2 of matrix, are analysed. They demonstrate that the flux of micrometeorites contains a significant fraction of hydrated, intensely altered, chondrule-poor material related to the <CM.2.2 chondrites.

Acknowledgements

The data presented here were acquired during M. Suttle's PhD research, funded by the UK's STFC (ST/M503526/1). Research continued whilst at the University of Pisa, funded through 2 Italian research grants: PNRA16_00029 [Programma Nazionale delle Ricerche in Antartide – CUP I52F17001050005] and PRIN2015_20158W4JZ7 [CUP I52F15000310001 for the "Meteoriti Antartiche"].

References

[1] Rubin, A.E., Trigo-Rodríguez, J.M., Huber, H. and Wasson, J.T: Progressive aqueous alteration of CM carbonaceous chondrites. Geochimica et Cosmochimica Acta, Vol.71, pp.2361-2382, 2007, doi:10.1016/j.gca.2007.02.008

[2] Nesvorný, D., Bottke, W.F., Levison, H.F. and Dones, L.: Recent origin of the Solar System dust bands. The Astrophysical Journal, Vo.591, p.486, 2003, doi:10.1086/374807

[3] Lee, M.R. and Lindgren, P.: Aqueous alteration of chondrules from the Murchison CM carbonaceous chondrite: Replacement, pore filling, and the genesis of polyhedral serpentine. Meteoritics & Planetary Science, Vo.51, pp.1003-1021, 2016, doi:10.1111/maps.12644.

[4] King, A.J., Schofield, P.F., Howard, K.T. and Russell, S.S.: Modal mineralogy of CI and CI-like chondrites by X-ray diffraction. Geochimica et Cosmochimica Acta, Vo.165, pp.148-160, 2015, doi:10.1016/j.gca.2015.05.038.

[5] Takir, D., Emery, J.P., Mcsween, H.Y., Hibbitts, C.A., Clark, R.N., Pearson, N. and Wang, A.: Nature and degree of aqueous alteration in CM and CI carbonaceous chondrites. Meteoritics & Planetary Science, Vol.48, pp.1618-1637, 2013, doi:10.1111/maps.12171.

[6] Lee, M.R., Sofe, M.R., Lindgren, P., Starkey, N.A. and Franchi, I.A.: The oxygen isotope evolution of parent body aqueous solutions as recorded by multiple carbonate generations in the Lonewolf Nunataks 94101 CM2 carbonaceous chondrite. Geochimica et Cosmochimica Acta Vo.121, pp.452-466, 2013, doi:10.1016/j.gca.2013.07.010.

EPSC Abstracts
Vol. 12, EPSC2018-202, 2018
European Planetary Science Congress 2018

Ground Observation of asteroids at mission ETA through JPL Horizons and SPICE

Flora Paganelli (1), Albert R. Conrad (2) and Marc Costa Sitjà (3)
(1) SETI, USA (fpaganelli@nccc.edu),
(2) LBTO, USA (aconrad@lbto.org),
(3) ESA-ESAC, Spain (mcosta@sciops.esa.int)

Abstract

This work presents an integrated approach for enhancing science return of targeted asteroids at spacecraft mission estimated time of arrival (ETA) through JPL Horizons and SPICE to inform ground-based and/or space-based telescope observations.

1. Introduction

NASA funding for ground-based support of spacecraft missions to small bodies has increased to enhance data science return. Thus emphasis for targeted asteroids (i.e. Lucy) data collected during observations carried out at ground-based observatories at mission estimated time of arrival (ETA), would provide to, and be recognized by, NASA as a valuable asset. Lucy, a SwRI mission proposal to study primitive asteroids among the Jupiter's Trojans, is one of five science investigations under the NASA Discovery Program [1]. Lucy's science payload/instrumentation is mirroring the New Horizons payload with: L'Ralph, Panchromatic and color visible imager and Infrared spectroscopic mapper (400nm -2.5µm); L'LORRI, high-resolution visible imager (350-850 nm); L'TES, thermal infrared spectrometer is similar to OTES on the OSIRIS-REx mission spectral range 5.71–100 µm (1750–100 cm^{-1}); and radio science investigation will determine the mass of the Trojans by using the spacecraft radio telecommunications hardware to measure Doppler shifts [2].

2. Approach

Observations through the Large Binacular Telescope (LBT) Multi-Object Double Spectrographs (MODS 1) - Imager and spectrograph covering 0.32-1.1 microns with a 6'x6' FOV - has been targeted for this assessment [3]. The importance of some Eurybates members spectra show a drop off in reflectance shortward of 0.52µm - similar features are seen in main belt C-type asteroids and commonly attributed to the intervalence charge transfer transition in oxidized iron [4,5]. Jupiter Trojan Asteroids targeted by Lucy are listed in Table 1.

Table 1. Lucy's Jupiter Trojan Asteroids albedo [4,5].

Mission	Number	Target	Vmag	Size (mas)	Albedo (µm)
Lucy	3548	Eurybates	16.8 to 17.7	13 to 20	0.052
	15094	Polymele	18.9 to 19.8	5 to 7	0.091
	11351	Leucus	17.8 to 18.8	7 to 11	0.079
	21900	Orus	16.9 to 17.9	11 to 16	0.075
	617	Patroclus	15.9 to 16.5	33 to 39	0.047
	52246	Donaldjohanson	18.3 to 20.1	2 to 4	

To derive Lucy targeted asteroids information for best ground-based observation at mission estimated time of arrival (ETA) we used data from JPL Horizons [6]. ETA of Lucy at Jupiter Trojan Asteroids are listed in Table 2.

Table 2. Lucy's Jupiter Trojan Asteroids ETA [1,2].

Lucy Mission	Encounter date	Location	Dia-meter (km)	Spectral type	**ETA targets**
Launch	Oct. 2021				
DonaldJohanson	April 2025	Main belt	3.9	C	
Eurybates	Aug. 2027	Greeks	64	C	12 Aug 2027
Polymele	Sept. 2027	Greeks	21	P	15 Sep 2027
Leucus	April 2028	Greeks	34	D	18 Apr 2028
Orus	Nov. 2028	Greeks	51	D	11 Nov 2028
Patroclus/Menoetius	March 2033	Trojans	113/ 104	P	02 Mar 2033

The workflow, shown in Figure 1, used *expect & tcl*, plus a *python* wrapper to access the JPL Horizons [6] database and extract observations of targeted asteroids at twilight conditions. The derived data provide the best suitable opportunities to observe the asteroids using LBT ground observations.

The SPICE implementation [7] has allowed to obtain details on observational parameters at ETA that could be utilized to optimize ground observations for added value on science return. Observational trajectories

used Spacecraft and Natural Bodies Trajectories Kernels (SPK) and Tcl to derive parameters/info for Lucy at the various considered targets to establish optimal geometry of observation that is then used as input for ground observation planning through JPL Horizons. The SPICE implementation is an addition to previous work, which mainly focused on the JPL Horizons implementation [8].

Figure 1. Workflow/pipeline for data extraction. (need to update)

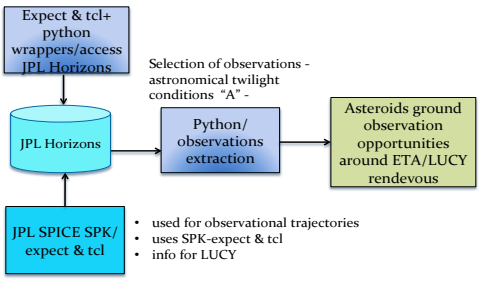

3. Results

The extracted observations for all targeted asteroids outlined several opportunities for suitable LBT ground observations. However, only one was found to be suitable during close approach of Lucy ETA to asteroid Leucus, as shown in Table 3.

Table 3. LBT ground observations.

Leucus

Date__UT___HR:MN:SS	Date_____JDUT	A/	R.A.___(ICRF/J2000.0)__DEC	dRA*cosD	d(DEC)/dt	APmag	S-brt	Ang_(O-Sppr)	Elev
2028-Apr-01 12:00:01	2461863.00001574	A	16 48 05.3186 -23 52 34.935	-2.03708	1.967076	18.61	0.16	180.7451	32.0560
2028-Apr-02 12:00:01	2461864.00001574	A	16 48 02.0360 -23 51 47.257	-2.47764	2.039883	18.60	0.16	189.8228	32.7334
2028-Apr-03 12:00:01	2461865.00001574	A	16 47 57.9864 -23 50 57.803	-2.91644	2.112077	18.59	0.15	190.8982	32.0952
2028-Apr-04 12:00:01	2461866.00001574	A	16 47 53.1706 -23 50 06.809	-3.35331	2.184463	18.58	0.15	191.9734	32.4413
2028-Apr-05 12:00:01	2461867.00001574	A	16 47 47.5929 -23 49 14.830	-3.78812	2.257043	18.57	0.15	193.0469	32.2716
2028-Apr-06 12:00:01	2461868.00001574	A	16 47 41.2569 -23 48 19.543	-4.22079	2.329823	18.56	0.14	194.1184	32.0863
2028-Apr-07 12:00:01	2461869.00001574	A	16 47 34.1662 -23 47 23.343	-4.65131	2.402808	18.55	0.14	195.1872	31.8853
2028-Apr-11 03:00:01	2461872.62501574	A	16 47 02.3258 -23 43 44.342	-5.64235	2.408793	18.51	0.12	97.9176	-34.7549
2028-Apr-12 03:00:01	2461873.62501574	A	16 46 51.7975 -23 42 40.171	-6.06957	2.558339	18.50	0.12	98.3705	-33.8900
2028-Apr-13 03:00:01	2461874.62501574	A	16 46 40.5368 -23 41 34.262	-6.49439	2.628069	18.49	0.11	98.8227	-33.0234
2028-Apr-14 03:00:01	2461875.62501574	A	16 46 28.5486 -23 40 26.614	-6.91652	2.699957	18.48	0.11	99.2744	-32.1550
2028-Apr-15 03:00:01	2461876.62501574	A	16 46 15.8382 -23 39 17.225	-7.33564	2.759975	18.47	0.10	99.7260	-31.2850
2028-Apr-16 03:00:01	2461877.62501574	A	16 46 02.4117 -23 38 06.092	-7.75148	2.830090	18.46	0.10	100.1776	-30.4134
2028-Apr-17 03:00:01	2461878.62501574	A	16 45 48.2757 -23 36 53.215	-8.16346	2.900269	18.44	0.09	100.6294	-29.5403
2028-Apr-18 03:00:01	2461879.62501574	A	16 45 33.4374 -23 35 38.595	-8.57145	2.970479	18.43	0.08	101.0817	-28.6658
2028-Apr-19 03:00:01	2461880.62501574	A	16 45 17.9047 -23 34 22.233	-8.97581	3.040684	18.42	0.08	101.5347	-27.7899
2028-Apr-20 03:00:01	2461881.62501574	A	16 45 01.6862 -23 33 04.131	-9.37308	3.110844	18.41	0.07	101.9885	-26.9129
2028-Apr-21 03:00:01	2461882.62501574	A	16 44 44.7980 -23 31 44.293	-9.76743	3.180921	18.40	0.07	102.4433	-26.0347
2028-Apr-22 03:00:01	2461883.62501574	A	16 44 27.2284 -23 30 22.723	-10.1555	3.250870	18.39	0.06	102.8995	-25.1554
2028-Apr-23 03:00:01	2461884.62501574	A	16 44 09.0894 -23 28 59.426	-10.5377	3.320647	18.38	0.05	103.3570	-24.2752
2028-Apr-24 03:00:01	2461885.62501574	A	16 43 50.1450 -23 27 34.408	-10.9136	3.390285	18.37	0.05	103.8162	-23.3941
2028-Apr-25 03:00:01	2461886.62501574	A	16 43 30.6468 -23 26 07.678	-11.2828	3.459496	18.35	0.04	104.2773	-22.5123

Observation days for Leucus are 22

4. Considerations

This effort could be enhanced by integrated spacecraft, space telescope, and ground observatory missions. A possible space telescope would be SOFIA, while candidate ground station to be considered in future work is the European Southern Observatory (ESO) in Chile. Also, the 23m Fizeau Imaging on LBT could fill the pre-ELT gap (~ 2018 to 2023) for resolved imaging of Lucy mission targets via appulse events, which are estimated to occur approximately once per week [9].

Acknowledgements

The authors acknowledge the support of LBTO and proprietary software in conducting this project.

References

[1] Levison H.F. and the Lucy Science Team. *LPSC 47th,* Abstract #2061, 2016.
[2] Weaver H.A. et al. *Space Sci. Rev. 140(1-4),* 75-91, 2008.
[3] Rothberg B. et al. Astrophysics, arXiv:1608.00037 [astro-ph.IM], 2016.
[4] Fornasier et al. *Icarus, 190 (2),* 622-642, 2007.
[5] Fernadez Y.R. et al. *The Astro. J.* 138, 240-250, 2009.
[6] JPL Horizons: ftp://ssd.jpl.nasa.gov/pub/ssd/Horizons_doc.pdf
[7] Acton C., Ancillary data services of NASA's Navigation and Ancillary Information Facility (1996), Planet. And Space Sci., 44, 65-70.
[8] Paganelli F. and Conrad A.R. *PSIDA,* Abstract#6032, 2018.
[9] Conrad A. et al. *AO4ELT5,* 1-8, 2017.

EPSC Abstracts
Vol. 12, EPSC2018-210, 2018
European Planetary Science Congress 2018

Using Gaia DR2 asteroid data: recommendations and example applications

Paolo Tanga (1), Federica Spoto (1,2)

(1) Université Côte d'Azur, Observatoire de la Côte d'Azur, CNRS, Laboratoire Lagrange, France (2) IMCCE, Observatoire de Paris, Université PSL, CNRS, Sorbonne Université, Univ. Lillen France

Abstract

We present the main properties of the Solar System data published in the Data Release 2 of the Gaia missions. Recommendations for their use are exposed, and applications to Yarkovsky determination illustrated.

1. Introduction

The Gaia mission by ESA regularly observes Solar System objects during its survey of the sky. The Data Relase 2 (Gaia DR2) includes for the first time epoch astrometry and photometry of asteroids. The time range covered by Gaia DR2 corresponds to nearly 22 months of operations.

2. Object selection and processing

Asteroids published in Gaia DR2 come from a pre-selected list of asteroids, covering different populations and maximizing the number of transits on the Gaia focal plane.

The data have been processed at the CNES facilities of Toulouse (France), one of the data processing centers of the Data Processing and Analysis Consortium (DPAC) of Gaia.

Processing has involved the rejection of clearly anomalous astrometric positions and fluxes, and a validation phase. This last task has involved a careful orbital fitting on Gaia data only, and an analysis of the residuals.

DR2 contains astrometry and photometry for 14.099 asteroids, consisting of nearly 2 million epoch data.

3. Astrometric accuracy

For objects brighter than V~18 the single-epoch astrometry is in general better than 1 mas, except at the bright end where size effects can play a role.

At the faint end (V~20.7) the accuracy decreases to a few mas. Photometry is in general accurate at a few mmag.

4. Orbit improvement

We used the data to attempt a bulk orbit improvement for all objects in DR2 showing that:

- An appropriate weighting, that takes into account the peculiar error model of Gaia data is required.

- The improvement in orbit quality is severely limited by the systematic errors present in the bulk of the other sources of astrometric data.

5. Conclusions and perspectives

In our talk we will discuss the approach to an appropriate debiasing of the non-Gaia astrometry, and on the possibility to improve the measurements of the Yarkovsky acceleration. New detections of Yarkovsky should also become possible.

References

[1] The Gaia collaboration, Spoto, F., Tanga, P. et al, A&A 2018.

EPSC Abstracts
Vol. 12, EPSC2018-259, 2018
European Planetary Science Congress 2018

A Comprehensive Model for Activation of Main Belt Comets

Nader Haghighipour (1) and Thomas Maindl (2)
(1) Institute for Astronomy, University of Hawaii, USA (nader@ifa.hawaii.edu), (2) Dept. Astrophysics, Univ. Vienna, Austria

Abstract

Main Belt Comets (MBCs) are asteroidal bodies with tails similar to those of comets. It has been suggested that the comet-like activity of these *activated asteroids* is due to the sublimation of sub-surface water-ice that is exposed when these objects are impacted by meter-sized bodies. We have developed a comprehensive model for this scenario where using a 3D SPH approach, we simulate collisions between m-sized and km-sized bodies, and determine the probability of ice exposure. Results show that ice is exposed in the bottom and surface of impact craters, and also accrete on the surface of the MBC. Impact craters have depths of ~ 15 m, implying that ice has been located within the top 15 m of the object. This has strong implications for models of ice longevity in the asteroid belt. Results also suggest that the activities of current MBCs are most probably from multiple impact sites. We present the details of our simulations and discuss their implications for the origin of Earth's water.

1. Introduction

Main-belt comets have attracted a great deal of interest since their identification as a new class of bodies by Hsieh & Jewitt in 2006 [1]. Much of this interest is due to the implication that MBCs activity is driven by the sublimation of volatile material (presumably water-ice). Analysis of the orbital evolution of MBCs suggests that these objects are native to the asteroid belt and formed in-situ as the remnants of the break-up of large icy asteroids [2,3]. The latter strongly argues in support of the idea that water-carrying planetesimals and planetary embryos from the outer part of the asteroid belt provided the majority of Earth's water during its formation.

Studies of the mass-loss in MBC 133P, combined with the observation of its recurrent activity from 1996 to 2004 [1,4] suggest that the impact crater(s) on this MBC must have been created by small 1–10 m-sized objects. These impacts excavate sub-surface ices, causing ice to sublimate and create a thin atmosphere and a tail when an MBC comes close to the Sun. In order to understand the nature of the activation of MBCs, and more importantly, to determine where ice is located in these bodies and in their parent asteroids, we have studied these collision processes and their outcomes by simulating impacts between km-sized bodies and m-sized objects using a smooth particle hydrodynamics (SPH) approach. Our SPH code includes material strength, fracture models, and porosity. We have carried out simulations for a large range of parameters allowing m-sized impactors to erode enough of an MBC's surface to trigger its activation. In the following, we discuss our methodology and present the results of our simulations.

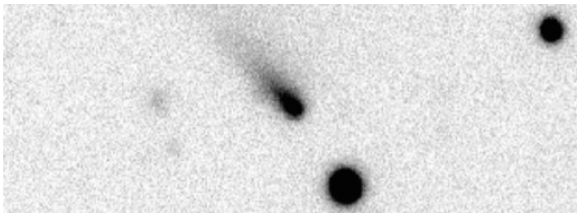

Figure 1: R-band, 90 s image of the MBC P/2008 R1(Garradd) taken UT2008 September 30 at the Keck telescope. A tail of material extends to the northeast from the nucleus of the object [5].

2. Simulations and Results

We have developed a full 3D SPH code capable of accurately simulating collisions of bodies of different sizes [5,6]. Our code includes material strength and self-gravity, and implements full elasto-plastic continuum mechanics. Fracture and brittle failure are treated using the Grady–Kipp fragmentation prescription. Our code also includes the p-alpha model for porosity with a time-varying α [7], and accounts for evaporation during the impact as well as the re-accretion of scattered materials.

To simulate collisions, we considered targets ranging from very soft (e.g., tuff) to very hard (e.g., basalt) with water contents varying from 0 to 50%. Given that

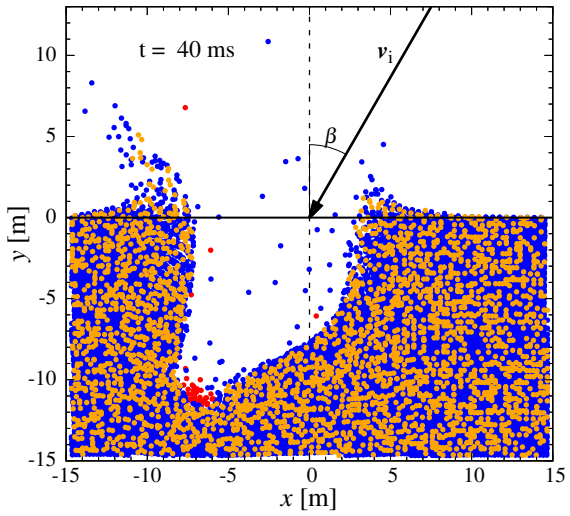

Figure 2: Impact crater for 4.4 km/s impact velocity.

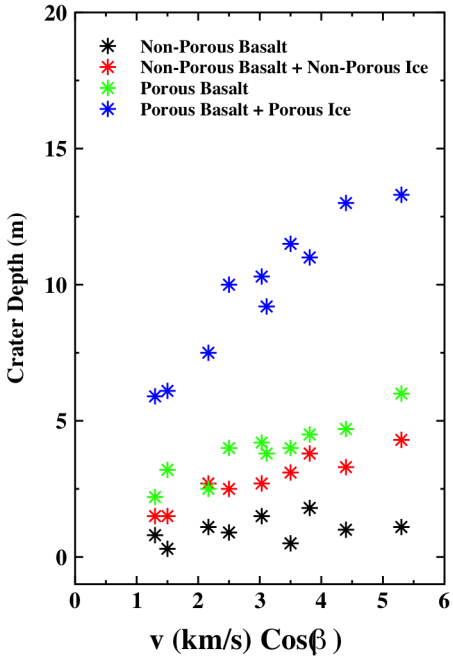

Figure 3: Graph of the depths of impact craters in terms of impact velocity for porous and non-porous targets, and with different water contents [9].

both the target and the projectile originate from the asteroid belt, we considered impact velocities in the range of 2.5 km/s to 5.3 km/s with the most probable value being around 4.4 km/s. The impact angle was varied between 0° (head-on) and 60°. We resolved the combined system of the impactor and target into ∼500,000 SPH particles. Because compared with the time of the influence of the gravitational force of the target body, the impact timescales are very short, we simulated collisions without self-gravity [8]. To analyze the evolution of the system during each impact, we took 100 snapshots every 1 ms. In between snapshots, time integration was continued with an adaptive step-size.

Figure 2 shows a snapshot of the final crater for an impact velocity of 4.4 km/s and an impact angle of 30°. The target is a mixture of 50% porous basalt (orange) and 50% porous water-ice (blue), and has a 50% water-mass fraction. As shown here, water-ice is exposed in the interior part of the impact crater and is also scattered out due to the impact [9,10].

Figure 3 shows the depth of impact craters for different material and water contents. As shown here, for the range of impact velocities corresponding to those in the asteroid belt, the depth of an impact crater is slightly below 15 m [9,10]. This indicates that in these bodies and in their parent asteroids, water-ice is located in the top 15 m, and as suggested by [11], has survived for the age of the solar system.

3. Conclusions

1) Impacts of small bodies present a viable mechanism for exposing sub-surface volatiles. 2) Water-ice is within the top 15 m. 3) The loss of ice due to the heat of impact is negligible. 4) Most of the ejected ice particles are lost and not re-accreted. 5) Activation of MBCs is most probably from multiple impact sites. 6) The water content of MBCs has to be larger than 20% in order be able to account for the observed activation of MBCs [9,10].

4. References

[1] Hsieh H. H. & Jewitt D. C. (2006) Science, 312, 561. [2] Haghighipour N. (2009) M&PS, 44, 1863. [3] Haghighipour N. (2010) IAU Symp., 263, 207. [4] Hsieh H. et al (2004) AJ, 127, 2997. [5] Jewitt, D. et al (2009) ApJ, 137, 4313. [5] Schäfer C. et al (2016) A&A, 590, A19. [6] Maindl T. et al (2013) AN, 334, 996. [7] Jutzi M. (2008) Icarus, 198, 242. [8] Maindl, T. I. et al (2015) A&A, 574, A22. [9] Haghighipour, N. et al (2016) ApJ, 830, 22. [10] Haghighipour N. et al (2018) ApJ, 855, 60. [11] Schörghofer, N. (2008) ApJ, 682, 697

EPSC Abstracts
Vol. 12, EPSC2018-315, 2018
European Planetary Science Congress 2018

Future orbital evolution of comets discovered in 2016-2018

Nataliya Kovalenko, Valeriy Kleshchonok
Astronomical Observatory of Kyiv National University, Kyiv, Ukraine (kievplanet@ukr.net)

Abstract

Each year dozens of new comets are being discovered. In order to investigate their future orbital evolution and potential hazard to Earth the orbits of new comets discovered in 2016-2018 were traced 100 kyr forward in time using Swifter integration package. The 8 planets and the Sun were taken into account and new comets were traced as massless test particles, without considering the non-gravitational forces caused by the outgazing. For comets that reached the 0.3 AU vicinity of Earth over the simulation period more detailed integrations were performed, for initial test particles along with their clones. Results of simulations are presented and discussed.

EPSC Abstracts
Vol. 12, EPSC2018-325-1, 2018
European Planetary Science Congress 2018

EPSC
European Planetary Science Congress

Asteroids observations from the ground and space: implications for our understanding of the main belt and of asteroid families

Marco Delbo (1)
(1) Université Côte d'Azur, CNRS–Lagrange, Observatoire de la Côte d'Azur, CS 34229 – F 06304 NICE Cedex 4, France (marcodelbo@gmail.com)

1. Asteroid surveys

Telescopes on the ground, such as the Catalina Sky Survey (CSS) and Pan-STARRS [1] and in space (NEOWISE) [2] discover everyday new asteroids and track the orbits of the known ones. Their data are organised by Minor Planet Center (MPC), which provides quick and accurate access for those who query their databases to obtain the final products: orbits and asteroid ephemerides. Photometric information from these telescopes are also used to obtain basic properties, such as rotation periods, shapes, and the direction of the rotational poles [3].

However, the information in these *databases of orbits* does not tell us what an asteroid actually is, because they do not contain physical properties such as albedo, size, mass, composition, and shape. Values for these physical parameters are obtained from different groups, using different techniques and different telescopes from ground and space.

For insatnce WISE, AKARI, IRAS, MMX, and Spitzer space telescopes [2] have provided infrared observation in the thermal infrared on which our knowledge of sizes and albedos is nowadays based (totalling to more than 140,000 asteroids).

On the other hand to study the composition of asteroids, spectra of the solar light reflected by these bodies are acquired with several different ground based telescopes (IRTF, TNG, Magellan...), analysed and compared to the millions of laboratory spectra of minerals and meteorites (see e.g smass.mit.edu). Spectrophometirc data from the SDSS [4] is used for the faintest asteroids.

2 Connecting physics & dynamics

Massively obtaining published data of asteroids, combining the physical and dynamical properties is key to future asteroid science, as it has been demonstrated in the case of interpreting of the compositional gradient of the Main Belt in term of the different events that sculpted our Solar System, [5] and in the discovery of asteroid families [6, 7, 8, 9].

However, this massive data exploitation is a problem. Hundred thousand of values for several physical properties exist, but are spread in numerous literature works or in other archives throughout the world [10, 11, 12, 13, 14, 15, 16, 17], usually hosted by the relevant space telescope internet sites or by the institutes of the scientists who obtained the values or even in supplementary materials of scientific publications [9].

One answer to this problem is the attempt of the Observatoire de la Côte d'Azur to develop and hosts an online, publicly open tool, the *Minor Planet Physical Properties Catalogue (mp3c.oca.eu)* that stores and distribute massive asteroid data. MP3C is also part of the *Virtual Observatory*.

3 The structure of the Main Belt

What are the original asteroids – those that formed as planetesimals by direct accretion of dust and pebbles in the protoplanetary disk ? Which asteroids are instead those of new generations – members of families of fragments created by the catastrophic fragmentation of the original parents bodies ? We need to identify all these possible families and remove them from our view in order to understand what were the sizes and the composition of the planetesimals that formed our planets. In the past, families have been identified as many tight clusters of asteroids on closely related orbits; this identification was performed solely on the basis of the orbits of the asteroids [18]. But this family identification was very conservative. New methods [19] based on the combination of dynamical and physical properties are very promising as they revealed ancient [6] and

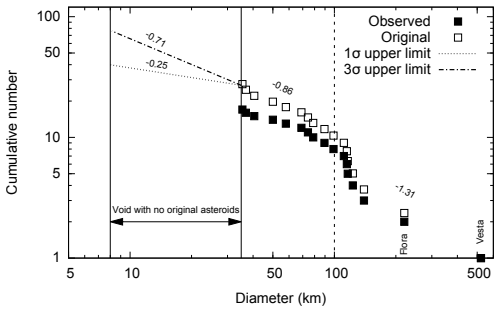

Figure 1: **Example of cumulative size distribution of original asteroids**. The cumulative size distribution of those asteroids that are outside families of the inner Main Belt (filled squares) is corrected for the maximum number of objects that were lost, due to the collisional and dynamical evolution, in order to obtain an upper limit for the distribution of the planetesimals (open squares). Functions of the form $N(> D) = N_0 D^{\beta}$, where N is the cumulative number of asteroids, are fitted piecewise in the size ranges $D >$ 100 km, $35 < D < 100$ km, and $8 < D < 35$ km. For the original planetesimals size distribution, we obtain the values of β reported by the labels in the plot. In the range of sizes between 8 and 35 km, we give the 1σ and the 3σ upper limits on the planetesimals size distribution. Adapted from [9]

primordial families [9], that, when removed, allowed us to identify the original planetesimals in a very restricted area of the Main Belt.

4 Future perspectives

ESA mission Gaia just released (DR2 on 25-04-18) the first milli-arcsec precise asteroid astrometry and in 2020 with the DR3 massive Gaia astrometry and spectroscopy will be released. The LSST first light in 2019 will provide an enourmous boost to asteroids physical characterisation, in particular for km-sized and smaller Main Belt objects: it will provide 5-band colour data, astrometry and photometry.

Acknowledgements

Asteroid physical properties data are from https://mp3c.oca.eu/, Observatoire de la Côte d'Azur. The author acknowledges support by the French National Research Agency under the project "Investissements d'Avenir" UCAJEDI with the reference number ANR- 15-IDEX-01.

References

[1] R JEDICKE, M Granvik, M Micheli, E Ryan, T Spahr, and D K Yeomans. Surveys, Astrometric Follow-Up, and Population Statistics. *in Asteroids IV (P. Michel, et al. eds.) University of Arizona Press, Tucson.*, pages 795–813, 2015.

[2] A Mainzer, F Usui, and D E Trilling. Space-Based Thermal Infrared Studies of Asteroids. *in Asteroids IV (P. Michel, et al. eds.) University of Arizona Press, Tucson.*, pages 89–106, 2015.

[3] J Durech, M Kaasalainen, B D Warner, M Fauerbach, S A Marks, S Fauvaud, M Fauvaud, J M Vugnon, F Pilcher, L Bernasconi, and R Behrend. Asteroid models from combined sparse and dense photometric data. *Astronomy and Astrophysics*, 493(1):291–297, January 2009.

[4] F E DeMeo and B Carry. The taxonomic distribution of asteroids from multi-filter all-sky photometric surveys. *Icarus*, 226(1):723–741, September 2013.

[5] F E DeMeo and B Carry. Solar System evolution from compositional mapping of the asteroid belt. *Nature*, 505(7):629–634, January 2014.

[6] Kevin J Walsh, Marco Delbo, William F Bottke, David Vokrouhlický, and Dante S Lauretta. Introducing the Eulalia and new Polana asteroid families: Re-assessing primitive asteroid families in the inner Main Belt. *Icarus*, 225(1):283–297, July 2013.

[7] Andrea Milani, Alberto Cellino, Zoran Knežević, Bojan Novaković, Federica Spoto, and Paolo Paolicchi. Asteroid families classification: Exploiting very large datasets. *Icarus*, 239:46–73, September 2014.

[8] J R Masiero, F E DeMeo, T Kasuga, and A H Parker. Asteroid Family Physical Properties. *in Asteroids IV (P. Michel, et al. eds.) University of Arizona Press, Tucson.*, pages 323–340, 2015.

[9] Marco Delbo, Kevin Walsh, Bryce Bolin, Chrysa Avdellidou, and Alessandro Morbidelli. Identification of a primordial asteroid family constrains the original planetesimal population. *Science*, 357(6355):1026–1029, September 2017.

[10] C R Nugent, A Mainzer, J Bauer, R M Cutri, E A Kramer, T Grav, J Masiero, S Sonnett, and E L Wright. NEOWISE Reactivation Mission Year Two: Asteroid Diameters and Albedos. *The Astronomical Journal*, 152(3):63, September 2016.

[11] C R Nugent, A Mainzer, J Masiero, J Bauer, R M Cutri, T Grav, E Kramer, S Sonnett, R Stevenson, and E L Wright. NEOWISE Reactivation Mission Year One: Preliminary Asteroid Diameters and Albedos. *The Astrophysical Journal*, 814(2):117, December 2015.

[12] Joseph R Masiero, A K Mainzer, T Grav, J M Bauer, R M Cutri, C Nugent, and M S Cabrera. Preliminary Analysis of WISE/NEOWISE 3-Band Cryogenic and Post-cryogenic Observations of Main Belt Asteroids. *The Astrophysical Journal Letters*, 759(1):L8, November 2012.

[13] Edward F Tedesco, Paul V Noah, Meg Noah, and Stephan D Price. The Supplemental IRAS Minor Planet Survey. *The Astronomical Journal*, 123(2):1056–1085, February 2002.

[14] Erin Lee Ryan and Charles E Woodward. Rectified Asteroid Albedos and Diameters from IRAS and MSX Photometry Catalogs. *The Astronomical Journal*, 140(4):933–943, October 2010.

[15] Fumihiko Usui, Daisuke Kuroda, Thomas G Müller, Sunao Hasegawa, Masateru Ishiguro, Takafumi Ootsubo, Daisuke Ishihara, Hirokazu Kataza, Satoshi Takita, Shinki Oyabu, Munetaka Ueno, Hideo Matsuhara, and Takashi Onaka. Asteroid Catalog Using Akari: AKARI/IRC Mid-Infrared Asteroid Survey. *Publications of the Astronomical Society of Japan*, 63(5):1117–1138, October 2011.

[16] Joseph R Masiero, A K Mainzer, T Grav, J M Bauer, R M Cutri, J Dailey, P R M Eisenhardt, R S McMillan, T B Spahr, M F Skrutskie, D Tholen, R G Walker, E L Wright, E DeBaun, D Elsbury, T IV Gautier, S Gomillion, and A Wilkins. Main Belt Asteroids with WISE/NEOWISE. I. Preliminary Albedos and Diameters. *The Astrophysical Journal*, 741(2):68, November 2011.

[17] Joseph R Masiero, T Grav, A K Mainzer, C R Nugent, J M Bauer, R Stevenson, and S Sonnett. Main-belt Asteroids with WISE/NEOWISE: Near-infrared Albedos. *The Astrophysical Journal*, 791(2):121, August 2014.

[18] D Nesvorný, M Brož, and V Carruba. Identification and Dynamical Properties of Asteroid Families. *in Asteroids IV (P. Michel, et al. eds.) University of Arizona Press, Tucson.*, pages 297–321, 2015.

[19] Bryce T Bolin, Marco Delbo, Alessandro Morbidelli, and Kevin J Walsh. Yarkovsky V-shape identification of asteroid families. *Icarus*, 282:290–312, January 2017.

EPSC Abstracts
Vol. 12, EPSC2018-354, 2018
European Planetary Science Congress 2018

Effect of surface roughness on the reflectance spectra of metallic meteorites

Sandra POTIN (1), Pierre Beck (1) and Guy Libourel (2,3)
(1)Institut de Planétologie et d'Astrophysique de Grenoble, France, (2) Observatoire de la Côte d'Azur, Nice, France, (3) Hawaii Institute of Geophysics and Planetology, School of Ocean, Earth Science and Technology, Honolulu, Hawaii, USA
(sandra.potin@univ-grenoble-alpes.fr)

Abstract

We studied the spectral effect (0.5-2.4 µm) of surface roughness on a sample of the Gibeon iron meteorite, using bidirectional reflectance spectroscopy around the specular direction, in the visible and near-infrared range. Photometry and spectral slopes for different illumination-emergence-azimuth configurations are compared.

1. Introduction

Visible and near-infrared reflectance spectra of M-class asteroids and metallic meteorites tend to present a strong red slope, typically associated to their iron-rich nature. Previous measurement on iron meteorite powders and comparison to M-type observations has led to the idea that the M-type surfaces are covered by fine regolith. Here we explore an alternative, that the signatures can be caused by a highly rough surface. For that, we conducted laboratory measurements to analyze the effect of geometry and surface roughness on reflectance spectroscopy of metallic meteorites, from polished surface to coarse grained rough surface.

2. Sample preparation

A sample of a few cubic centimeters of the Gibeon metallic meteorite was used for our study. This meteorite is in majority composed of iron mixed with 8% of nickel [1]. The first step was to polish one of the flat surfaces of the sample, resulting in a smooth mirror-like surface. Then SiC abrasive disks of increasing grain sizes were used to create roughness on the same surface (see fig.1). After each roughening step, bidirectional reflectance spectra were taken around the specular direction.

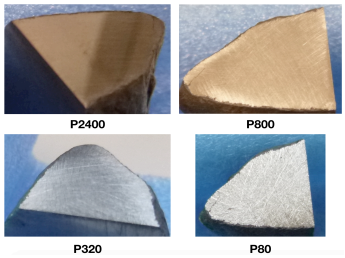

Figure 1: Pictures of the flat surface of the sample of the Gibeon meteorite after the four alterations by the abrasive disks P2400, P800, P320 and P80.

3. Bidirectional reflectance spectra

The reflectance spectra were acquired with the spectrogonio radiometer SHADOWS [2] installed at IPAG. To observe the modification of the spectra around the specular direction, the illumination angle has been set to 20°, and spectra were acquired at emergence angles from 10° to 30° by 2° steps, in and outside the principal plane. The two detectors of the goniometer caught the reflected light in a 1.6° solid angle around the emergence position. The spectral range was set from 500 nm to 2400 nm with a step of 100 nm. The spectrogonio radiometer measures the reflectance of any sample, compared to a lambertian surface.

3.1 Decrease of reflectance

The rougher the surface, the lower the reflectance. This effect can be represented by drawing the bidirectional reflectance distribution function, or BRDF (see fig. 2).

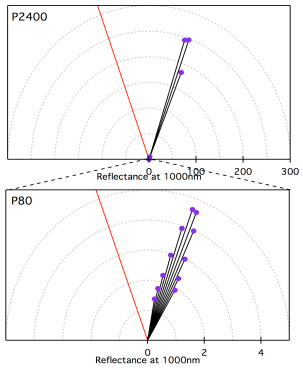

Figure 2: BRDF at 1000nm of the Gibeon meteorite, polished (disk P2400, top panel) and after alteration by the roughest abrasive disk (disk P80, bottom panel). The illumination direction of 20° is represented by the red line, the purple dots are the reflectance measurements at each emergence angle (note the measurements around 0 on the top panel). The grey doted semi-circles represent values of reflectance.

A highly polished or fine-grained surface behaves like a mirror and almost all the incident light is reflected in the specular direction in the principal plane. Compared to a lambertian surface, we measured at 2400 nm a reflectance of 35300 % in the specular direction and a reflectance of 4% at an emergence angle of 10° (phase=10°). We observed a factor of 10 between the reflectance measured in the specular direction in the principal plane and with an azimuth angle of 10°. For the roughest surface, we measured reflectance between 100% and 700% in the principal plane, including the specular reflectance, and the factor between the reflectance in the principal plane and at an azimuth angle of 10° decreases to 1.

3.2 Spectral slope

We observed a strong dependence of the spectral slope with the roughness of the surface, as well as with the geometry (see fig. 3).

For the polished surface, the specular reflection tends to present a red slope, while spectra outside the specular position present a strong blue slope. This

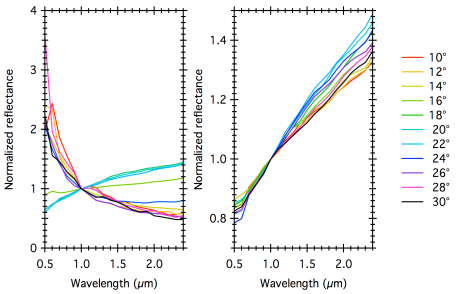

Figure 3: Normalized reflectance spectra in the principal plane of the Gibeon meteorite after being polished (left) and after alteration (right) for different emergence angles. The specular reflection is at emergence 20°. Note the different scales for the reflectance axis.

blue slope rapidly disappears after the abrasions of the surface, until all spectra become red, with a geometry dependant slope. In the case of the roughened samples, the surface becomes a diffuse reflector and all spectra roughly present the same spectral reddening and slope.

4. Conclusion

We conducted bidirectional reflectance spectra on a sample of the Gibeon meteorite. Spectra show a strong variability du to the surface roughness of the meteorite and the geometry of the system, incidence, emergence and azimut angles. Value of reflectance, as well as the spectral slope is impacted. Fine-grained or polished surfaces show a high and red specular reflection, while other geometries present low and blue reflectance spectra. For coarse grains, the differences between spectra in and out of the specular reflection decrease and all spectra tend to present a rather low reflectance coupled with a soft red slope.

References

[1] Weller M., Wegst U. Fe-C Snoek peak in iron and stony meteorites: Metallurgical and cosmological aspects, Materials Science and Engineering A, vol.521-522, pp 39-42 (2009)

[2] Potin S., et al.: SHADOWS: spectrogonio radiometer for bidirectional reflectance studies of dark meteorites and terrestrial analogues, EPSC Abstracts, Vol. 11, EPSC2017-243 (2017)

EPSC Abstracts
Vol. 12, EPSC2018-396, 2018
European Planetary Science Congress 2018

Chaotic transport of Main Belt asteroids in Martian resonances

Apostolos Christou (1), Stanley Dermott (2) and Dan Li
(1) Armagh Observatory and Planetarium, Armagh, UK (aac@arm.ac.uk / Fax: +44-2837-527174), (2) University of Florida, Gainesville, USA (3) University of Pennsylvania, Philadelphia, USA.

Abstract

A major question in planetary science is the source regions and parent bodies of NEAs and meteorites [1]. In the contemporary view, these are first produced as fragments of larger asteroids in the Main Belt [2, 3], then mobilized by chaotic orbital evolution [4, 5] and Yarkovsky radiation forces [6, 7] until their injection to the terrestrial planet region through dynamical "escape hatches" [8]. The process of orbit mobilisation of MB asteroids is a relatively unexplored chain in this link, with implications for the past evolution and genealogy of bodies in the asteroid belt [5, 9] but also efforts to debias the observed NEA population [10, 11].

We are pursuing a project to quantify the efficiency of Mars resonances to mobilise Inner Main Belt asteroids (ie those with a<2.5 au) through intensive numerical simulations. We complement, and expand on, earlier work [4, 12, 13] by systematically mapping out the mobility rate of asteroids both within and outside resonances and over a wide region of phase space. We initially consider only point-mass gravitational forces, since these would affect all asteroids independently of size. Pinning down the long-term effect of gravity alone would also help to separate it out in later simulations that include non-gravitational forces.

Here, we focus our attention on the 1:2 & 4:7 exterior mean motion resonances with Mars. Both of these, but especially the 1:2 resonance, visibly affect the orbital distribution of asteroids in their vicinity (Fig 1) and therefore we expect them to be important individual drivers of asteroid orbit evolution.

Our principal finding from these simulations is that, while there is little change in e & I outside these resonances, asteroids in the resonances undergo significant chaotic evolution. This implies that resonant asteroids can slowly migrate away from the family they belong to and ultimately become Mars-orbit crossers.

However, the magnitude of the changes is different for the two resonances and even between asteroids within the same resonance. For instance, the change in I is significantly higher within the 4:7 than the 1:2 resonance, probably because the 3rd order resonance allows interaction between numerous strong multiplets involving the node. At the same time, orbits in the 1:2 resonance with $e \simeq e_{\rm Mars}$ diffuse faster in e than more eccentric orbits within that resonance. There, the varying eccentricity of Mars may be modulating the frequency of hopping between the two principal multiplets, with strengths proportional to e and $e_{\rm Mars}$ respectively.

In conclusion, our findings show that local dynamics play an important role in mobilising asteroid orbits. Therefore, models of the IMB as a dynamically evolving population with asteroid production and loss will require careful calibration over a sufficiently large number of different locations.

1. Figures

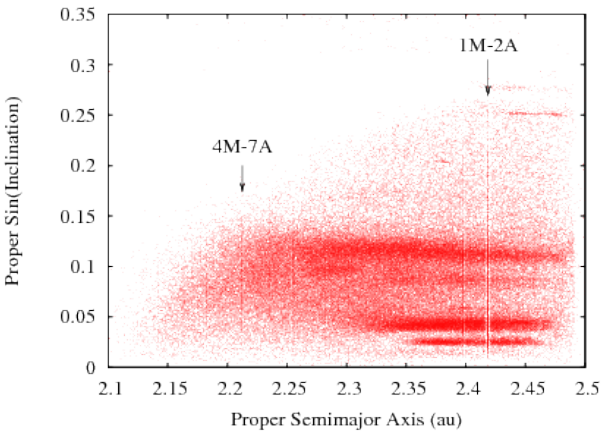

Figure 1: Phase portrait of asteroid orbits in the IMB. The arrows indicate the locations of the xM-yA exterior Martian resonances where the asteroid completes x revolutions for every y revolutions of Mars.

Acknowledgements

Astronomical research at the Armagh Observatory and Planetarium is funded by the Northern Ireland Department for Communities (DfC).

References

[1] Burbine, T.H., et al: Meteoritic parent bodies: Their number and identification, In: Asteroids III, University of Arizona Press, Tucson, pp. 653-667, 2002.

[2] Michel, P., et al: Collisions and gravitational reaccumulation: Forming asteroid families and satellites, Science, Vol. 294, pp. 1696-1700, 2001.

[3] Jacobson, S.A., et al: Effect of rotational disruption on the size-frequency distribution of the Main Belt asteroid population, MNRAS, Vol. 439, pp. L95-L99, 2014.

[4] Morbidelli, A., Nesvorný, D.: Numerous weak resonances drive asteroids toward terrestrial planet's orbits, Icarus, Vol. 139, pp. 295-308, 1999.

[5] Minton, D.A., Malhotra, R.: Dynamical erosion of the asteroid belt and implications for large impacts in the inner solar system., Icarus, Vol. 207, pp. 744-757, 2010.

[6] Vokrouhlický, D., Farinella, P.: Efficient delivery of meteorites to the Earth from a wide range of asteroid parent bodies, Nature, Vol. 407, pp. 606-608, 2000.

[7] Bottke, W.F., et al: The effect of Yarkovsky thermal forces on the dynamical evolution of asteroids and meteoroids, In: Asteroids III, University of Arizona Press, Tucson, pp. 395-408, 2002.

[8] Wisdom, J.: Chaotic behavior and the origin of the 3/1 Kirkwood gap, Icarus, Vol. 56, pp. 51-74, 1983.

[9] Dermott, S.F., et al: The common origin of family & non-family asteroids, Nature Astronomy, in press, 2018.

[10] Bottke, W.F., et al: Debiased orbital and absolute magnitude distribution of the near-Earth objects, Icarus, Vol. 156, pp. 399-433, 2002.

[11] Greenstreet, S., et al: The orbital distribution of Near-Earth Objects inside Earth's orbit, Icarus, Vol. 217, pp. 355-366, 2012.

[12] Gallardo, T.: The Mars 1:2 resonant population, Icarus, Vol. 190, pp. 280-282, 2007.

[13] Gallardo, T., et al: Origin and sustainability of the population of asteroids captured in the exterior resonance 1:2 with Mars, Icarus, Vol. 214, pp. 632-644, 2011.

EPSC Abstracts
Vol. 12, EPSC2018-481, 2018
European Planetary Science Congress 2018

Chondrules alteration study of NWA2086 CV3 meteorite by using µ-IR and SEM/EDS combined analysis and implications for asteroid parent body

Fabrizio Dirri (1), Marco Ferrari (1), Ernesto Palomba (1), Stefania Stefani (1), Andrea Longobardo (1,2), Alessandra Rotundi (1,2)
(1) Institute for Space Astrophysics and Planetology, Via del Fosso del Cavaliere 100, 00133, Rome, Italy (fabrizio.dirri@iaps.inaf.it); (2) Dipartimento di Scienze e Tecnologie, Università di Napoli "Parthenope", CDN, IC4 , 80143, Naples, Italy.

Abstract

The aim of this work is to characterise two different chondrules (from intact chondrule to matrix area) of NWA2086 CV3 type meteorite by using the Infrared µ-spectroscopy (µ-IR) and Scanning Electron Microscope with Energy Dispersive Spectroscopy (SEM/EDS) coupled technique. The Christiansen and Reststrahlen features of the main minerals were identified by using µ-IR (spectral region 7-15µm). The µ-IR results were compared with SEM/EDS analysis able to provide chemical information of meteorite samples and high resolution images of the inclusions morphology. The coupled technique will provide a comprehensive mineralogical characterization of NWA2086 meteorite, giving implications about the CV3 parent body evolution.

1. Introduction

The CV Carbonaceous Chondrite meteorite with many large olivine chondrules and CAIs (Ca-Al-rich inclusions), are among the most studied meteorites founded on Earth [1]. The CV3 were considered primitive and representative of primitive solar nebula [2] and although belong to petrologic type 3, some signatures related to hydration and interaction with water could also be present [3] and should provide information about chemical processes in relatively small planetesimals [4]. In this work, we analysed two portions of NWA2086 meteorite, belonging to the reduced subtype of CV3s, with low shock stage (S = 1) and weathering grade (W = 1). Four types of Chondrules, i.e. 1. plagioclase-rich (PRCs), 2. porphyritic olivine (PO), 3. porphyritic olivine pyroxene (POP), and 4. barred olivine (PO) and three types of CAIs, i.e. 1. spinel-rich, 2. clinopyroxene assemblages plus andradite and perovskite, 3. gehelenite-rich plus perovskite and spinel have been identified by Fintor et al. (2013) by using petrographic and micro-Raman methods.
In this framework, we focused our analysis on mineral characterization of two intact chondrules and matrix area of NWA2086 by coupling the spectral features obtained with µ-IR technique and coupling the results with SEM/EDS chemical data.

2. Method

A preliminary analysis was performed on NWA2086 by using a Stereo Microscope (Leica M205c) equipped with a digital camera in order to select the sample regions characterized by a significant mineralogical heterogeneity. Thus, two chondrules (A, B area; Fig.1) were selected and spectral data acquired with µ-IR Microscope (Bruker Hyperion 3000) and analysed in the spectral range of interest: 7-15 µm.

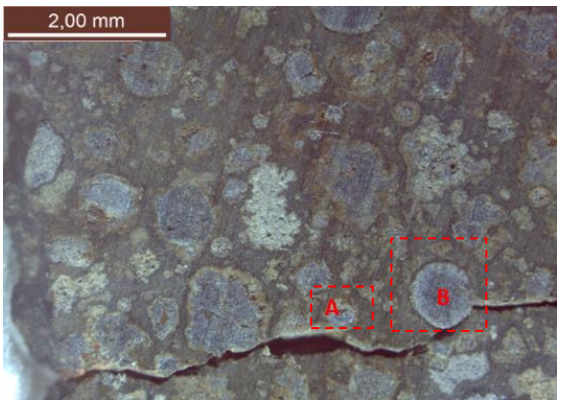

Figure 1. Image of A and B area, analysed with the µ-IR and SEM/EDS techniques.

The A and B regions have been also analysed by using chemical information provided by SEM/EDS technique and compared with the Reststrahlen bands of the main minerals identified and summarized in Table 1.

Table 1. Mineral bands identified by means of μ-IR technique and compared with SEM/EDS data.

NWA2086	**Res. - Christ. features (μm)**	**μ-IR minerals**	**SEM minerals**
A(chondrule)	9.5,10.8, 11.2, 12 - 8.7	Mg-rich oliv. clinopyr., An	Mg-rich olivine
A(matrix)	10.4, 11.3, 12 - 9.3	Fe-rich olivine	Fe-rich olivine
A(chondrule)	9.1, 10.6 - 8.2	an-rich, olivine clinopyroxene	anorthitic plag., clinopyr., oliv., sulphides
B(matrix)	10.4, 11.3, 12 - 9.4	olivine	Fe-rich olivine, poor-phyllosil.

3. Discussion

The matched data of A, B area indicate that:

- the chondrule spectral bands (*"A"* area) can be ascribed to clino-pyroxene and Mg-rich olivine while the matrix spectral bands indicate the presence of Fe-rich olivine. From intact chondrule to matrix area the chemical analysis shows as: 1. MgO decreases; 2. FeO increases (up to 55%); 3. small quantity of Al2O3 (<2%); 4. Fe-rich mineral is present in the rim where Mg content decreases and Fe content increases as stated by Kareszturi et al. (2014).

- the chondrule spectral bands (*"B"* area) can be ascribed to clino-pyroxene and plagioclase while the matrix spectral bands indicate the presence of olivine. Chemical data shows as from intact chondrule to matrix area: 1. Al2O3 and CaO decreases (35 to 3% and 24 to 4%, respectively); 2. FeO and MgO increases (up to 45% and 22%, respectively) that can be ascribed to Fe-rich olivine largely present in the matrix area.

An example of spectral bands variation from chondrule to matrix of B area is shown in Fig. 2 where mainly composition of An-plagioclase (probably PRCs chondrule) gives way to Fe-rich olivine composition (matrix).

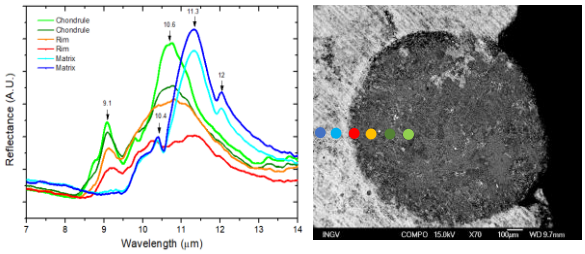

Figure 2. B area: spectral bands from chondrule to matrix (*left*) and location of μ-IR measurements *(right)*.

4. Conclusion and future aims

The chondrules showed a different composition, i.e. clino-pyroxene and Mg-rich olivine ("A"), clino-pyroxene and plagioclase ("B") while the composition of matrix area, i.e. Fe-rich, is mainly ascribed to Fe-rich olivine. In particular, from intact chondrule to matrix the Fe content increases and Mg decreases which suggests, as stated by [6], a chondrule rim composition close to matrix composition (as confirmed by our data), due to fluid interaction during the re-accretion phase of this meteorite. The chondrules rim characterization will be in depth studied in the next future (the comparison of NWA2086 with other CV3 meteorites as well) in order to understand the formation or chemical processes involved in the CV3 parent body evolution.

Aknowledgments

This work is supported by the Italian Space Agency, PRIN-MIUR and Regione Campania. This research has been performed using the spectra from ASTER database (courtesy of the JPL) and RRUFF database.

References

[1] McSween H.Y. (1977), *Geochin. Cosmochim. Ac*. 41, 1777-1790; [2] McSween H.Y. (1977), *Rev. of Geoph. And Space Phys.*, 17, 1059-1078; [3] Beck P. et al. (2010), *Geochem. And Cosmochem. Acta* 74, 4881-4892; [4] Gyollai I. et al., (2011), *LPSC Abs. #1608*; [5] Fintor K. et al. (2013), *LPSC Abs.#1152*; [6] Kareszturi, A. et al. (2014), *M&PS 49*, 1350-1364.

EPSC Abstracts
Vol. 12, EPSC2018-498, 2018
European Planetary Science Congress 2018

μ-IR + SEM/EDS combined technique for Carbonaceous Chondrite meteorites characterization as possible analogues of Hayabusa2 and Osiris-REx asteroid targets

Fabrizio Dirri (1), Marco Ferrari (1), Ernesto Palomba (1), Stefania Stefani (1), Andrea Longobardo (1,2), Alessandra Rotundi (1,2)
(1) Institute for Space Astrophysics and Planetology, Via del Fosso del Cavaliere 100, 00133, Rome, Italy (fabrizio.dirri@iaps.inaf.it); (2) Dipartimento di Scienze e Tecnologie, Università di Napoli "Parthenope", CDN, IC4 , 80143, Naples, Italy.

Abstract

We used the Infrared μ-spectroscopy (μ-IR) and Scanning Electron Microscope with Energy Dispersive Spectroscopy (SEM/EDS) coupled technique on CM2 and CV3 Carbonaceous Chondrites (CC) meteorites, as possible analogues of the Hayabusa2 and Osiris-REx Space Missions asteroid targets. Chondrules, CAIs, and mineral inclusions were identified and analysed in detail in the spectral region 7-15 μm by using μ-IR. Chemical information on chondrules, inclusions and matrix were acquired by using SEM/EDS technique and the results were combined with the main absorption bands, Christiansen and Reststrahlen features identified. This technique is going to be applied to CI, CR and CK meteorites because of their strict relation with C-type and B-type asteroids.

1. Why study Carbonaceous Chondrites?

Different groups of Carbonaceous Chondrite were associated with different asteroidal parents and most are thought to come from low-albedo C-type asteroid, the most abundant type between 2.7 A.U. and 3.7 A.U. [1]. In particular, CI, CM and CI/CM unusual are consistent with C-type asteroids [2,3] while from recent spectral analysis CK, CO and CV can be associated to B-type asteroids (e.g., Pallas group) [4]. Thus, in order to know the asteroids evolution and to support the space data interpretation from remote-sensing infrared spectroscopes, the mineralogical and spectral analysis on extraterrestrial samples are fundamental. We applied μ-IR + SEM/EDS combined technique to CM2 and CV3 meteorites, as possible analogues of 101955 Bennu (B-type) and 162173 Ryugu (C-type), targets by Hayabusa 2 and Osiris Rex missions [5,6].

2. CCs samples and measurement procedure

We analysed the following meteorites: 1. Murchison (CM2 group); 2. NWA8267 (CM2 group), characterized by small chondrules and refractory inclusions [7]; 3. Allende characterized by coarse-grained, Al-rich inclusions and chondrules [8] and 4. NWA2086 (CV3 group) with considerable amount of large mm-size chondrules and Calcium Aluminum Inclusions (CAIs), many surrounded by igneous rims [9]. A preliminary analysis was performed by using a Stereo Microscope (Leica M205c) equipped with a digital camera in order to select the sample regions characterized by a significant mineralogical heterogeneity (e.g. chondrules, inclusions) (Fig.1).

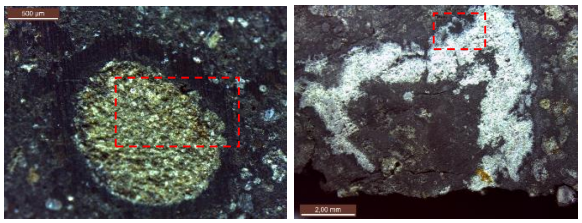

Figure 1. Examples of selected regions analysed with the μ-IR+SEM/EDS technique. *Left*: NWA8267 (CM2) chondrule. *Right*: Allende inclusion (CV3).

The infrared spectra of selected regions (Fig.2a, 2b) were acquired with μ-IR Microscope (mod. Bruker Hyperion 3000) and analysed in the spectral range: 7-15 μm. The Christiansen features and Reststrahlen bands of the main minerals were identified and coupled with chemical data provided by SEM/EDS technique. Preliminary results are summarized in Table 1.

Table 1. Reststrahlen and Christiansen features identified and compared with SEM/EDS data.

CC samples	Res. - Christ. features (μm)	μ-IR minerals	SEM minerals
Murchison - inclusion	9, 9.9,10.5, 11.6 - 8.4	olivine, low-Ca pyroxene, serpentine	olivine, serpentine
NWA8267 -chondrule	9.1, 9.8, 10.5 - 8.5	low-Ca pyroxene	low-Ca pyroxene
NWA2086 - chondrule	9.1, 10.8 – 8.3	clino-pyroxene, olivine, Anorth.	Mg-rich olivine, sulphides
Allende - inclusion	9.1, 10.3, 11.1, 15 – 8.5	clino-pyroxene, melilite, spinel	-

3. Discussion and results

The combined data μ-IR+SEM/EDS technique (Fig. 2c, 2d) of chondrules and inclusions indicate that the main spectral bands:

- in Murchison can be ascribed to the Fe-rich olivine, to a pyroxene mixture and phyllosilicates [7];
- in NWA8267 can be assigned to a mixture of low-Ca pyroxene an sulphides [10];
- in NWA2086 can be ascribed to Mg-rich olivine, clinopyroxene and phyllosilicates in the intact chondrules and Fe-rich olivine in matrix area [9];
- in Allende can be ascribed to clinopyroxene, melilite and spinel (inclusion) and Fe-rich olivine (matrix) [8].

The analysis is going to be extended to other CCs class like CK and CO as well CM/CI anomalous and comparing the results with C-type and B-type asteroids data to find similar spectral features. In order to help the analysed CC sample characterization, FT-IR spectra of packed powder meteorite samples should be acquired between 1.5 and 4.2 μm in order to identified the distinct absorption band and their relationship with minerals founded with μ-IR+SEM/EDS combined technique. Thus, these combined analyses will provide a comprehensive mineralogical framework of Carbonaceous Chondrites meteorites, which will help the returned samples characterization of next sample return missions.

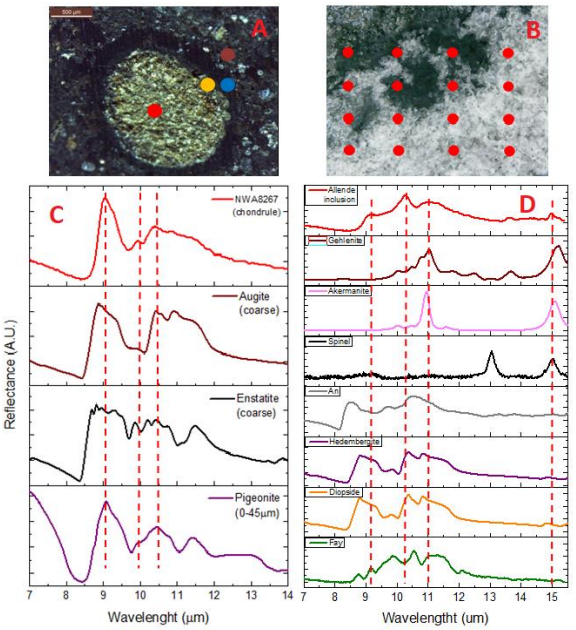

Figure 2. A, B: selected areas and μ-IR measurements location. C, D: μ-IR spectra in comparison with main minerals.

Acknowledgments

This work is supported by the Italian Space Agency, PRIN-MIUR and Regione Campania. This research has been performed using the spectra from ASTER database (courtesy of the JPL) and RRUFF database.

References

[1] Bell J.F. (1989), *Icarus* 78, 426; [2] Gaffey M.J. & McCord T.B. (1978), *SSR* 21, 555-628; [3] Hiroi et al., (1996), *M&PS* 31, 321-327; [4] Clark B.E. et al. (2010), *Jour. Geochem. Res.* 115, E06005; [5] Chasley, R. et al. (2014), *Icarus* 235, 5-22; [6] Yoshikawa, M. et al. (2016), *47th LPSC Abs.*; [7] Morlok, A. et al. (2010), *Icarus* 207, 45-53; [8] Grossman L. 1975, *Geochem. Cosmochem. Data* 39, 433-454; [9] Kareszturi, A. et al. (2014), *M&PS* 49, 1350-1364; [10] Meteoritical Bulletin N°104 (2017), in preparation.

EPSC Abstracts
Vol. 12, EPSC2018-504, 2018
European Planetary Science Congress 2018

Unusual properties of asteroid (3200) Phaethon from polarimetric observations and modeling

Nikolai Kiselev (1,2), Viktor Afanasiev (3), Dmitry Petrov (2), Vera Rosenbush (1,4)
(1) Main Astronomical Observatory of the NAS of Ukraine, Kyiv, Ukraine (kiselevnn42@gmail.com), (2) Crimean Astrophysical Observatory, Nauchnij, Crimea, (3) Special Astrophysical Observatory of the RAS, Nizhnij Arkhyz, Russia, (4) Taras Shevchenko National University of Kyiv, Kyiv, Ukraine

Abstract

The results of imaging and aperture polarimetric observations of the near-Earth asteroid (3200) Phaethon in November-December 2017 are presented. The unique phase-angle dependence of polarization within the range of phase angles 19.2–134.9° with $P_{max} = 48\%$ at $\alpha_{max} = 110°$ is obtained. To calculate the scattering properties of surface of Phaethon we used the modified *T*-matrix method, so called *Sh*-matrix method, for the conjugated random Gaussian particles. The best fit of simulated polarization curve and observational data was obtained for the particles composition of amorphous carbon (80%) with sizes within the range $r_{carb} = 0.09$–1.33 μm and silicon dioxide SiO_2 (20%) with $r_{carb} = 0.31$–1.91 μm.

1. Introduction

The polarimetric study of the near-Earth asteroids (NEAs) allows us to cover the large range of phase angles, including the value and position of polarization maximum, and thereby supplement the inaccessible angles for the Main Belt asteroids. Despite the long history of polarimetric studies, only several NEAs were studied at large phase angles and the most complete phase dependences of polarization were determined, including polarization maximum. The unprecedented close passage of Phaethon to the Earth at distance of 0.069 au on December 16, 2017 provided a good opportunity to measure the polarization in the large range of phase angles.

2. Observations

Observations of asteroid (3200) Phaethon were carried out at the 6-m BTA telescope with the multimode focal reducer SCORPIO-2 of the Special Astrophysical Observatory (Russia) in the imaging polarimetry (filter V) and spectropolarimetric (λ4100−8000 Å) modes from November 27 to December 26, 2017 within the range of phase angles 19.2–134.9°. The aperture polarimetry was made at the Crimean Astrophysical Observatory with the 2.6-m telescope in the B, V, and wide-R filters and 1.25-m telescope in the V, R, and I filters on December 8−16, 2017 within the range of phase angles 19.6–61.6°.

3. Results

We found that the maximum of polarization for Phaethon is $P_{max} = 48\%$ at phase angle 110° in the V band. The inversion angle α_{inv} and polarimetric slope *h* are 20.5° and 0.46 ± 0.01 %/°, respectively. Phaethon has the highest maximum degree of polarization that was determined among the earlier observed bodies in the Solar System, including the recently observed NEA (152679) 1998 KU_2 with a high polarization degree up to 44% at phase angle 81° [1]. The degree of polarization of asteroid Phaethon is slightly higher in the blue filter B than that in the red filter R. A similar spectral dependence of polarization was observed for two others low-albedo asteroids (1580) Betulia [2] and (2100) Ra-Shalom [3].

4. Modeling and analysis

For simulation of the scattering properties of the surface particles of enigmatic asteroid Phaethon, we used the modified *T*-matrix method [4], called *Sh*-matrix method [5] to calculate the scattering properties of arbitrary shaped particles. The small perihelion distance of Phaethon (0.14 au) can affect the surface properties, and particles of Phaethon may be rather smooth. Therefore, the model of conjugated random Gaussian particles was used for modeling our data. The best fit to the observational data was

obtained for the particles composition of amorphous carbon (80%) with sizes within the range $r_{carb} = 0.09–1.33$ μm and silicon dioxide SiO_2 (20%) with $r_{carb} = 0.31–1.91$ μm, which have power law distribution. Note, that our observations of Phaethon do not include the negative polarization branch which should be also described by our simulation. Since Phaethon could be a fragment of asteroid (2) Pallas [6], we used polarimetric data for this asteroid which were obtained at the small phase angles [7].

5. Conclusions

Our polarimetric data showed that asteroid Phaethon has the highest degree of polarization ($P_{max} = 48\%$) in the maximum of positive polarization branch ($\alpha_{max} = 110°$) among all earlier observed bodies in the Solar System, including the recently observed NEA (152679) 1998 KU_2 with a high polarization degree up to 44% at phase angle 81° [1]. Probably this property of the asteroid is associated with its close approach to the Sun and corresponding processes on the surface due to heat.

Acknowledgements

We wish to thank K. Antoniuk, S. Belan, N. Pit', E. Zhuzhulina, and S. Kolesnikov for help in observations. The researches by VR are supported, in part, by the project 16BF023-02 of the Taras Shevchenko National University of Kyiv.

References

[1] Kuroda, D., Ishiguro, M., Watanabe, M., et al.: Significantly high polarization degree of the very low-albedo asteroid (152679) 1998 KU_2. Astron. Astrophys., Vol. 611, id.A31, 9 pp., 2018

[2] Tedesco, E.J., Drummond, J., Candy, M., Birch, P., Nikoloff, I., and Zellner, B.: 1580 Betulia: An unusual asteroid with an extraordinary lightcurve. Icarus, Vol. 35, pp. 344–359, 1978.

[3] Kiselev, N.N., Rosenbush, K., and Jockers, K.: Polarimetry of asteroid 2100 Ra-Shalom at large phase angle. Icarus, Vol. 140, pp. 464–466, 1999.

[4] Mishchenko, M.I., Travis, L.D., and Mackowski, D.W.: T-matrix computations of light scattering by nonspherical particles: a review. J. Quant. Spectrosc. Radiat. Transfer, Vol. 55, pp. 535–575, 1996.

[5] Petrov, D., Shkuratov, Yu., and Videen, G.: Light scattering by arbitrary shaped particles with rough surfaces: Sh-matrices approach. J. Quant. Spectrosc. Radiat. Transfer, Vol. 113, pp. 2406–2418, 2012.

[6] de León, J., Campins, H., Tsiganis, K., Morbidelli, A., and Licandro, J.: Origin of the near-Earth asteroid Phaethon and the Geminids meteor shower. Astron. Astrophys., Vol. 517, id.A23, 25 pp., 2010.

[7] Lupishko, D., Ed.: Asteroid Polarimetric Database V8.0. EAR-A-3-RDR-APD-POLARIMETRY-V8.0., NASA Planetary Data System, 2014.

EPSC Abstracts
Vol. 12, EPSC2018-591-1, 2018
European Planetary Science Congress 2018

Unique Multi-Tailed Active Asteroid 311P/(2013 P5) Panstarrs

David Jewitt (1,2), Harold Weaver (3) and Max Mutchler (4), Jing Li (1), Jessica Agarwal (5) and Stephen Larson (6)
(1) Department of Earth, Planetary and Space Sciences, UCLA, USA, (2) Department of Physics and Astronomy, UCLA, USA, (jewitt@ucla.edu), (3) Johns Hopkins University Applied Physics Laboratory, Laurel, USA, (4) Space Telescope Science Institute, Baltimore, USA, (5) Max Planck Institute for Solar System Research, Gottingen, Germany, (6) Lunar and Planetary Laboratory, Tucson, USA

Abstract

The unique inner-belt active asteroid 311P/(2013 P5) PANSTARRS is notable for its sporadic, comet-like ejection of dust in nine distinct epochs spread over ∼250 days in 2013. This curious behavior has been interpreted as the product of localized, equator-ward landsliding from the surface of an asteroid rotating at the brink of instability [1,2,3, but see also 4]. We obtained new Hubble Space Telescope observations to directly measure the nucleus and to search for evidence of its rapid rotation. We find a nucleus with mid-light absolute magnitude H_V = 19.14±0.02, corresponding to an equal-area circle with radius 190±30 m (assuming geometric albedo p_V = 0.29). However, instead of providing photometric evidence for rapid nucleus rotation, our data set a lower limit to the lightcurve period, $P \geq 5.4$ hour. The dominant feature of the lightcurve is a V-shaped minimum, ∼0.3 magnitudes deep, that is suggestive of an eclipsing binary. Under this interpretation, the time-series data are consistent with a secondary/primary mass ratio, $m_s/m_p \sim$ 1:6, a ratio of separation/primary radius, $r/r_p \sim 4$ and an orbit period ∼0.8 days. These properties lie within the range of other asteroid binaries that are thought to be formed by rotational breakup. While the lightcurve period is long, centripetal dust ejection is still possible if one or both components rotates rapidly ($\leq$ 2 hour) and has a small lightcurve variation because of azimuthal symmetry. Indeed, radar observations of asteroids in critical rotation reveal "muffin-shaped" morphologies which are closely azimuthally symmetric and which show minimal lightcurves. Our data are consistent with 311P being a close binary in which one or both components rotates near the centripetal limit. The mass loss in 2013 suggests that breakup occurred recently and could even be on-going. A search for fragments that might have been recently ejected beyond the Hill sphere reveals none larger than effective radius $r_e \sim$ 10 m. These results are described in detail in the literature [5].

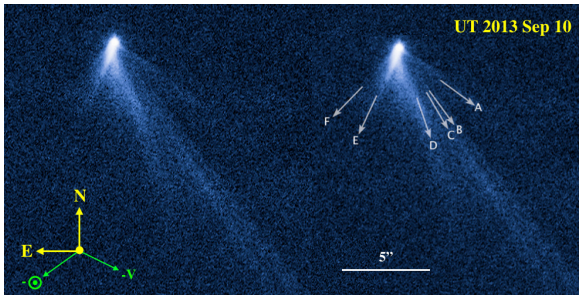

Figure 1: 311P imaged in an active state on UT 2013 September 10 (Jewitt et al. 2013). Letters mark individual dust tails. Three additional tails (G - I) were ejected after this image was taken (Jewitt et al. 2015b). The cardinal directions are indicated by yellow arrows while the projected antisolar vector (-⊙) and the negative heliocentric velocity vector (-V) are shown in green..

References

[1] Jewitt, D., Agarwal, J., Weaver, H., Mutchler, M., & Larson, S. 2013, Ap. J., 778, L21

[2] Jewitt, D., Agarwal, J., Weaver, H., Mutchler, M., & Larson, S. 2015b, Ap. J., 798, 109

[3] Hirabayashi, M., Sánchez, D. P., & Scheeres, D. J. 2015, Ap. J., 808, 63

[4] Hainaut, O. R., Boehnhardt, H., Snodgrass, C., et al. 2014, Astron. Ap., 563, A75

[5] Jewitt, D., Weaver, H., Mutchler, M., et al. 2018, A. J., 155, 231

EPSC Abstracts
Vol. 12, EPSC2018-611, 2018
European Planetary Science Congress 2018

Multi-phase melt percolation during core formation

Marc A. Hesse (1,2)
(1) Institute of Computational Engineering and Science, University of Texas at Austin, U.S.A.
(2) Department of Geological Sciences, University of Texas at Austin, U.S.A.
(mhesse@jsg.utexas.edu)

Abstract

The segregation of dense core-forming melts by porous flow is a natural mechanism for core formation in early planetesimals. It has long been thought that texturally equilibrated metallic melts reside in isolated pores that prevent percolation. It has recently been shown that hysteresis in the network connectivity allows melts that overcome the percolation threshold to drain almost entirely [1]. However, the drainage of metallic melts may occur in the presence of a silicate melt, in particular in S-poor planetesimals where higher temperatures are required to overcome the percolation threshold of metallic melts. Percolative core formation therefore likely involves the flow of two melts in a compacting medium. The dynamics of this complex process are currently poorly understood, both on the pore-scale and on the Darcy-scale.

1. Introduction

Experimental observations show that texturally equilibrated metallic melt does not wet the silicate grain boundaries and tends to reside in isolated pockets that prevent percolation [2]. This leads to a percolation threshold, a minimum melt fraction required to connect the pores and induce porous flow. Although typical planetesimals likely contain enough metal to overcome this threshold, it has been thought that melt segregation is prevented by a pinch-off at melt fractions slightly below the percolation threshold. Recently, it has been shown that texturally equilibrated melt networks experience significant hysteresis and remain connected down to melt fractions of only 1-2% [1]. This hysteresis in melt connectivity allows percolative core formation in planetesimals that contain enough metal to exceed the percolation threshold. Some primitive achondrite meteorites preserve metal distributions that are reminiscent of a connected network of metallic melt, suggesting that hysteretic melt segregation is a viable mechanism for core formation.

2. Two-phase melt percolation

If the partial melting of metallic melts and the silicate melts overlap, melt segregation requires multi-phase percolation and additional physical processes have to be considered. The overlap in the partial melting regimes depends strongly on the overall composition. In an ordinary chondrite assemblage, progressive internal heating initially leads to the formation of a metal-sulphide melt at the Fe,Ni-FeS eutectic at 988°C and later to the formation of a silicate melt at approximately 1050°C-1150°C, depending on composition and pressure [3]. In S-rich compositions up to 40% of the metallic melt may form at the eutectic temperature, before the onset of silicate melting. In S-poor bulk compositions more overlap in melting regions is expected.

2.1. Silicate melt as wetting phase

In the simplest case, the silicate melt is the wetting phase and the metallic melt is the non-wetting phase. In this limit, the silicate melt entirely coats the silicate grain boundaries and hence determines the shape and connectivity of the melt network. In this case, the metallic melt forms ganglions in the center of the pore space, as shown in Figure 1.

The dynamics of two-phase percolation introduce a

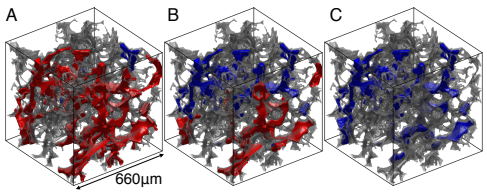

Figure 1: Trapping of non-wetting (metallic) melt during drainage, from left to right. Connected and mobile metallic melt is shown in red, while isolated trapped metallic melt is shown in blue. [4].

new phenomenon, called *capillary trapping*, currently not considered in literature on percolative core formation. This process is shown in Figure 1 and leads to the immobilization of up to 40% of the metallic melt. Capillary trapping might therefore prevent efficient percolative core formation in the presence of silicate melt.

However, the simulation shown in Figure 1 does not consider the simultaneous compaction of the pore space as melt segregation occurs. It is possible that metallic melt remains connected during compaction, because its connectivity is typically a function of the fraction of the pore space it occupies rather than its absolute volume fraction. Hence, if compaction reduces porosity as the metallic melt drains, its saturation and hence connectivity may remain the same and allow percolation. This has potentially been observed in centrifuged experiments of metal migration [5].

2.2. Mixed-wet three-phase systems

The wetting properties of the silicate and metallic melts are highly dependent on their composition. Experiments show that silicate melts do not wet the grain boundaries entirely [6]. In this case, the shape of the pore network itself becomes dependent on the volume fractions of the two melt phases (Figure 2).

Past work on such mixed-wet three-phase systems has assumed that connectivity of phases can be determined from the classical two-phase connectivity criterion [6]. The connectivity of the two-phase system depends only on the volume fraction of the melt and the dihedral angle [7]. In contrast, the three phase system has at least two additional parameters, the volume fraction and wetting angle of the second melt. This increased parameter space allows for many melt configurations, and their connectivity has not yet been explored. Such systems are also likely to exhibit significant hysteresis, similar to the two-phase system.

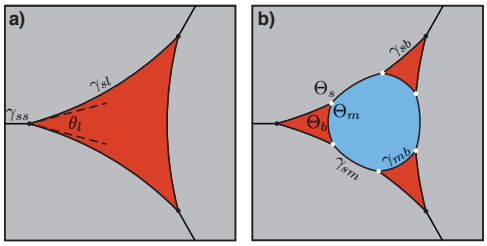

Figure 2: **a**) Two-phase textural equilibrium in 2D. **b**) Potential three-phase mixed-wet equilibrium configuration.

3 Conclusion

Despite recent improvements in our understanding of melt percolation, the effect of silicate melt on the mobility of core forming melts is unclear. The presence of a second melt phase introduces new capillary phenomena that determine melt mobility and hence the possibility of percolative core formation. Therefore, we are working to extend current two-phase pore-scale simulations for equilibrium melt distributions to mixed-wet three-phase systems.

References

[1] S. Ghanbarzadeh, M. A. Hesse, and M. Prodanović. Percolative core formation in planetesimals enabled by hysteresis in metal connectivity. *Proceedings of the National Academy of Sciences*, 114(51):13406–13411, 12 2017.

[2] W.G. Minarik, F.J. Ryerson, and E.B. Watson. Textural Entrapment of Core-Forming Melts. *Science*, 272(5261):530–533, 1996.

[3] E.R. Mare, A.G. Tomkins, and B.M. Godel. Restriction of parent body heating by metal-troilite melting: Thermal models for the ordinary chondrites. *Meteoritics and Planetary Science*, 49(4):636–651, 2014.

[4] S. Ghanbarzadeh, M.A. Hesse, M. Prodanović, and J.E. Gardner. Deformation-assisted fluid percolation in rock salt. *Science*, 350(6264):1069–1072, 2015.

[5] N. Bagdassarov, G. Solferino, G.J. Golabek, and M.W. Schmidt. Centrifuge assisted percolation of Fe-S melts in partially molten peridotite: Time constraints for planetary core formation. *Earth and Planetary Science Letters*, 288(1-2):84–95, 2009.

[6] A. Holzheid. Sulphide melt distribution in partially molten silicate aggregates: implications to core formation scenarios in terrestrial planets. *European Journal of Mineralogy*, 25(November 2012):267–277, 2013.

[7] N. von Bargen and H.S. Waff. Permeabilities, interfacial areas and curvatures of partially molten systems: Results of numerical computations of equilibrium microstructures. *Journal of Geophysical Research*, 91(B9):9261–9276, 1986.

EPSC Abstracts
Vol. 12, EPSC2018-620, 2018
European Planetary Science Congress 2018

European component of the AIDA mission: science investigation of a binary system

Patrick Michel (1), Michael Küppers (2), Jens Biele (3), Adriano Campo Bagatin (4), Benoît Carry (1), Sébastien Charnoz (5), Alan Fitzsimmons (6), Simon Green (7), Alain Herique (8), Martin Jutzi (9), Ozgur Karatekin (10), Julia de Leon (11), Naomi Murdoch (12), Petr Pravec (13), Holger Sierks (14), Paolo Tortora (15) , Kleomenis Tsiganis (16), Jean-Baptiste Vincent (17), Kai Wünnemann (18), Ian Carnelli (19)
(1) Laboratoire Lagrange, Université Côte d'Azur, Observatoire de la Côte d'Azur, CNRS, France, (2) ESA-ESAC, Madrid, Spain, (3) DLR, Germany, (4) Universidad de Alicante, Spain, (5) Institut de Physique du Globe de Paris / Université Paris Diderot, France, (6) Queen's University Belfast, Northern Ireland, (7) The Open University, UK, (8) Institut de Planétologie et d'Astrophysique de Grenoble, Université Grenoble Alpes, France, (9) Physics Institute, University of Bern, Switzerland, (10) Royal Observatory of Belgium, Belgium, (11) Instituto de Astrofísica de Canarias, Centro de Astrofísica en La Palma, Spain, (12) ISAE-SUPAERO, France, (13) Ondrejov Observatory, Czech Republic, (14) Max-Planck Institute for Solar System Research, Germany, (15) Università di Bologna, Italy, (16) Aristotle University of Thessaloniki, Greece, (17) DLR Institute of Planetary Research, Germany, (18) Museum für Naturkunde & Freie Universität Berlin, Germany, (19) ESA HQ, Paris, France, (michelp@oca.eu)

Abstract

The European component of the Asteroid Impact & Deflection Assessment (AIDA) mission has been redesigned and is called Hera hereafter. Hera is a small mission of opportunity built on the previous AIM concept, whose objectives are to investigate a binary asteroid, the outcome of a kinetic impactor test, and thus to provide extremely valuable information for asteroid impact threat mitigation and science purposes [1]. The second component of AIDA is NASA's DART mission [2]. The target is the binary near-Earth asteroid (NEA) (65803) Didymos. In particular, its secondary is the target of the DART mission. With its 163 m-diameter, it allows for the first time to gather detailed science data not only from a binary asteroid but also from the smallest asteroid ever visited.

1. Introduction

The science return of Hera is similar to that of AIM [1] except for the direct measurement of the internal structure from a low-frequency radar instrument placed on the surface of the asteroid, which is not included in the current Hera baseline [3].

2. Science return

Although the requirements for Hera are focused on planetary defense, the bonus science return from this mission will be outstanding as it will include:

- First detailed images of a binary asteroid in orbit, offering informed constraints to models describing binary formation and dynamics, and verifying/constraining predictions from the radar shape model.
- First images and in-situ compositional analyses of the smallest asteroid ever visited, enabling the determination of the geophysical and compositional properties of such a small body compared to larger ones.
- Understanding of physical/compositional properties and geophysical processes in low gravity, with implications for our understanding of small-body surface properties and their evolution.
- First documentation of an asteroid-scale impact outcome (from DART), orders of magnitude beyond laboratory scales.

The last item will provide crucial data to validate numerical simulations of hyper-velocity impacts that are used in planetary science (planet and satellite formation, impact cratering and surface ages, asteroid belt evolution). It will offer new constraints for collisional evolution models of small-body populations and planetary formation.

About 15% of NEAs larger than 200 m in diameter are binaries, and many of these may be similar to Didymos. Therefore, some systematic process is expected to be at the origin of the creation of such

systems. According to current knowledge, the YORP spin-up of a rubble pile is the most likely process. The characterization of Didymos by Hera will provide information not only about an individual asteroid but also about a sizable fraction of near-Earth and potentially hazardous asteroids.

Hera will perform the geophysical characterization of the target. A big step will be achieved in our knowledge in such a low-gravity environment, in terms of shape, mass (and density), surface features, presence and kind of surface regolith, crater abundance and size distribution, boulder size distribution down to the resolution limit of the camera, as well as local slopes.

In addition to surface properties, indirect information on the internal structure will be obtained. Surface images allow for the evaluation of surface structures, such as lineaments, crater shapes, crater ejecta, boulder existence/distribution, and mass wasting features. From these features, information on material strength, cohesion, porosity, etc., can be derived both for the asteroid regolith and interior. For instance, if the largest boulders found at the surface are comparable in size to the asteroid itself, this can indicate that they were produced during a catastrophic disruption or reaccumulation event (like in some binary formation scenarios), and the asteroid is more likely to have a rubble-pile structure. The Radio Science Experiment will also contribute to internal structure estimates.

3. Conclusion and main message

Hera provides a robust and cost-effective means to perform a planetary defense validation test with a solid balance between risk and innovation. In the frame of the AIDA collaboration, Hera contributes to a truly international planetary defense initiative. It will bring completely new knowledge and insights on asteroid science that will be of great benefit not only to the planetary defense community as a whole but also to those seeking a deeper understanding of the processes underlying solar system formation. Hera builds upon a unique knowledge base gained in Europe with the Rosetta mission on close-proximity operations and offers a great opportunity to develop them further by increasing on-board autonomy and testing new technologies developed for future in-orbit servicing missions.

We note that: (1) NASA's New Frontier OSIRIS-REx sample return mission is on its way to the asteroid Bennu. Two other asteroid missions, namely Psyche to the metallic asteroid of the same name and Lucy to Trojan asteroids, have been selected in its Discovery program. Finally the CAESAR sample return mission to the comet 67P/Churyumov-Gerasimenkos pre-selected in the New Frontier program for a one year study with final selection at the end of 2018, for a possible launch in the mid-2020s; (2) JAXA's Hayabusa-2 sample return mission is currently visiting the asteroid Ryugu, and two other Japanese small body missions are under study, namely the sample return mission MMX to the martian moon Phobos and OKEANOS to Trojan asteroids; (3) CNSA is planning several sample return missions, including to the Moon and to Near Earth Asteroids.

Given the demonstrated international interest in small body science and all the studies and efforts made in Europe since the early 2000s, starting with the Don Quijote study (asteroid deflection test), the MarcoPolo and MarcoPolo-R studies (asteroid sample return) and the AIM study, this is the right time for the next European small body mission. Hera is a great opportunity to demonstrate that Europe keeps being on the front of small body research and maintains the visibility and expertise gained with Rosetta. A mission like Hera will certainly fire the imagination of young people and adults, as the science is accessible and understandable and is associated with fascinating challenges and goals.

Acknowledgements

P.M. acknowledges the support from ESA.

References

[1] Michel, P., et al.: Science case for the Asteroid Impact Mission (AIM): a component of the Asteroid Impact & Deflection Assessment (AIDA) Mission, Advances in Space Research, Vol. 57, pp. 2529-2547, 2016.

[2] Cheng, A. et al.: AIDA DART Asteroid Deflection Test: Planetary Defense and Science Objectives. Planetary and Space Science, accepted, 2018.

[3] Michel, P. et al.: European component of the AIDA mission to a binary asteroid: characterization and interpretation of the impact of the DART mission, Advances in Space Research, in press, 2018.

EPSC Abstracts
Vol. 12, EPSC2018-626, 2018
European Planetary Science Congress 2018

Investigation of Mobility-related Surface Features on Asteroids and their Relation to Volatiles

R. Parekh (1), K. Otto (2), Ralf Jaumann (2)
(1) Geoscience Division, Physical Research Laboratory, Ahmedabad, India (rutu@prl.res.in) (2) Institute of Planetary Research, German Aerospace Center (DLR), 12489 Berlin, Germany

Abstract

The identification of regolith material and mass movement processes on icy planetary bodies has grabbed the attention of scientist in the past decades. The well preserved signatures of these materials have been well studied on Moon and Mars. In fact, studies show strong synergy between these physical processes and chemical properties of the planetary objects. With the aim to get better understanding of asteroid surface we plan to analyse mobility related features and establish an inventory.

1. Introduction

Recent space missions provided the opportunity to study the complex surface signatures of asteroids and comets. Observations include regolith covered terrains [1] that show uneven distribution of ejecta and large number of degraded craters [1],[11],[12]. Through these signatures, it is possible to reconstruct the interior and surface geological processes that asteroids might have undergone in the past. Our view will soon be complemented by the Hayabusa2 and Osiris-Rex Missions arriving at their target asteroids this year.

2. Evidences of regolith motion on asteroids

Regolith is defined as the layer or pile of debris which consists of loose material and forms the upper surface of a planetary object [10]. Depending upon the material properties the debris consist of small particles or large boulders [8] that are held together by gravity, cohesive forces or bonding between the particles. Regolith covered surfaces are characteristic for asteroids and have been observed on Eors [2], Vesta [4], Luteia [5] and Itokawa [9].

Depending upon the particle size, gravitational pull and material properties, there are differences in the geomphological properties of regolith. For example, the regolith of Eros is 20-40 m thick and may have been produced and redistributed by seismic activity. In agreement, Eros shows an abundance in impact craters [6]. The debris of regolith is usually confined in sloppy terrain with preserved signature of aprons on Eros (Fig. 1A) [6]. Whereas the regolith surface of Ikotawa is smooth and rough [9], with relatively few craters (<100). Itokawa's rough terrain consists of large boulders (up to 40 m in size) (Fig. 1C). In case of Vesta, extensive evidences of regolith studies have been conducted [4]. Debris avalanches show lobate tong like features (Fig. 1B) with dark and bright material at the rims or walls of craters, scarps at the top of the dislocated material [3,14] and the presence of large boulders (up to 200 m) [3,14] with confined boundaries. This is interpreted as a gravity driven mass wasting process or impact induced melt phenomena [3,14]. The regolith surface of Lutetia shows a diverse range of an active regolith layer [1] (Fig. 1B). The thickness of the regolith layer is ~ 600 m [13] with an uneven distribution of slopes of 30º or less [2,10].

Other than dynamical surface processes, regolith studies also help to understand the processes that may include volatiles. However, the presence of volatiles on asteroid surfaces is debated and volatiles may have been delivered through meteorite impacts [2], as it has been suggested for the asteroid Vesta. The abundance of volatile elements tells us about the local geochemistry and enriches our knowledge about the evolutionary processes of asteroids.

3. Future Study

Currently, high resolution data from various missions provide valuable information on the morphologies and composition related to sublimation and out-gassing of volatiles on asteroid surfaces. The active processes and distribution of ices on asteroids and comets are of particular interest to understand the distribution of water and other volatiles in our Solar System. Volatiles are often trapped along with minerals.

Here we present an inventory of regolith features on asteroids related to dynamic processes such as landslides, debris aprons and particle sorting. Based on the image data provided by space missions, we aim to characterize and classify these features and correlate them with the properties of the host body, such as the gravity, internal structure, and volatile content. The effect of volatiles on the dynamic features will be constrained by comparison with cometary surface features.

References

[1]Cheng et al., 1997, JGR:Planets, 102(E10):23695–708.

[2] Hearn et al., 2011,Science, 334(6055):487–490.

[3] Jaumann et al., 2012, Science, 336(6082):687–90.

[4] Otto et al. 2013, JGR, 118:1–16.

[5] Miyamoto et al., 2007, Science, 316(5827):1011–14.

[6] Murdoch et al., 2015, Asteroid Surface Geophysics, ch039.

[8] Richardson et al., Asteroids III, 501–15.

[9] Saito et al., 2006, Science, 312(5778):1341–44.

[10]Thomas et al. 2002, Icarus, 155(1):18–37.

[11]Veverka et al., 2000, Science 289(5487):2088–97.

[12]Veverka et al., 2001, Nature 413(6854):390–93.

[13]Vincent et al., 2012, PSS, 66(1):79–86.

[14]Williams et al., 2014, PSS, 103:24–35..

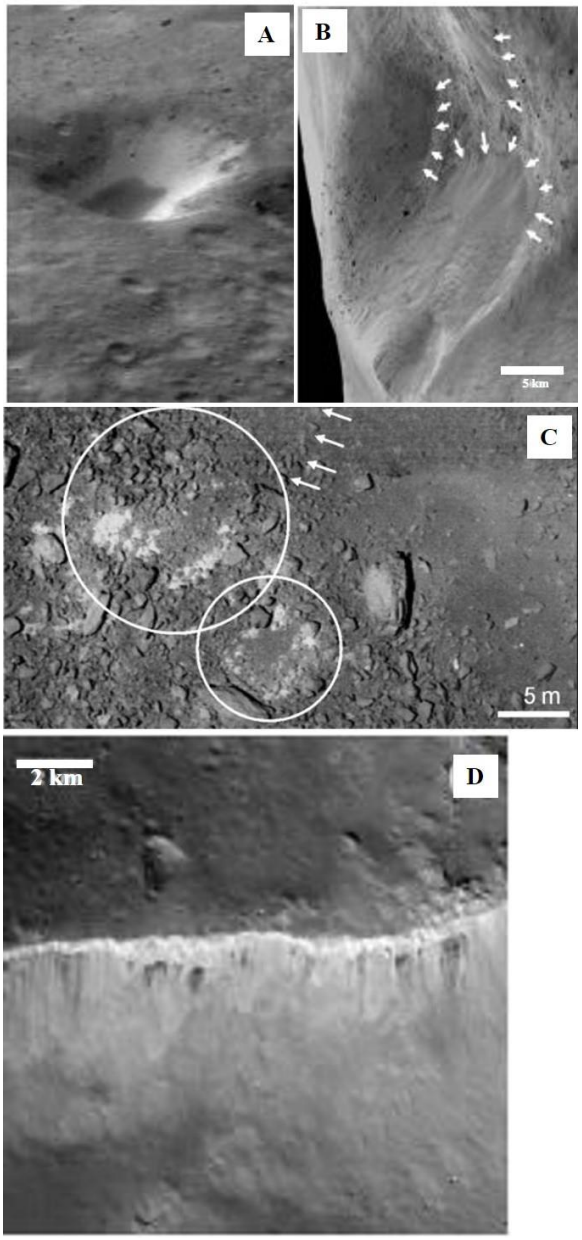

Figure 1 Evidences of regolith movements on various asteroids (A) Eors, pond like feature shows displaced material [6] (B) Lutetia, the arrows shows landslide material [6] (C) Itokawa, arrow indicates debris material piled up, circle indicates circular feature like crater [5] (D) Vesta, fresh bright material at crater rim [6]. Image credit: (A)http://ser.sese.asu.edu/near.html (B) ID 216820, ESA 2010 MPS for OSIRIS Team MPS/UPD/LAM/IAA/RSSD/INTA/UPM/DASP/IDA. (C) Miyamoto et al., 2007(D)NASA/JPLCaltech/UCLA/MPS/ DLR/IDA/LPI/ASU.

EPSC Abstracts
Vol. 12, EPSC2018-662, 2018
European Planetary Science Congress 2018

The interior of Enceladus one year after Cassini

Gaël Choblet (1), Gabriel Tobie (1), Ondřej Čadek (2), Christophe Sotin (3), Mathieu Bouffard (4), Frank Postberg (5), Mathilde Kervazo (1,3), Marie Běhounková (2) and Ondřej Souček (6)
(1) Laboratoire de Planétologie et Géodynamique, UMR-CNRS 6112, Université de Nantes, France,
(2) Charles University, Department of Geophysics, Prague, Czech Republic,
(3) Jet Propulsion Laboratory, Caltech, Pasadena, USA,
(4) Max Planck Institute for Solar System Research, Göttingen, Germany,
(5) Institut für Geowissenschaften, Universität Heidelberg, Germany,
(6) Charles University, Mathematical Institute, Prague, Czech Republic.
(gael.choblet@univ-nantes.fr)

1. Introduction

While the observation of a large-scale plume emitted by Enceladus occurred early after the insertion of the Cassini spacecraft around Saturn, a coherent view on the interior processes that power and feed this activity started emerging only in the latest year of the mission. Thanks to a flexible payload as well as multiple flybys during the extended mission, analyses of Enceladus data (composition of materials originating from the moon's interior [7, 8], geophysical measurements and long series of surface images [5, 9, 1]) composed a view where a global salty ocean is present underneath an ice crust of very uneven thickness (20-25 km in average, less than 5 km beneath the south pole, more than 30 km in some equatorial regions). Density of the rock core implies a significant ($\sim$ 20-30 %), water-filled, porosity. Furthermore, several independent chemical clues indicate that high-temperature (>363 K) hydrothermal processes probably occur at present, deep in the moon [4, 12].

2. The vibrating hot sandy core [2]

These observations require a huge heat power and a mechanism to focus the release of heat in the South Polar Terrain (SPT), most probably related to tidal dissipation yet unexplained by previous models. Assuming the ice shell thickness is known locally, a conductive thermal equilibrium provides a rough estimate of the heat emanating from Enceladus' interior: while, in the SPT, tidal heating within the ice crust could match the local heat budget (3-5 GW) owing to an extremely thin shell and to the presence of faults [10], the considerable amount of heat extracted elsewhere (i.e. at moderate and northern latitudes) exceeds 20 GW, a figure that requires a deeper origin since a thicker ice shell is less dissipative.

Mechanical tests on water saturated unconsolidated rock materials subjected to cyclic deformation point to the likelihood that, at tidal frequency, a significant amount of energy can be dissipated in a rock core filled with interstitial liquid water. We show in 3D spherical simulations that thermal convection of interstitial water within such a tidally heated core leads to strongly focused hot upwellings, especially beneath the poles (Fig. 1). While the permeability of Enceladus' core is unknown and could vary within a range involving orders of magnitude, modeled temperatures obtained for a relatively limited interval within the admissible parameter space (typically 10^{-14}-10^{-13} m^2) agree with the estimate inferred from compositional measurements by Cassini that indicate water-rock interaction. Powerful hotspots (several GW) are thus predicted at the seafloor with maxima located beneath the poles and along the leading and trailing meridians.

3. Polar ocean Plumes

Ocean dynamics could partly filter this strongly heterogeneous heat flux at the seafloor, mostly if rotational effects overcome thermal convection. We have recently conducted 3D simulations dedicated to the buried ocean of Enceladus with a heterogeneous heat flux prescribed at the inner boundary (not shown in [2]): while the precise balance between the Coriolis and the buoyancy forces is not known, our first results demonstrate that although in some cases, the heat flux pattern at the seafloor can be significantly blurred at moderate latitudes bounded by the the tangent cylinder, it remains globally unaffected in polar regions where ocean plumes supply a significant amount of heat in regions coinciding with the lowest ice thickness (Fig. 1). Scaling relationships also indicate that

the transport time of organic products by ocean thermal vents would match the constraints derived from Cassini measurements (typically a few months).

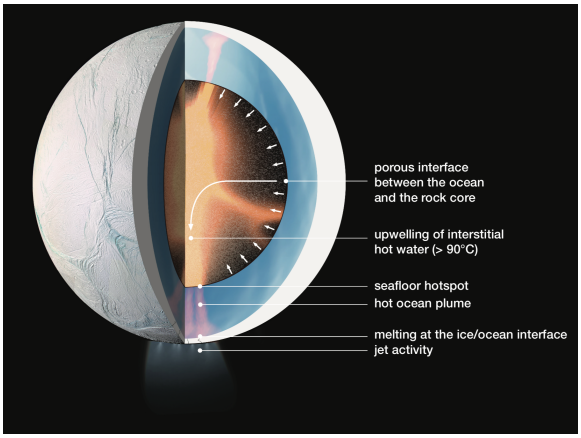

Figure 1: A general scheme describing our "vibrating hot sandy core" model for the interior of Enceladus and its relationship to the main properties inferred from Cassini observations: intense jet activity, uneven ice shell, buried global ocean and hydrothermal activity. *Credit: ESA-LPG*

4. The very uneven ice shell

We also refined our model for the ice shell thickness based on the shape data recently published by Tajeddine et al. (2017) [11] still considering the long-wavelength gravity model of Iess et al. (2014) [5] (again not described in [2]), globally confirming our earlier results [1]. Based on this new inversion, this presentation will briefly address the mechanical and thermal stability of the ice shell. We consider in particular how lateral heat flux variations delivered by the ocean at the base of the ice shell leads to melting/thinning and show that density anomalies caused by thermal convection in the porous core might affect the interpretation of the compensation mechanism.

5. Summary and conclusions

While the vibrating hot sandy core model for Enceladus (Fig. 1) accounts for the main features inferred from Cassini observations, a key question remains (especially with regard to habitability): since how long can such an intense activity have occurred ? The answer mostly relies on the dissipation mechanism within Saturn that controls the eccentricity of Enceladus and thus, ultimately, the power generated by tides in its core. Based on the latest estimates from astrometric data [6], we predict that hydrothermal activity can persist for several tens of millions of years. Assuming tidal evolution results from resonance locking as suggested by Fuller et al. [3], it could have lasted for billions of years.

References

[1] Čadek, O., et al.: Geophys. Res. Lett., 43, pp. 5653-5660, 2016.

[2] Choblet, G., et al.: Nat. Astro., 1, pp. 841-847, 2017.

[3] Fuller, J., et al.: Mon. Not. R. Astr. Soc. 458, pp. 3967-3879, 2016.

[4] Hsu, H.W., et al.: Nature, 519, pp. 207-210, 2015.

[5] Iess, L., et al.: Science, 344, pp. 78-80, 2014.

[6] Lainey, V., et al.: Icarus, 281, pp. 286-296, 2017.

[7] Postberg, F., et al.: Nature, 459, pp. 1098-1101, 2009.

[8] Postberg, F., et al.: Nature, 474, pp. 620-622, 2011.

[9] Thomas, P.C., et al.: Icarus, 264, pp. 37-47, 2016.

[10] Souček, O., et al.: Geophys. Res. Lett., 43, pp. 7417-7423, 2016.

[11] Tajeddine, R., et al.: Icarus, 295, pp. 46-60, 2017.

[12] Waite, J.H., et al.: Science, 356, pp. 155-159, 2017.

EPSC Abstracts
Vol. 12, EPSC2018-670-1, 2018
European Planetary Science Congress 2018

Dreams came true – the first results from inversion of Gaia DR2 asteroid photometry

Josef Ďurech and Josef Hanuš
Astronomical Institute, Faculty of Mathematics and Physics, Charles University, Prague, Czech Republic
(durech@sirrah.troja.mff.cuni.cz)

Abstract

The Gaia Data Release 2 from April 2018 contains observations of about 14,000 asteroids. These photometric data with a typical accuracy of $\sim 1\%$ can be used for reconstruction of the rotation state (the rotation period and the direction of spin axis) and shape of asteroids. We applied a triaxial ellipsoid model and a convex shape model [6] to fit Gaia photometry and to derive models of individual asteroids. We were successful in 338 cases, out of which 270 were new models.

1. Introduction

Sparse-in-time photometry of asteroids can be successfully used for the reconstruction of asteroid shapes and spin states [4, 2]. So far, the main problem has been the low quality of sparse photometry from ground-based sky surveys. For this reason, a reliable solution of the inverse problem based on sparse data was possible only when hundreds of data points were available and when the lightcurve amplitude was high enough not to be lost in noise. The situation has changed dramatically with the Gaia DR2 that contains also asteroid photometry [3]. Although the number of data points in DR2 for a given asteroid is a few tens at most, thanks to very good photometric accuracy of $\sim 1\%$ or even better, the unique solution of the inverse problem is possible for hundreds of asteroids.

2. Inversion of Gaia photometry

We tested the potential of Gaia data to reconstruct spin states and shapes of asteroids. We used essentially the same approach as with our analysis of sparse data from astrometric ground-based surveys [4, 5, 2]. Using a gradient-based optimization, we searched for the best-fitting shape/spin model. For each asteroid with more than 10 independent observations in DR2 (~ 5400), we scanned the period interval 2–1000 hours and for each trial period we looked for the best pole direction and the corresponding shape. Then we selected the globally best solution and tested its reliability with the approach described in [2]. We derived 328 unique models out of which 270 were new models. We compared the remaining 68 models with those derived from independent data and stored in the Database of Asteroid Models from Inversion Techniques (DAMIT, [1]). This comparison showed us that with our approach, the rate of false positive solutions is only few percent and that Gaia data alone can be used for reliable spin and shape reconstruction.

Not surprisingly, the success of the inversion process critically depends on the number of data points N. For $N \simeq 10-15$, unique solutions are rare, for $N \simeq 20$ they are common, and for $N \gtrsim 30$ they are frequent. This obvious dependence on the number of data points is demonstrated in Fig. 1, where we show the comparison between the best-fitting period computed from Gaia data (without any check of the reliability of the spin/shape solution) and the period taken from the Lightcurve Database (LCDB, [7]). The solutions based on a convex shape model sometimes produce false half periods, while the solutions based on ellipsoids do not have this problem. On the other hand, ellipsoidal models often produce wrong period solutions when $N \lesssim 20$.

3. Summary

It is possible to reconstruct correct spin states and coarse shapes of asteroids from Gaia photometry even if the number of observations $N < 20$, but the success rate is high only when $N \gtrsim 30$. The number of such high-cadence asteroids in DR2 is very small (~ 160), but this should change with next data releases and we can expect an order-of-magnitude increase of the number of reconstructed asteroid models. Another promising possibility is the combination of 'subcritical' Gaia data with other low-quality photometry or dense lightcurves form archives. With proper weight-

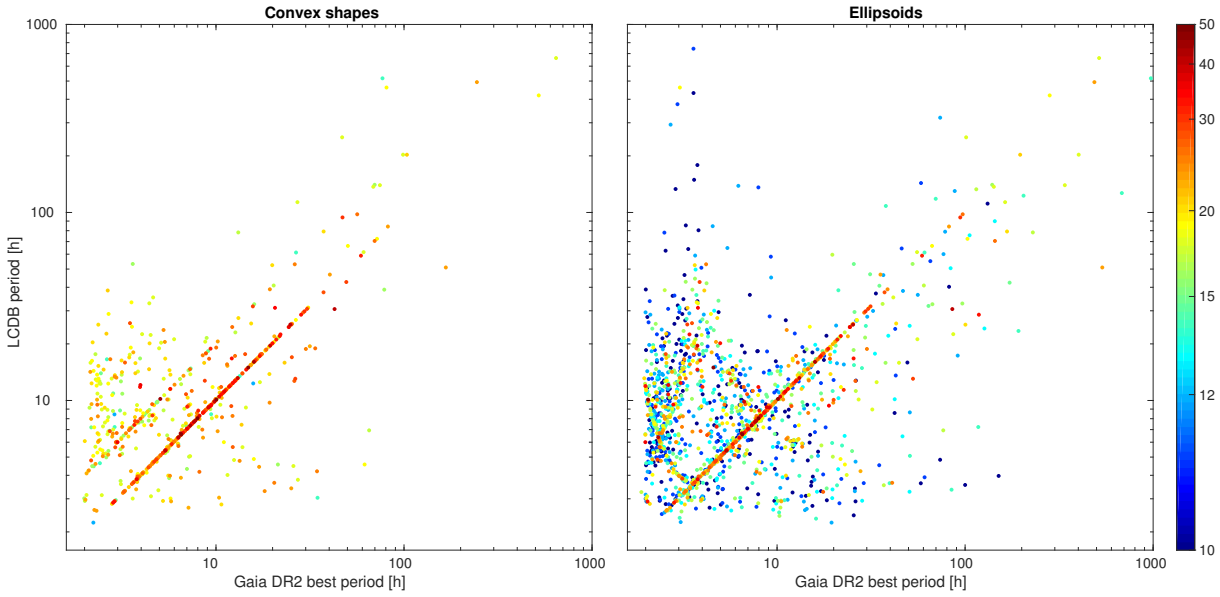

Figure 1: The comparison between the best period derived from Gaia photometry with convex models (left) and ellipsoids (right) with the period in the LCDB. The color corresponds to the number of data points.

ing of Gaia data, this should lead to other thousands asteroid models.

Acknowledgements

This work was supported by the grant 18-04514J of the Czech Science Foundation.

References

[1] Ďurech, J., Sidorin, V., and Kaasalainen, M. DAMIT: a database of asteroid models. *A&A* 513, A46, 2010.

[2] Ďurech, J., Hanuš, J., Oszkiewicz, D., and Vančo, R. Asteroid models from the Lowell photometric database. *A&A* 587, A48, 2016.

[3] Gaia Collaboration, F. Spoto, P. Tanga, F. Mignard, et al. Gaia Data Release 2: Observations of solar system objects. *ArXiv e-prints*, 2018.

[4] Hanuš, J., Ďurech, J., Brož, M., et al. A study of asteroid pole-latitude distribution based on an extended set of shape models derived by the lightcurve inversion method. *A&A* 530, A134, 2011.

[5] Hanuš, J., Ďurech, J., Oszkiewicz, D., et al. New and updated convex shape models of asteroids based on optical data from a large collaboration network. *A&A* 586, A108, 2016.

[6] Kaasalainen, M., Torppa, J., and Muinonen, K. Optimization methods for asteroid lightcurve inversion. II. The complete inverse problem. *Icarus* 153, 37–51, 2001.

[7] Warner, B. D., Harris, A. W., and Pravec, P. The asteroid lightcurve database. *Icarus* 202, 134–146, 2009.

EPSC Abstracts
Vol. 12, EPSC2018-671, 2018
European Planetary Science Congress 2018

Binary main-belt comet 288P

J. Agarwal[1], D. Jewitt[2,3], M. Mutchler[4], H. Weaver[5], S. Larson[6]
(1) Max-Planck-Institut für Sonnensystemforschung, Göttingen, Germany (agarwal@mps.mpg.de), (2) Department of Earth, Planetary and Space Sciences, University of California at Los Angeles, USA (3) Department of Physics and Astronomy, University of California at Los Angeles, USA, (4) Space Telescope Science Institute, Baltimore, USA, (5) The Johns Hopkins University Applied Physics Laboratory, Laurel, USA, (6) Lunar and Planetary Laboratory, University of Arizona, USA.

Abstract

The binary asteroid 288P (300163) [1, 2, 3, 4] is unique among the known binary asteroids due to its combination of a large semi-major axis ($\sim$100$\times$ the radius of one of the components), near-equal component size, and sublimation-driven, comet-like activity [5]. We report on new Hubble Space Telescope observations obtained between August 2017 and May 2018 that show 288P inactive. We use a refined method to measure the component separations in both the new data set and the Hubble observations from 2016/17 [5], and derive the orbit solution from the combined data set. We also study the dust environment during the 2016/17 perihelion passage, exploiting the knowledge on the inactive components obtained from the 2017/18 data to separate the light contribution from dust and the parent bodies.

References

[1] Hsieh, H. H. et al. (2012): Discovery of Main-belt Comet P/2006 VW_{139} by Pan-STARRS1, ApJL 748, L15.

[2] Licandro, J. et al. (2012): Exploring the nature of new main-belt comets with the 10.4 m GTC telescope: (300163) 2006 VW139, A&A 550, A17.

[3] Novaković, B. et al. (2012): P/2006 VW_{139}: a main-belt comet born in an asteroid collision?, MNRAS 424, 1432-1441.

[4] Agarwal, J. et al. (2016): Hubble and Keck Telescope Observations of Active Asteroid 288P/300163 (2006 VW139), AJ 151, 12.

[5] Agarwal, J. et al. (2017): A binary main-belt comet, Nature, 549, 357-359.

EPSC Abstracts
Vol. 12, EPSC2018-741, 2018
European Planetary Science Congress 2018

Extended photometric survey of Near-Earth Objects

S. Ieva (1), E. Dotto (1), E. Mazzotta Epifani (1), D. Perna (1,2), A. Rossi (3), A. Di Paola (1), A. Giunta (1), M. Micheli (1,4), E. Perozzi (5), R. Speziali (1), M. Lazzarin (6), I. Bertini (6), P. Ochner (6), V. Petropoulou (6), D. Lazzaro (7), P. Arcoverde (7), H. Medeiros (7), F. Monteiro (7)
(1) INAF – Osservatorio Astronomico di Roma, Via Frascati 33, 00078 Monte Porzio Catone (Roma), Italy
(2) LESIA, Observatoire de Paris, PSL Research University, CNRS, Univ. Paris Diderot, Sorbonne Paris Cité, UPMC Univ., Paris 06, Sorbonne Université, 5 Place J. Janssen, Meudon Cedex F-92195, France
(3) IFAC-CNR, Via Madonna del Piano 10, 50019 Sesto Fiorentino (Firenze), Italy
(4) ESA SSA-NEO Coordination Centre, Frascati (Roma), Italy
(5) Agenzia Spaziale Italiana - ASI, Via del Politecnico, snc, 00133 Roma, Italy
(6) Department of Physics and Astronomy 'Galileo Galilei', University of Padova, Vicolo dell'Osservatorio 3, I-35122 Padova, Italy
(7) Observatório Nacional, R. Gal. José Cristino 77, 20921-400 Rio de Janeiro, Brazil

Abstract

More than 85% of the 18,000 NEOs discovered up to now lack a physical characterization. The situation is even more dramatic for the small NEO population (D < 300 m). We conducted photometric observations for a large collection of uncharacterized NEOs in order to design future space missions towards them and assess the consequences of a possible impact on Earth. We discovered that carbonaceous C-complex NEOs deserve particular attention, since they are sometimes located in orbits that are challenging from a mitigation point of view, but also because the lack of carbonaceous material might not be due to an observational bias alone.

1. Introduction

The study of the near-Earth object (NEO) population is important because they represent the most accessible vestiges of the building blocks that formed the solar system approximately some 4.5 billion years ago. Furthermore, NEOs can help us answer fundamental questions about the presence of water and organics on the early Earth, and last but not least, of life itself. Recent astrobiological studies suggest that it is plausible that comets and NEOs are responsible for the delivery of organic and prebiotic molecules to the Earth [2].
The study of the physical characteristics of NEOs is also compelling in view of the potential hazard posed to our planet. NEOs are linked with all kinds of meteorite falls, from the recent Chelyabinsk event [4] to the occasional catastrophic impact events (like the K-T event, [5]). Unfortunately, NEOs have a great variation in terms of mitigation-relevant quantities (size, albedo, composition, etc.) and less than 15% of them have been characterized to date. Their increasing discovery rate (currently almost 2.000 objects/year) makes the situation progressively worse. There is therefore an urgent need to undertake a comprehensive characterization of the NEO population, particularly for the small NEO population (with a diameter below a few hundred meters), given that:
- there are many more of them than larger objects;
- their small sizes make them intrinsically fainter and therefore harder to study;
- they could cause severe regional damage [3].

In the framework of a 2-year Long-Term Program at the Telescopio Nazionale Galileo (TNG, La Palma, Spain) we carried out visible photometry of NEOs, with a focus on the small population, in order to derive visible color indexes and the taxonomic classification for 191 NEOs previously uncharacterized. To the same purpose, we also made use of the Italian Asiago Schmidt telescope and the Large Binocular Telescope (LBT, Arizona, US), observing a final sample of 226 objects. Finally, we obtained phase curve characterization for several high-profile NEOs using the the Campo Imperatore telescope (L'Aquila, Italy) and the Observatório Astronômico do Sertão de Itaparica (Nova Itacuruba, Brazil).

2. Results

The overall majority of NEOs characterized in our survey belong to the S-complex [1], although the most dangerous objects in our sample are represented by porous C-complex targets with a low MOID and on high inclination (>10 deg) orbits. The design of a mitigation mission toward these objects could be

particularly challenging since the ΔV for these objects is greater than current technological capabilities.

Moreover, our size analysis has pointed out that there seems to be a lack of carbonaceous asteroids going to smaller sizes (D < 300 m). While it is possible that observational selection effects are at play, we suggest that a physical phenomenon could also be responsible for the lack of smaller carbonaceous NEOs [6]. However, more observations of the small NEO population at different wavelength ranges are needed in order to settle the question of what is causing these selection effects.

Acknowledgements

We acknowledged financial support from the European Commission - grant agreement no: 640351 H2020- PROTEC-2014 - Access technologies and characterisation for Near Earth Objects (NEOs) and from ASI (contract No. 2013-046-R.0: "OSIRIS-Rex Partecipazione Scientifica alla missione per la fase B2/C/D").

References

[1] Ieva, S., Dotto, E., Mazzotta Epifani, E., et al. 2018, accepted in A&A https://doi.org/10.1051/0004-6361/201732154

[2] Izidoro, A., de Souza Torres, K., Winter, O. C., Haghighipour, N., ApJ, 767, 54, 2013

[3] Perna, D., Barucci, M. A., Drube, L., et al. 2015, Planet. Space Sci., 118, 311

[4] Popova, O. P., Jenniskens, P., Emel'yanenko, V., et al. 2013, Science, 342, 1069

[5] Rehan, S. M., Leys, R., & Schwarz, M. P. 2013, PLoS ONE, 8, e76683

[6] Scheeres, D. J. 2018, Icarus, 304, 183

EPSC Abstracts
Vol. 12, EPSC2018-770, 2018
European Planetary Science Congress 2018

The NEOSHIELD-2 project: results from the spectroscopic survey of small NEOs

S. Fornasier (1), D. Perna (2), M.A. Barucci (1), M. Popescu (3), A. Doressoundiram (1), F. Merlin (1), M. Fulchignoni (1), C. Lantz (4)
(1) LESIA, Observatoire de Paris, PSL Research University, CNRS, Univ. Paris Diderot, Sorbonne Paris Cité, Sorbonne Université, 5 Place J. Janssen, 92195 Meudon Principal Cedex, France; (2) INAF-Osservatorio Astronomico di Roma, Via Frascati 33, I-00078 Monte Porzio Catone, Rome, Italy; (3) Astronomical Institute of the Romanian Academy, 5 Cuţitul de Argint, 040557 Bucharest, Romania; (4) IAS, UMR 8617, CNRS, Université Paris-Sud, Bat 121, F-91405 Orsay, France

Abstract

The NEOShield-2 project was funded by European Commission (2015-2017) in the framework of the EU H2020 programme, and it is a follow-up of the first NEOShield (2012-2015) project. The main objectives of NEOShield-2 project are: i) to investigate the most promising mitigation techniques of an asteroid impact risk ; ii) to characterize the physical properties of NEOs of small sizes.
In this work we report the results of the spectroscopic survey on about 150 NEOs, most having sizes lower than 300 m, in order to constrain their surface composition.
The observations were carried out at the 3.6-meter NTT telescope of the European Southern Observatory under a Guaranteed Time Observations programme of 30 nights spanning two years (April 2015 to March 2017). The EFOSC2 spectrograph was used with the Grism #1 diffraction element. This configuration covers the spectral interval 0.40–0.92 μm with a resolution R$\sim$500. The objects with an absolute magnitude larger than 20 were selected, with a priority for the very small newly discovered ones.
The observed asteroids include 29 asteroids with diameters smaller than 100 meters, 71 with diameters between 100 m and 300 m, and 47 larger than 300 m. After standard reduction procedures and normalization of the spectra at 550 nm, we taxonomically classified 147 NEOs having good signal to noise ratio spectra by performing curve matching of their data with the visible part of the 25 template spectra defined by the Bus–DeMeo scheme [1], using the M4AST online tool [2].
We thus compare our results with those available in the literature from the European Asteroid Research Node (EARN) database of NEO physical properties.
Our main findings are the following [3, 4, 5]:
(1) The distribution we found from our observations is dominated by the S -complex at all sizes, in agreement with previous results for larger NEOs
(2) when comparing our sample with data reported in the literature, we observe an overabundance of A- and D-type for NEOs smaller than 300m compared to the bigger ones.
More specifically, A-type are 5.4% of the NEOs observed in our survey. Such olivine-rich bodies are very rare among larger NEOs and in the asteroid main belt, where objects of just a few hundred metres in size are not usually observable. Our results cast light on the missing olivine problem in the main belt, and they support the “battered to bits” scenario [6]: mantle fragments from disrupted differentiated parent bodies could have been shattered to dimensions below a few hundreds of metres, below the limit of detectability of previous spectroscopic surveys.
Nine new D-type asteroids were observed in our sample, with important exo-biological implication as these asteroids are considered the most primitive in the solar system and suppose to have a high abundance of organics and volatiles. D-type asteroids were considered to be very rare in the NEA population. Our results could conversely indicate that they are quite abundant among the small sized bodies, probably as a consequence of the high fragility of these carbonaceous asteroids, which favors the fragmentation of larger bodies. Six of them have also a ΔV lower than 6 km/s, and are good candidates for a sample-return mission to a D-type primitive asteroid.

Acknowledgements

This work is based on observations collected at the European Organisation for Astronomical Research in the Southern Hemisphere under ESO programme 095.C-0087. We acknowledge financial support from the NEOShield-2 project, funded by the European Union's Horizon 2020 research and innovation programme (contract No. PROTEC-2-2014–640351). This work was also supported by the Programme National de Planétologie (PNP) of CNRS/INSU, co - funded by CNES. DP has received further funding from the Horiz on 2020 programme also under the Marie Sklodowska-Curie grant agreement n. 664931.

References

[1] DeMeo, F. E., Binzel, R. P., Slivan, S. M., Bus, S. J. 2009, Icarus, 202, 160

[2] Popescu, M., Birlan, M., Nedelcu, D. A. 2012, A&A, 544, A13

[3] Perna et al., 2018. Planetary and Space Science, in press (DOI: $10.1016/j.pss.2018.03.008$)

[4] Barucci, M. A., et al. 2018. MNRAS, 476, 4481

[5] Popescu, M., et al. 2018. MNRAS, 477, 2786

[6] Burbine, T. H., Meibom, A., Binzel, R. P. 1996, Meteoritics, 31, 607

EPSC Abstracts
Vol. 12, EPSC2018-807, 2018
European Planetary Science Congress 2018

Search for possible differences in dynamical and physical properties of L4 an L5 Jupiter Trojans

Ivan Slyusarev (1,2), Daniella Glezina (1) and Irina Belskaya (1,2)
(1) Department of Astronomy and Space Informatics, V.N. Karazin Kharkiv National University. (2) Institute of Astronomy, V.N. Karazin Kharkiv National University. Kharkiv, Ukraine (i.slyusarev@karazin.ua)

Abstract

We search for possible differences in rotational frequencies, diameters, albedos and orbital parameters between Trojans belonging to the L4 and L5 swarms using our own observations and literature data. With increasing number of observational data it becomes evident that the L4 and L5 populations have very similar distributions of most parameters with an exception of orbital inclination distribution.

1. Introduction

In the second half of 2000's, after the emergence of new class of models of evolution of the early Solar system (Nice, Nice2, Grand Tack) [1,2] interest to Jupiter Trojans increased. The mechanism of Trojans capture and the place of their origin (outer part of Solar system) was the significant part of these models. Therefore, investigation of this population is necessary to the testing of these models. New surge of interest to this resonance group of minor bodies is caused by the future space mission "Lucy" (NASA) in 2021 which is aimed to study Trojans in both swarms [3]. Probably the most intriguing characteristic of the Jupiter Trojans is the observed asymmetry between the populations in L4 and L5. From the beginning of the study of Jupiter Trojans, there is a well-known difference in number of objects between L4 and L5 groups. For a long time, this difference has been attributed to the observational selection effect. However, as the number of discovered Trojans increase the difference become even more noticeable. At present, there are 4599 objects known in L4 and 2433 in L5 population, i.e. L4 Trojans are more numerous than L5 in 1.9 times. Except this well-known asymmetry in the number of bodies between L4 and L5 swarm [4], in our previous work [5] we found possible difference in orbit inclinations distribution. Here we search for possible differences in dynamical and physical properties using increasing set of observational data.

2. Physical and dynamical properties of Jupiter Trojans

Thanks to to the all-sky surveys Pan-STARRS, Palomar Transient Factory and Kepler K2 mission large extent of data about Trojans rotational properties were obtained. There are more than 400 Trojans with rotational periods and lightcurve amplitudes known to date. This data taken from [6] after qualification analysis for each asteroid and our own unpublished data allows us to perform the comparative analysis of rotational frequency distribution in both swarms (Fig.1.). Also we have compared distributions of albedos and diameters using data from WISE database [7] (Fig.2, 3).

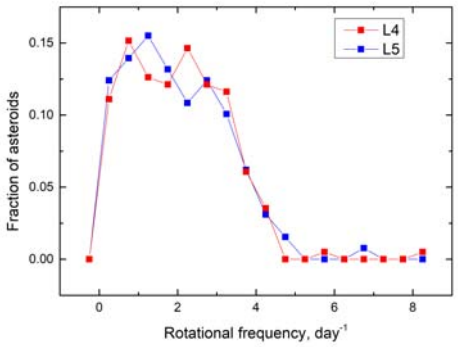

Figure1: Rotational frequency distribution.

3. Summary and Conclusions

The excess of the number of asteroids in L4 over the number of asteroids in L5 is observed in the entire range of absolute magnitude values, including the area that not distorted by the effect of observational selection (H<14).

There are possible slight differences in the diameter and albedo distribution.

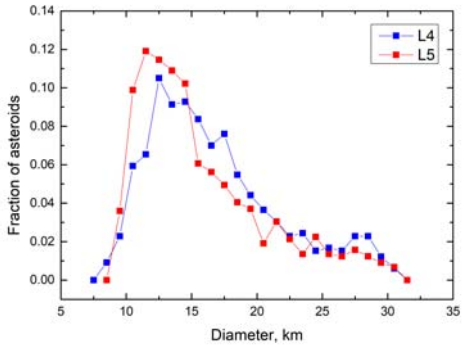

Figure 2: Diameter distribution.

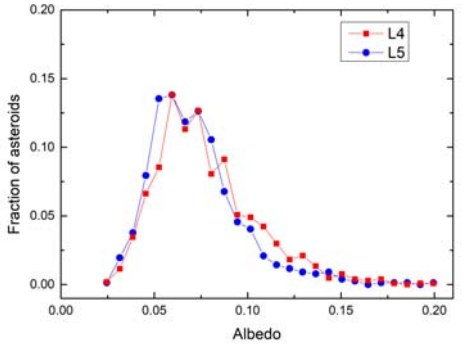

Figure 3: Albedo distribution.

Updated plot of the distribution of orbital inclinations is shown in Fig.4.

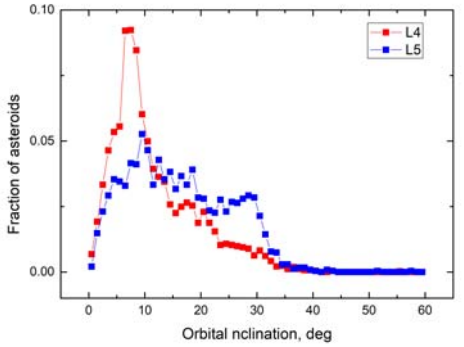

Figure 4: Orbital inclinations distribution.

There is no significant difference between L4 and L5 swarms in distribution of their rotational properties.

As for the orbital inclinations distribution in the L4 and L5 swarms (Fig.4) the differences in their shape is evident. The L5 population shows significantly wider distribution with a plateau in the range from 5° to 17° and a weak maximum at 27°. The distribution of the L4 population demonstrates a sharp maximum at 7°, after which the number of Trojans with specified inclinations decreases exponentially. Thus, in L4 bodies with small inclinations dominate in range 5°-10°, in L4 and L5 also there is a weak maximum near 18°. The distribution of eccentricities is identical in both subgroups.

References

[1] Morbidelli, A., Levison, H.F., Tsiganis, K., and Gomes, R.,Chaotic capture of Jupiter's Trojan asteroids in the early solar system, Nature Lett., Vol. 435, pp. 462–465.2005.

[2] Nesvorny D., Vokrouhlicky D., Morbidelli A., The Capture of Jupiter Trojans, ApJ, Vol. 768, 8 pp. 2013.

[3] Levison, H. F., Olkin, C., Noll, K.S., Marchi, S. Lucy: Surveying the Diversity of the Trojan Asteroids, the Fossils of Planet Formation. 48th Lunar and Planetary Science Conference. 20–24 March 2017. The Woodlands, Texas. LPI Contribution No. 1964, id. 2025.

[4] Szabo G. M. et al. The properties of Jovian Trojan asteroids listed in SDSS Moving Object Catalogue 3. MNRAS, Vol. 377, pp. 1393-1406, 2007.

[5] Slyusarev I.G. Asymmetry Between the L4 and L5 Swarms of Jupiter Trojans. 44th Lunar and Planetary Science Conference, held March 18-22, 2013 in The Woodlands, Texas. LPI Contribution No. 1719, p.2223.

[6] http://alcdef.org/

[7] Mainzer, A.K., Bauer, J.M., Cutri, R.M., Grav, T., Kramer, E.A., Masiero, J.R., Nugent, C.R., Sonnett, S.M., Stevenson, R.A., and Wright, E.L., NEOWISE Diameters and Albedos V1.0. EAR-A-COMPIL-5-NEOWISEDIAM-V1.0. NASA Planetary Data System, 2016;

EPSC Abstracts
Vol. 12, EPSC2018-877-1, 2018
European Planetary Science Congress 2018

Cooling rates of chondrules from diffusion profiles in relict olivine grains

S. C. Stockdale (1), I. A. Franchi (1), D. J. Morgan (2), M. Anand (1), M. M. Grady (1)
(1) School of Physical Science, The Open University, Milton Keynes, MK7 6AA, UK (2) School of Earth and Environment, University of Leeds, Leeds, LS2 9JT, UK (Shannon.Stockdale@open.ac.uk)

Abstract

Chondrule cooling rates are one of the important constraints on chondrule formation and can be used to distinguish between different chondrule formation mechanisms. Here we have modelled diffusion profiles observed across the boundary between forsteritic-olivine relict grains and more fayalitic overgrowth. We show that the cooling of chondrules is complex and good model fits are produced with non-linear cooling rates, offering additional scope for constraining the origin of chondrules.

1. Introduction

Chondrules are small, up to millimetre sized, spherical melt droplets composed of ferromagnesian minerals, olivine and pyroxene. They are one of the main components of chondritic meteorites, up to 80 vol % in some chondrites [1], and therefore appear to represent one of the main stages in the development of the rocky planets. They are products of widespread heating in the protoplanetary disk, however, the nature of this event is poorly understood. Pb-Pb ages of chondrules indicate they formed in the first few Myrs of the solar system [2]. As such, chondrules provide evidence of energetic processes occurring in the early solar system. Proposed chondrule formation mechanisms vary from shockwaves in the solar nebula [3] to impacts between planetesimals [4]. Chondrule cooling rates are one of the important constraints on chondrule formation and can be used to distinguish between competing chondrule formation models. Dynamic crystallisation experiments are the most widely cited methods of determining chondrule cooling rates and this indirect method has provided cooling rates from 1 to 3000 Kh^{-1} [1]. In order to assess whether this is a true representation of chondrule cooling rates, it should be validated or better constrained using a more direct method. Modelling of diffusion profiles observed across the boundary between forsteritic-olivine relict grains and more fayalitic overgrowth provides such an approach to determining chondrule cooling rates.

2. Methods

Forsteritic-olivine relict grains have been identified in a thin-section of ALHA 77307 CO3.0. They were characterised using Back Scattered Electron (BSE) imaging, Energy Dispersive X-ray Spectroscopy (EDS) mapping and EDS point analyses, with the FEI Quanta 3D FIB-SEM at The Open University. Chondrule liquidus temperatures were calculated from chondrule bulk compositions using geochemical modelling software, Petrolog3 [5]. Bulk compositions were calculated using a modal recombination analysis, combining the density, composition, and proportion of each phase identified in each chondrule [6]. The composition of each phase was determined by electron microprobe analyses using the Cameca SX-100 electron microprobe at The Open University. Fe-Mg diffusion profiles have been measured using BSE greyscale images, calibrated to electron microprobe analyses and extracted using open source software ImageJ [7]. As diffusion in olivine crystals is highly anisotropic, the crystal orientations have been determined by Electron Back Scatter Diffraction (EBSD) using the Zeiss SUPRA^{TM} 55VP FEG-SEM equipped with an Aztec HKL EBSD system and HKL Nordlys Nano high-sensitivity camera at The Open University. For oxygen fugacity, we use a value of 1 log unit beneath the Iron-Wüstite buffer.

3. Modelling

Fe-Mg diffusivity in olivine is well constrained [8] and Fe-Mg diffusion profiles were modelled using a one-dimensional, finite-difference method incorporating shifting boundary conditions and the effects of olivine composition, crystal orientation oxygen fugacity, and chondrule liquidus temperature.

4. Results

Fe-Mg diffusion profiles from 8 relict grains in 6 chondrules have been modelled. Good diffusion model fits to the observed diffusion profiles are

generally produced with non-linear cooling rates over the modelled temperature range, e.g. Fig. 1. Initial cooling rates range from 5 to 500 Kh^{-1} and increase to final cooling rates of 50 to 2000 Kh^{-1}. The change in cooling rate varies from a near-constant cooling rate to an increase in cooling rate of an order of magnitude.

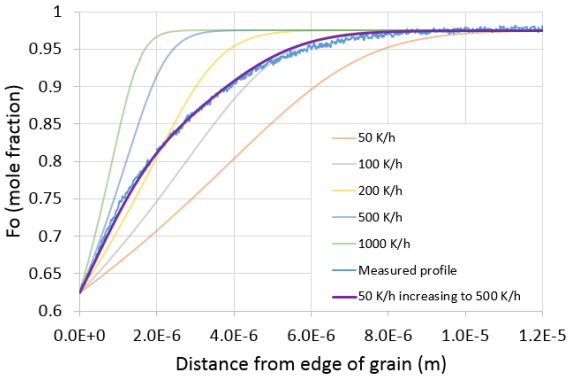

Figure 1: Fe-Mg diffusion profile showing model runs for constant cooling rates. The purple line shows a model fit with an initial cooling rate of 50 Kh^{-1} which increases to 500 Kh^{-1} and matches well with the measured profile.

5. Discussion

These cooling rates of 5 to 2000 Kh^{-1} are broadly consistent with experimental constraints on chondrule formation [1]. They are also consistent with cooling rates determined from modelling olivine zoning profiles in chondrules [9] and previous work determining chondrule cooling rates from diffusive exchange between a forsteritic-olivine relict grain and the fayalitic overgrowth [10]. However, the results here indicate that chondrule cooling was more complex than has previously been considered, requiring up to a tenfold increase in cooling rate at high temperatures, when diffusion is most efficient (~1900 to ~1785 K). This new detail offers additional scope for constraining the origin of chondrules. One possible situation where this could occur is during a planetary embryo bow-shock. Immediately after passing through the bow-shock, chondrules cool relatively slowly. As chondrules pass through the post-shock region, adiabatic expansion of gas causes more rapid cooling of the region [11]. However, some of the measured cooling rates may be lower than have been modelled so far for planetary embryo bow-shocks. We will, therefore, consider the detailed implications of our results for a range of bow-shock models as well as other chondrule formation scenarios.

Acknowledgements

This work is funded by an STFC PhD studentship to Shannon Stockdale. We would also like to thank the MWG, NASA JSC for the loan of the sample that makes this work possible.

References

[1] Hewins, R., Connolly, and H. C. Jr.: Experimental Constraints on Chondrule Formation, Chondrites and the Protoplanetary Disk, ASP Conference Series, Vol. 341, pp. 286-316, 2005.
[2] Connelly, J. N., Bizzaro, Krot, A. N., Nordlund, Å., Wieland, D., and Ivanova, M. A.: The Absolute Chronology and Thermal Processing of Solids in the Solar Protoplanetary Disk, Science, Vol. 338(6107), pp. 651-655, 2012.
[3] Morris, M. A. and Desch, S. J.: Thermal Histories of Chondrules in Solar Nebula Shocks, Astrophys. J., Vol. 722(2), pp.1474, 2010.
[4] Johnson, B. C., Minton, D. A., Melosh, H. J., and Zuber, M.T.: Impact jetting as the origin of chondrules, Nature, Vol. 517(7534), pp. 339-341, 2015.
[5] Danyushevsky, L. V. and Plechov, P.: Petrolog3: Integrated software for modelling crystallization processes, Geochem. Geophy. Geosy., Vol. 12(7), 2011.
[6] Berlin, J., Jones, R. H., Brearley, A. J. and Spilde, M. N.: Determining Bulk Compositions of Chondrules by Electron Microprobe: Modal Recombination Analysis versus Defocused Beam Analysis, Microsc. Microanal., Vol. 14(S2), pp. 110, 2008.
[7] Schneider, C. A., Rasband, W. S. and Eliceiri, K. W.: NIH Image to ImageJ: 25 years of Image Analysis, Nature methods, Vol. 9(7), pp. 671-675, 2012.
[8] Dohmen, R. and Chakraborty, S.: Fe-Mg diffusion in olivine II: point defect chemistry, change of diffusion mechanisms and a model for calculation of diffusion coefficients in natural olivine, Phys. Chem. Miner., Vol. 34, pp. 409-430, 2007.
[9] Miyamoto, M., Mikouchi, T. and Jones, R. H.: Cooling rates of porphyritic olivine chondrules in the Semarkona (LL3.00) ordinary chondrite: A model for diffusional equilibration of olivine during fractional crystallization, Meteorit. Planet. Sci., Vol. 44(4), pp. 521-530, 2009.
[10] Hewins, R. H., Ganguly, J. and Mariani, E.: Diffusion modelling of cooling rates of relict olivine in Semarkona chondrules, 40th Lunar and Planetary Science Conference, #1513, 2009.
[11] Boley, A. C., Morris, M. A. and Desch, S. J.: High-temperature processing of solids through solar nebular bow shocks: 3D radiation hydrodynamics simulations with particles, Astrophys. J., Vol. 776, pp. 101, 2013.

EPSC Abstracts
Vol. 12, EPSC2018-899, 2018
European Planetary Science Congress 2018

Mesosiderites and HEDs characterized combining by µ-IR and SEM/EDS analyses in relation to infrared spectra of Vesta-like asteroids

M. Ferrari (1), F. Dirri (1), E. Palomba (1), S. Stefani (1) and A. Rotundi (2,1)

(1) Institute for Space Astrophysics and Planetology, IAPS-INAF, Via del Fosso del Cavaliere 100, 00133, Rome, Italy.
(2) Dipartimento di Scienze e Tecnologie, Università degli Studi di Napoli "Parthenope", CDN, IC4; 80143 Naples, Italy.
(marco.ferrari@iaps.inaf.it)

Abstract

We present the results of a µ-IR and SEM/EDS combined study of three Howardite-Eucrite-Diogenite meteorites (HEDs) [1] and two mesosiderites [2] compared to the spectroscopic data collected by VIR onboard Dawn spacecraft [3]. The origin of HED group is thought to be linked to the asteroid 4 Vesta [4]. This hypothesis is reinforced by the data provided by the Dawn mission [5]. However, understanding the origin of mesosiderites is still challenging, since it is not clear whether a connection between these two groups of meteorites actually exists [6].

1. Introduction

In order to acquire a fuller grasp of remotely sensed compositional data, it is fundamental to compare them to analogue samples analyzed by means of spectroscopy techniques. Here, we report a SEM/EDS and µ-IR spectroscopy combined study of five meteorite samples: 1) NWA 7159, a monomictic brecciated eucrite consisting of exolved orthopyroxene and anorthite with accessory silica polymorph and ilmenite; 2) NWA 7490 a diogenite with a cumulate texture dominated by orthopyroxene, with Ca-plagioclase, minor olivine and chromite and troilite as accessory minerals; 3) NWA 2698, an howardite with eucritic pyroxene; 4) Vaca Muerta and 5) NWA 6266 (Fig. 1) two mesosiderites with subequal silicate and metallic components.

2. Experimental set up

For the µ-IR analyses on meteorites fragments we used a microscope (mod. Bruker Hyperion 3000) connected to the Vertex 80 interferometer. This set-up is able to acquire spectra in reflection mode on a single feature with minimum dimensions of 50 µm. For the SEM/EDS analyses we used a Field-Emission Gun Scanning Electron Microscope (FEG-SEM) equipped with an energy dispersive spectrometer (EDS) operating at 20 kV with an ultimate resolution of 1.5 nm, and a magnification up to 400.000x.

Figure 1: The NWA 6266 meteorite

3. Discussion

The µ-IR analysis performed on meteorite slabs provided punctual information on the mineralogy of the samples. The mid-IR reflectance spectra on pyroxenes present in the three analysed HEDs are shown in figure 2.

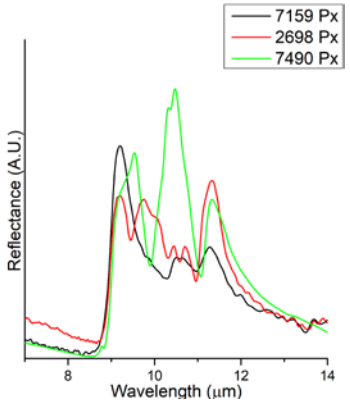

Figure 2: Spectra of pyroxenes in NWA 7159, NWA 2698 and NWA 7490.

The spectrum of NWA 2698 meteorite (red in fig. 2) shows the bands at 9.1, 10.4, 10.7 and 11.3 µm that can be attributed to pigeonite, whereas the bands at 9.7 can be ascribed to an "impurity" of calcium plagioclase. The bands at 9.2, 10.4, 10.7 and 11.3 µm in the spectrum of NWA 7159 meteorite (black in fig.2) can be attributed to pigeonite. The reflectance spectrum of NWA 7490 (green in fig.2) shows the bands at 9.5, 10.3, 10.4 and 11.3 µm attributable to hypersthene. Figure 3 shows two spectra collected on the NWA 6266 mesosiderite, the black one on the metal fraction whereas the red one the silicates portion, pyroxene dominated.

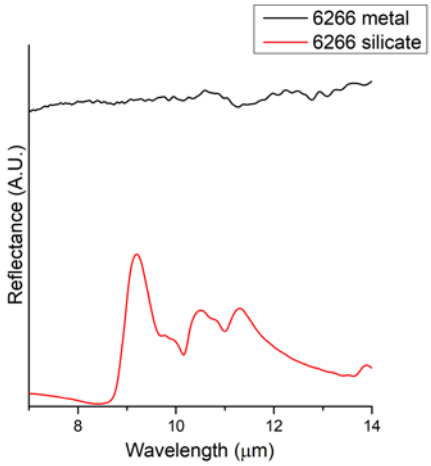

Figure 3: Spectra collected on the NWA 6266 meteorite.

While the µ-IR analysis provided reflectance spectra of single phases, the SEM/EDS analysis corroborated the results adding chemical and textural information on the samples. By means of combined analyses, we obtained a comprehensive mineralogical framework for the HEDs and mesosiderites. It has been verified that the mineralogical heterogeneity of the HED meteorites is consistent with the spectroscopic diversity seen on Vesta, and proven that the silicate fraction of the mesosiderites and HEDs are isotopically identical [7]. Therefore, this work helps to better constrain and characterize the reflectance spectra performed on Vesta-like bodies through the spectroscopic study of these two meteorite families.

4. Conclusions

The laboratory data acquired on three HEDs and on two mesosiderites indicate that:

- the pyroxene of NWA 2698 is a pigeonite in accordance with the composition of the eucritic pyroxene, as reported in the Meteoritical Bulletin N°90;
- the NWA 7159 sample shows a predominant presence of anorthite, as confirmed by the value of Christiansen feature. The presence of pigeonite is in accordance with the pyroxene composition reported in the Meteoritical Bulletin N°104;
- the meteorite NWA 7490 shows the presence of Ca-plagioclase and Mg-olivine, in addition to the predominant occurrence of hypersthene, as reported in the Meteoritical Bulletin N°101;
- the composition of the two mesosiderites is consistent with mixtures of metallic iron and pyroxene;
- based on the obtained results the near-IR spectra of these HEDs are directly comparable to those of asteroid (4)Vesta;
- the next step will be the comparison of the mid-IR data with spectra obtained by means of earth observation on the Vesta-like asteroids.

Acknowledgements

This work is supported by the Italian Space Agency, PRIN-MIUR and Regione Campania. We are grateful to the PLab (INAF-IAPS) for making available their instrumentation. This research uses spectra reproduced from the ASTER database (courtesy of the JPL) and the Berlin Emissivity Database (Helbert et al. 2007).

References

[1] Takeda H., et al., 1983. Mem. Natl. Inst. Polar Res., 30, 181-205.
[2] Delaney J. S., et al., 1981 Proc. Lunar Planet. Sci. 12B, 1315–1342.
[3] De Sanctis M.C. et al., 2012. Science, 336, 697-700.
[4] Keil K., 2002. In Asteroids III, The University of Arizona Press, 573-584.
[5] McSween Jr., H.Y. et al., 2013. Meteorit. Planet. Sci., 48(11), 2090-2104.
[6] Greenwood R. C et al., 2015. Geochim. Cosmochim. Acta 169 (2015) 115–136.
[7] Greenwood R. C. et al. 2006 Science, 313, 1763-1765.

EPSC Abstracts
Vol. 12, EPSC2018-930, 2018
European Planetary Science Congress 2018

The meteorite flux of the last 2 Myr recorded in Atacama

Alexis Drouard (1,2), Jérôme Gattacceca (2) Aurore Hutzler (2) Pierre Rochette (2) Régis Braucher (2) Didier Bourlés (2) ASTER Team (2) Matthieu Gounelle (3) Alessandro Morbidelli (4) Vinciane Debaille (5) Millarca Valenzuela (6)
(1) Aix Marseille Univ, CNRS, LAM, Laboratoire d'Astrophysique de Marseille, Marseille, France (alexis.drouard@lam.fr) (2) Aix-Marseille Univ, CNRS, IRD, Coll France, INRA, CEREGE, Aix en Provence, France (3) IMPMC, MNHN, Paris, France (4) Laboratoire Lagrange, UMR7293, Université de la Côte d'Azur, CNRS, Observatoire de la Côte d'Azur, Nice, France (5) Laboratoire G-Time, Université Libre de Bruxelles, Belgium (6) SERNAGEOMIN, Santiago de Chile

Abstract

The delivery of meteoroids to the Earth is controlled by the complex dynamical evolution of the Solar System bodies. Although the intensity of the current flux of meteoroids to the Earth can be estimated by meteor observations [1], the characterization of the longer term flux and its possible variability in intensity and composition requires the study of meteorites. Large meteorite collection recovered from deserts are particularly suited for this purpose, as they terrestrial age can be estimated from cosmonogenic nuclides measurements. In this work, we show that meteorites from the Atacama desert allow studying the meteorite flux variability over the last 2 Myr.

The Atacama desert is an important meteorite reservoir with very high number of meteorites per surface units [2, 3]. Terrestrial ages of 54 ordinary chondrites from this desert were determined by measuring the ^{36}Cl content of their metallic fraction. These meteorites (25 H, 26 L, and 3 LL) were randomly selected among the 385 meteorites found in the El Médano dense collection area. Care was taken to discard possibly paired meteorites to avoid overrepresentation of large fall events that can produce hundreds of meteorites. The protocol used to extract the chlorine was inspired by the works of [4] and [5]. Typically, the samples were crushed, washed in hydrochloridric and fluoridric acids and dried in order to magnetically separate the metal fraction. These fractions were then dissolved, spiked with ^{35}Cl, and silver chloride precipitates were formed. The isotopic ratio measurements were performed at ASTER AMS facility. Finally, terrestrial ages T_{age} were derived from the measured activity in the samples A_{mes}:

$$T_{\mathrm{age}} = \frac{1}{\lambda} \ln\left(\frac{A_{\mathrm{sat}}}{A_{\mathrm{mes}}}\right) \quad (1)$$

where λ is the ^{36}Cl half-life (λ = (301 $\pm$ 0.01) kyr [6]) and A_{sat} the saturated activity in chondritic meteorites exposed to cosmic rays (A_{sat} = (22.8 $\pm$ 3.1) dpm kg^{-1} [7]).

The cumulative distribution distribution of these terrestrial ages is displayed in Fig. 1. About 30% of the samples are older than 1 Myr, and that the oldest are older than 2 Myr. The distribution can be fitted as an exponential decrease, with an half-life of 568 kyr. The uncertainties on the ages range from 60 to 100 kyr. For comparison, meteorites from other hot deserts and Antarctica have an average terrestrial age of only ∼20 kyr and ∼50 kyr respectively [8]. These results are consistent with the old surface ages of the Atacama desert surfaces and the long-standing hyperarid climate [9, 10] and offer an explanation for the unusually high number of meteorites that were found in the El Médano area (∼160 meteorites per km^2 [3]).

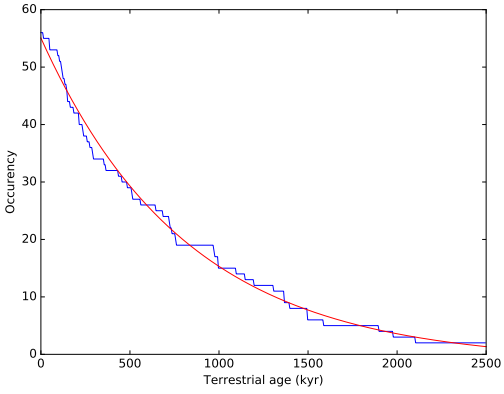

Figure 1: Cumulative terrestrial age distribution measured by ^{36}Cl (blue) and the exponential best-fit (red).

We then studied the flux variability between H and L chondrites over the last million years, statically more representative. The H chondrite fraction with respect to the total (H+L) chondrites is presented in Fig. 2. Our results show a variability over the last million years, where H are dominant within the 600-1400 kyr and L are dominant within the 200-600 kyr.

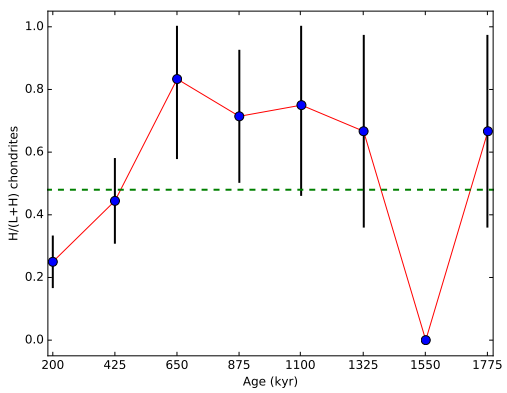

Figure 2: H chondrite fraction (with respect to the total H+L chondrite) for bins of 225 kyr. The green dotted line is the current ratio computed from the meteorite fall population (800 over the last two centuries)

Because we took care to select meteorites that were not paired, we rule out the hypothesis of a large meteorite shower that could bias the statistics. We have started to investigate dynamically the possibilities for the encounter between Earth and a meteorite swarm. The low probability to keep a stable swarm after ejection from resonant orbits within the main belt is probably not consistent with catastrophic collision in the main-belt, but periodic encounters between Earth and Near-Earth-Objects due to precession cycles could be investigated. Further work should be done, especially measurement of cosmic ray exposure ages (i.e., the transfer time to the Earth under the form of a meteoroid), in order to investigate this potential link. Also, this result will need to be confirmed by conducting the same type of study in a different area of the Atacama desert.

The El Médano meteorite collection from the Atacama meteorite collection is exceptionally old and allows for the first time a statistical approach to study the possible variations of the flux of meteoroids to the Earth over the last million years.

References

[1] Halliday, I., Blackwell, A.T. and Griffin, A.A., Meteoritics, 24, p. 173-178, 1989.

[2] Gattacceca, J., Valenzuela, M., Uehara, M. et al., M& PS 46, Nr 9, pp. 1276-1287, 2011.

[3] Hutzler, A., Gattacceca, J., Rochette, P. et al., M& PS 51, Nr 3, pp. 468-482, 2016.

[4] Vogt, S., and Harpers, U., Fresenius Z. Anal. Chem., Vol. 331, pp. 186-188, 1988.

[5] Merchel, S, and Herpers, U., Radiochimica Acta, Vol. 84, pp. 215-220, 1999.

[6] Bartholomev, R.B., Boyd A.W., Brown, F *et al.*, Canadian Journal of Physics, Vol. 33, pp. 43-48, 1955.

[7] Nishiizumi, K. , Elmore, D. and Kubik, P.W., Earth and Planetary Science Letters, Vol 93, Issue 3-4, pp. 299-313, 1989.

[8] Jull, A.J.T.: Terrestrial Ages of Meteorites, in Meteorites and the Early Solar System, University of Arizona Press.

[9] Clarke, J., Geomorphology, 73, pp. 101-114, 2005.

[10] Dunai, T.J., Gonzalez-Lopez, G.A and Juez-Larré, J., Geology, 33, no4, p. 321-324, 2005.

EPSC Abstracts
Vol. 12, EPSC2018-953, 2018
European Planetary Science Congress 2018

Astrometry and photometry of TNOs and asteroids using Gaia DR2

R. Duffard (1), P. Santos-Sanz (1), N. Morales (1), and J.L. Ortiz (1)

(1) Instituto de Astrofísica de Andalucía, CSIC, Apt 3004, 18080 Granada, Spain (duffard@iaa.es)

Abstract

We will present the astrometry and photometry of a selected sample of main belt asteroids and TNOs using data from the Gaia DR2.

We analyzed the astrometry of selected TNOs and Main belt asteroids to know if it's possible to detect the presence of a satellite. We also analyzed the photometry of a selected list of main belt asteroids searching for variation in the absolute magnitude and confirming the determination of the rotational period if it is known. On the other hand, applying a shape model, an absolute size can be reached, assuming an albedo.

1. Introduction

Gaia DR2 released the data of more than 14 000 minor bodies. On these data the astrometry and photometry of only a few TNOs are presented, the rest is the astrometry and photometry of main belt asteroids, Jupiter Trojans, a small number of NEOs and Hildas. In this work we selected two particular cases from this sample, to test the potentiality of the DR2 data.

Haumea is one of the largest TNOs and it is known to have two satellites. The largest one can be detected using astrometry from ground-based telescopes following the movement of the system photocenter [1]. Rings are also detected around this TNO [2].

(596) Scheila is a main belt asteroid that presented activity in 2010 [3]. The impact of a small body could be the cause of this activity [4].

In this work, we will present the results on the astrometry and photometry of Haumea. We also will present the results on the analysis of the photometry of Scheila and its implications.

Finally, we will present the result on the variation of absolute magnitude along time for a selected sample of main belt asteroids.

2. Analysis of the data

All the data was extracted from the Gaia Archive and processed with own software.

The search for the rotational period was done applying the PDM technique. To obtain the absolute magnitude H, the magnitudes were distance and phase angle corrected using the ephemerides from the Gaia spacecraft.

After the distance and phase correction we used the equations presented by [5] to obtain the calculated absolute magnitude for a given triaxial ellipsoid with fixed albedo.

3. Main results

When analyzing the astrometry data for Haumea we realize that the data did not reach enough precision to determine the movement of the photocenter. DR2 astrometry precision for a single observation for this TNO reached 50 milli-arcsecond (mas), not enough for the detection.

Results on absolute magnitude were obtained for the entire sample. In figure 1 it is shown an example for asteroid (596) Scheila.

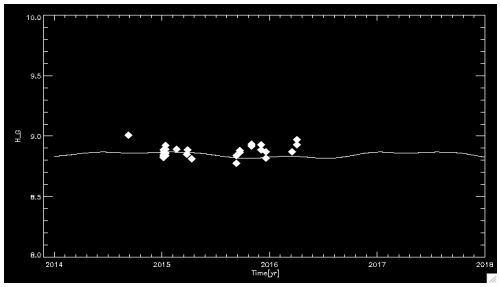

Figure 1: Absolute magnitude versus time in years for (596) Scheila. The points are the data from DR2 and the line is the generated model.

4. Summary and Conclusions

After the analysis of the astrometry of Haumea we can say that the individual measurements made with GAIA DR2 until now has not enough precision to detect the largest satellite of Haumea. We need to wait the following releases the increase the precision on the astrometry.

The rotational period based on the photometry, meanwhile, is correctly found on the data of Haumea.

On the main belts, an absolute magnitude in the Gaia system can be determined and its variation along time. The time spam on the data is from 2014 to 2017 mainly, corresponding to this release.

Acknowledgements

Spanish grant AYA-2014-56637-C2-1-P and the Proyecto de Excelencia de la Junta de Andalucía J.A. 2012-FQM1776 is acknowledged. The research leading to these results has received funding from the European Union's Horizon 2020 Research and Innovation Programme, under Grant Agreement No. 687378.

References

[1] Ortiz et al. 2011. A mid-term astrometric and photometric study of trans-Neptunian object (90482) Orcus. Astronomy and Astrophysics, 525, A31, 12p

[2] Ortiz et al (2017), The size, shape, density and ring of the dwarf planet Haumea from a stellar occultation. Nature, Volume 550, Issue 7675, pp. 219-223

[3] Larson, S. M., (2010), International Astronomical Union Circular, 9188.

[4] Moreno, F., Licandro, J., Ortiz, J. L. et al. (2011), (596) Scheila in outburst: A probable collision event in the Main Asteroid Belt, Astrophysical Journal (ApJ), 738, 130.

[5] Tegler et al. 2005. The period of rotation, shape, density, and homogeneous surface color of the Centaur 5145 Pholus. Icarus, vol 175, pp390-396.

EPSC Abstracts
Vol. 12, EPSC2018-1012, 2018
European Planetary Science Congress 2018

Fifteen years of Antarctic micrometeorite research by the Italian Programma Nazionale delle Ricerche in Antartide

Luigi Folco (1) (luigi.folco@unipi.it)

(1) Dipartimento di Scienze della Terra, Università d Pisa, Via S. Maria 53, 56126 Pisa, Italy

Abstract

This is an overview of the contribution to cosmic dust studies provided by fifteen years of Antarctic micrometeorite research by the Italian Programma Nazionale delle Ricerche in Antartide (PNRA) since the discovery of the Transantarctic Mountain micrometeorite collection in 2003.

1. Introduction

The Earth accretes some tens of thousands of tonnes of extraterrestrial material each year [1]. Most of this is interplanetary dust produced by collisions and evaporation of rocky and icy bodies in the Solar System. A fraction of this dust survives hypervelocity impact with the Earth's upper atmosphere and is collected at the Earth's surface in the form of microscopic particles (<2 mm) called micrometeorites. Significant quantities of micrometeorites are recovered mainly from deep-sea sediments, and snow, ice and loose sediments in polar areas. Micrometeorites are relevant for planetary science because they provide samples of a variety of dust-producing bodies in the Solar System for laboratory analysis, most notably primitive asteroids and comets which allow exploration of the first stages in the evolution of the protoplanetary disk [2]. Furthermore, the systematic study of unbiased and time-constrained micrometeorite collections allows investigation of the cycles of extraterrestrial input to the global geochemical budget of planet Earth, including its bearing on the emergence of life. Lastly, knowledge of the physical and compositional properties of micrometeorites provides constraints for modelling the source regions and dynamic evolution of the cosmic-dust complex in the near-Earth space, as well as for assessing the potential hazard to space activities of dust in the vicinity of the Earth.

During the Italian 2003 and 2006 Programma Nazionale delle Ricerche in Antartide (PNRA) expeditions, we discovered of large accumulations of micrometeorites from the tops of Victoria Land Transantarctic Mountains (TAM) [3]. Since then, four more PNRA micrometeorite collection campaigns led to the collection of thousands of micrometeorites available for cosmochemical studies. This material is under investigation in a collaborative effort by a number of European research teams (Pisa University, INAF and Parthenope, Italy; CEREGE and ISTerre France; Imperial College, UK; Max Plank Institute Mainz, Germany; Vrije Universiteit Brussel, Belgium) with the aim of understanding the composition of the near Earth dust complex - an outstanding issue in Solar System science.

2. The TAM micrometeorite collection

TAM micrometeorites are found within the loose fine-grained bedrock detritus accumulated in the joints and decimeter-sized weathering pits of flat, glacially eroded granitoid summits of the TAM - the so called TAM micrometeorite traps [3]. These are windows into the last ~1 million years of micrometeorite flux. This relatively long accumulation time is documented by the occurrence of ~480,000 year old debris from a large meteorite impact over Antarctica [4] and ~800,000 year old Australasian microtektites [5]. As micrometeorites are found within a loose soil, extraction of particles <200 μm in size is difficult, though feasible. Due to the relatively long accumulation time, TAM micrometeorites show variable degrees of alteration [6]. This collection contains thousands of micrometeorites in the 200–800 μm range and hundreds in the 800–2000 μm range with many up to 3000 μm in size. [3] and [7] concluded that the TAM micrometeorite collection is representative of the

micrometeorite flux >200 µm in size over the last one million years. This is based on the match with the frequency by type and size distribution of the South Pole Water Well cosmic spherule collection [8], as secondary accumulation processes and weathering act selectively on micrometeorites with different physical properties (mainly density) and compositions.

3. Research highlights and outlook

The extraordinarily large number of specimens and their relatively large size which enables investigation through a multi-analytical approach are unique characteristics of the micrometeorites in the TAM collection. Combined petrographic, bulk compositional and oxygen isotopic data has allowed identification of new micrometeorite types from a number of different, primitive and evolved parent bodies [e.g., 9, 10]; in particular, data from cosmic spherules has allowed to establish their relative contribution to the modern composition of the <200 µm dust complex at ~1 AU [11]. Besides evidence of complex exposure histories in some particles, current noble gas research is providing information on the micrometeoroid source regions in the solar system with implications on their orbital evolution (Baecker et al. 2018, GCA, under review).

Future research will focus on i) parent body identification in a statistically representative selection of >200 µm unmelted micrometeorites, combining petrographic, geochemical and oxygen isotopic compositional data; ii) mineralogical and geochemical investigation of the intense acqueous alteration observed in giant fine-grained micrometeorites to explore parent body processes on hydrous C-type asteroids (see Suttle et al., this meeting).

Acknowledgements

Italian MIUR: PNRA grant PNRA16_00029 and PRIN grant PRIN15_20158W4JZ7.

References

[1] Taylor S, Messenger S, Folco L: Cosmic dust: finding a needle in a haystack. Elements, Vol.12, pp.171-176, 2016.

[2] Folco L, Cordier C: Micrometeorites. In European Mineralogical Union Notes in Planetary Mineralogy, Vol. 15, pp. 253-29, 2015.

[3] Rochette P, Folco L, Suavet C, van Ginneken M, Gattacceca J, Perchiazzi N, Braucher R, Harvey R, Micrometeorites from the Transantarctic Mountains. Proceedings of the National Academy of Sciences of the United States of America, vol. 105, pp. 18206-18211, 2008.

[4] van Ginneken M, Folco L, Perchiazzi N, Rochette P, Bland PA: Meteoritic ablation debris from the Transantarctic Mountains: Evidence for a Tunguska-like impact over Antarctica ca. 480 ka ago. Earth and Planetary Science Letters, vol. 293, pp.104-113, 2010.

[5] Folco L, Rochette P, Perchiazzi N, D'Orazio M, Laurenzi M, Tiepolo M: Microtektites from Victoria Land Transantarctic Mountains. Geology, vol. 36, pp. 291-294, 2008.

[6] van Ginneken M, Genge M J, Folco L, Harvey RP: The weathering of micrometeorites from the Transantarctic Mountains. Geochimica et Cosmochimica Acta, vol. 179, pp. 1-31.

[7] Suavet C, Rochette P, Kars M, Gattacceca J, Folco L, Harvey R: Statistical properties of Transantarctic Mountain (TAM) micrometeorite collection. Polar Science, vol. 3. pp. 100-109, 2009.

[8] Taylor S, Lever JH, Harvey RP: Accretion rate of cosmic spherules measured at the South Pole. Nature vol. 392, pp. 899–903, 1998.

[9] Cordier C, Folco L, Taylor S: Vestoid cosmic spherules from the South Pole Water Well and Transantarctic Mountains (Antarctica): A major and trace element study. Geochimica et Cosmochimica Acta, vol. 75, pp. 1199-1215, 2011.

[10] van Ginneken M, Folco L, Cordier C, Rochette P: Chondritic micrometeorites from the Transantarctic Mountains. Meteoritics and Planetary Science, vol. 47, pp. 228-247, 2012.

[11] Cordier C, Folco L, Oxygen isotopes in cosmic spherules and the composition of the near Earth interplanetary dust complex. Geochimica et Cosmochimica Acta, vol. 146, pp. 18-26, 2014.

[12] Cordier C, Baecker B, Ott U, Folco L, Trieloff M: A new type of oxidized and pre-irradiated micrometeorite. Geochimica et Cosmochimica Acta (in press, https://doi.org/10.1016/j.gca.2018.04.010).

EPSC Abstracts
Vol. 12, EPSC2018-1030, 2018
European Planetary Science Congress 2018

The second joint Italian – Iranian expedition to Dasht-e Lut for meteorite recovery

M. Ferrari (1), V. Moggi Cecchi (2), G. Pratesi (3), M. Di Martino (4), G. Giuli (5), M. Nemati (6), M.C. De Sanctis (1)

(1)Institute for Space Astrophysics and Planetology, IAPS-INAF, Rome, Italy, marco.ferrari@iaps.inaf.it; (2)Museo di Storia Naturale dell'Università di Firenze, Firenze, Italy; (3)Dipartimento di Scienze della Terra dell'Università di Firenze, Firenze, Italy; (4)INAF – OATO, Torino, Italy; (5)Scuola di Scienze e Tecnologie, Università di Camerino, Camerino, Macerata, Italy; (6)Department of Geology, Shahid Bahonar University, Kerman, Iran.

Abstract

After the first expedition in 2017 a second field trip in the Lut Desert has been realized in April/May 2018 by the University of Florence, the Italian Institute for Space Astrophysics and Planetology-INAF and the Shahid Bahonar University of Kerman.

1. Introduction

Dasht-e Lut is a large salt desert located in south-eastern Iran (Fig. 1), with an area of ~52,000 km^2. Being part of the Afro-Asian desert belt, the area is considered as one of the driest (annual rainfall less than 50 mm) and hottest places (surface temperatures of 70°C or more) in the world. The central part of the desert has been wind-sculpted into a series of parallel ridges, troughs, ravines, and sinkholes, while the eastern part is an extended area of sand, containing dunes that reach heights of 300 m. Previous expeditions in this area, including the first joint Italian-Iranian expedition during last year (3,67 Kg of samples), have confirmed that it is suitable for meteorite conservation and recovery [1-4]. According to the international agreement signed between the University of Florence and the Shahid Bahonar University of Kerman, a second field trip to Lut Desert -and the related fieldwork for searching and collecting meteorites- has been realized from April 27 to May 7, 2018.

Figure 1: Map of Iran, the star indicates the location of the Dasht-e Lut.

2. The 2018 field campaign

The explored area is located in the Kalut desert (Fig. 2), which is the north-western part of the Dasht-e Lut. This area is characterized by the presence of 50-100 meters high ridges consisting of loess deposits. These reliefs have been modeled by the action of wind forming long channels oriented northwest to south-east.

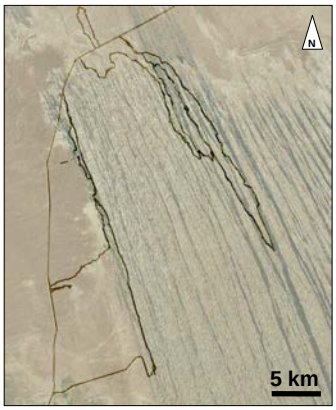

Figure 2: Trail of the field trip in the Lut desert.

During this expedition some specimens (Fig. 3) of meteorites and several doubtful stones have been recovered in the field.

Figure 3:Meteorite samples recovered during the 2018 campaign.

3. Preliminary characterization of meteorites collected during the 2017 campaign

As concerns the 2017 expedition a long time occurred for the authoritative procedure needed for releasing the samples and shipping them to Italy. After the samples arrival they have been analyzed following a procedure which started from the weight and density measurement, polyester resin mount preparation, optical microscope and SEM analysis. An essay of each sample has been analyzed and photographed by means of a Zeiss Axioplan metallographic microscope. After this they have been analyzed by means of a Zeiss EVO 15 Scanning Election Microscope to determine the major phases composition. Preliminary results appear interesting: 146 fragments belonging to 42 separate specimens of meteorites and 11 doubtful stones have been recovered. The weight of the samples ranges from few grams to one kilo with a total amount of 3670 grams. The density measurement allowed discriminate terrestrial rocks form true meteorites and, for meteorites, to single out three separate clusters of values in the range 3.2-3.4 g/cm^3. Moreover two separate specimens with values of 3.5 and 3.6 g/cm^3 have been evidenced. The analytical results are reported in table 1.

4. Summary and Conclusions

Most of the small samples appear to belong to the L5 group of ordinary chondrites, while larger samples can be assigned to other 5 groups of ordinary chondrites. Moreover the largest sample (LE26), provisionally assigned to the H4 group, displays very interesting characteristics that need more detailed analyses, like the presence of chondrules with a zoned phase distribution.

Acknowledgements

We wish to acknowledge the Lut Travel Agency of Kerman for support and logistic in the organization of both the 2017 and 2018 field trips.

Field label	Frag. #	Weight	Density (g/cm3)	Met (Y/N)	Lat (N)	Long (E)	Classification (provisional)
LE1	1	52.2	3.322	Y	30° 46' 25"	57° 47' 45"	OC (L5)
LE2	1	10.2	3.323	Y	30° 46' 25"	57° 47' 45"	OC (L5)
LE3	5	6.8	3.333	Y	30° 46' 25"	57° 47' 45"	OC (L5)
LE4	1	14.8	3.354	Y	30° 46' 25"	57° 47' 45"	OC (L5)
LE5	1	35.6	3.342	Y	30° 46' 25"	57° 47' 45"	OC (L5)
LE6	1	23.0	3.317	Y	30° 46' 25"	57° 47' 45"	OC (L5)
LE7	1	20.6	3.377	Y	30° 46' 25"	57° 47' 45"	OC (L5)
LE8	15	51.9	3.287	Y	30° 46' 25"	57° 47' 45"	OC (L5)
LE9	8	9.9	3.224	Y	30° 46' 25"	57° 47' 45"	OC (L5)
LE10	1	19.9	3.334	Y	30° 46' 25"	57° 47' 45"	OC (H5)
LE11	1	28.8	3.379	Y	30° 46' 25"	57° 47' 45"	OC (L5)
LE12	1	16.7	3.298	Y	30° 46' 25"	57° 47' 45"	OC (H5)
LE13	5	14.5	3.307	Y	30° 46' 25"	57° 47' 45"	OC (L5)
LE13/2	1	6.9	3.051	N	30° 46' 25"	57° 47' 45"	Terrestrial
LE14	1	50.5	2.564	N			Terrestrial
LE15	1	14.2	2.687	N			Terrestrial
LE16	1	10.6	3.426	Y	30° 44' 9"	57° 48' 50"	OC (L5)
LE17	2	5.5	3.310	Y	30° 44' 9"	57° 48' 50"	OC (L5)
LE17/2	1	1.6	2.670	N	30° 44' 9"	57° 48' 50"	Terrestrial
LE18	1	1.6	3.262	Y	30° 43' 21"	57° 49' 18"	OC (L5)
LE19	1	13.2	3.253	Y	30° 45' 5"	57° 48' 36"	OC (L5)
LE20	45	106.3	3.200	Y	30° 45' 5"	57° 48' 36"	OC (L5)
LE21	1	4.0	3.324	Y	30° 46' 27"	57° 47' 45"	OC (L5)
LE22	1	2.5	3.344	Y	30° 46' 27"	57° 47' 45"	OC (L5)
LE23	1	58.1	2.619	N	30° 43' 21"	57° 49' 18"	Terr.
LE24	1	9.9	3.346	Y	30° 44' 33"	57° 48' 31"	OC (L5)
LE25	1	229.0	3.455	Y	30° 39' 59"	57° 50' 20"	OC (H5)
LE26	1	954.9	3.232	Y	30° 42' 25"	57° 49' 24"	OC (H4)
LE27	1	134.7	3.315	Y	30° 40' 40"	57° 50' 34"	OC (L5)
LE27b	2	4.3	3.404	Y	30° 35' 27"	57° 52' 23"	OC (L5)
LE27b/2	1	1.2	2.620	N	30° 35' 27"	57° 52' 23"	Terrestrial
27b/3	1	0.5	3.576	N	30° 35' 27"	57° 52' 23"	Terrestrial
LE28	3	230.5	3.361	Y	30° 40' 40"	57° 50' 34"	OC (LL4)
LE29	1	404.6	3.396	Y	30° 39' 51"	57° 50' 56"	OC (L4)
LE29b	1	3.5	3.297	Y	30° 39' 51"	57° 50' 56"	OC (L4)
LE30	1	88.6	3.315	Y	30° 46' 14"	57° 48' 11"	OC (L5)
LE31	1	207.2	3.379	Y	30° 46' 14"	57° 48' 11"	n.a.
LE32	1	125.4	3.648	Y	30° 46' 14"	57° 48' 11"	OC (H4)
LE32b	4	70.7	3.390	Y	30° 46' 14"	57° 48' 11"	OC (L5)
LE32c/6	1	4.7	2.723	N	30° 46' 14"	57° 48' 11"	Terrestrial
LE32c	3	16.6	3.276	Y	30° 46' 14"	57° 48' 11"	OC (L5)
LE32/t	1	76.9	n.a.	Y	30° 47' 17"	57° 47' 52"	n.a.
LE33	1	8.6	3.362	Y	30° 35' 31"	57° 51' 48"	OC (L5)
LE34	5	14.6	3.367	Y	30° 46' 24"	57° 49' 10"	OC (L5)
LE35	1	255.0	3.360	Y	30° 39' 59"	57° 58' 9"	OC (L5)
LE36	1	31.2	3.372	Y	30° 46' 1"	57° 47' 28"	OC (L5)
LE37	1	68.9	3.358	Y	30° 45' 53"	57° 47' 31"	OC (L5)
LE38	1	13.2	3.354	Y	30° 45' 50"	57° 47' 35"	OC (L5)
LE39	1	9.1	3.311	Y	30° 45' 51"	57° 47' 33"	OC (L5)
LE40	14	90.7	3.386	Y	30° 45' 33"	57° 47' 44"	OC (L5)
LE41	2	54.0	3.410	Y	30° 45' 22"	57° 47' 43"	OC (L5)
LE42	3	4.7	3.250	Y	30° 45' 22"	57° 47' 43"	OC (L5)
LE45	1	31.1	2.652	N			Terrestrial
LE46	2	13.2	2.695	N			Terrestrial
LE47	1	17.0	3.312	Y	30° 32' 44"	57° 45' 56"	OC (LL5)
Total	157	3670.8	///	///	///	///	///

Table 1: Summary of provisional results obtained from the analyses performed on the 2017 Lut Expedition meteorite samples.

References

[1] J. Gattacceca et al. 2011. Meteoritics & Planetary Science 46:1276–1287.

[2] A. Al-Khatiri et al. 2005. Meteoritics & Planetary Science 40:1215–1239.

[3] H. Pourkhorsandi et al. 2016. Journal of the Earth and Space Physics 41:125–130.

[4] H. Pourkhorsandi et al. 2016. 79th Annual Meeting of the Meteoritical Society, abs. 6195.

EPSC Abstracts
Vol. 12, EPSC2018-1043, 2018
European Planetary Science Congress 2018

Meteorite 4.5Gyr halite crystals likely to originate from Comets

Max K. Wallis and N. Chandra Wickramasinghe (1)
(1) Buckingham Centre for Astrobiology, University of Buckingham, Buckingham, UK (maxkwallis@gmail.com)

Abstract

Halite crystals in the ZAG and Monahans meteorites have been of special interest because they imply a watery crystallisation environment.. The crystals contain some organic-rich brine inclusions, so the recent dating at 4.5Gyr implies a watery organic pool in the very early solar system. Media publicity in January 2018 talked of finding the "building blocks of life", much as comets have been depicted as bringing the building blocks of life to planet Earth. Indeed, the organic complement shows similarities with comet Wild 2 and Stardust particles.

We hypothesise that the organics in the meteorite halite inclusions are biotic or pre-biotic chemicals from the first 10Myr of comets. This corresponds to the few Myr radiogenic heating by short-lived ^{26}Al and ^{60}Fe.

1. Evidence from the Zag and Monahans meteorites

Both these 1998 meteorites are regolith breccias containing mm-sized halite crystals (NaCl; KCl), blue in colour due to extensive cosmic-ray processing. Rubin et al [3] identified shock metamorphism, thermal metamorphism and aqueous alteration on the asteroid (H-chondrite) parent body. Subsequent studies [6] found µm-sized zones of complex mixtures of primitive organics (aliphatic, aromatic/olefinic, vinyl-keto, carboxyl/ester and carbonate) .

Recently Chan et al. [1] made a comprehensive analysis of soluble and insoluble organic compounds trapped in brine inclusions in the mm-sized halite crystals. They summarised them as organic precursors, intermediates and reaction products that make up precursor bio-molecules such as amino acids. The organic compounds also contain a mixture of C-, O-, and N-bearing macromolecular carbon materials, including aromatics, ketones and imine or imidazole compounds.

Their data showed nitrogen ^{15}N is enriched but carbon ^{13}C is depleted. Enrichment compared with solar system values can arise from preferential retention on partial evaporation to space, whereas depletion of ^{13}C is normally taken as indicative of biological fixing processes. A C-rich area of Monahans was found as $\delta^{13}C$=37.6+/-4.2 $^{o}/_{oo}$, mid-range for terrestrial biological carbon ($\delta^{13}C$ = 25-60 $^{o}/_{oo}$) whereas C-rich meteorites Murchison and Orgeil are less depleted $\delta^{13}C$ ~17-19$^{o}/_{oo}$

2. Comets as a source

The origin suggested [1] for the halite crystals was icy moons such as Enceladus and Europa, but their gravitational pull and that of the parent planet means such ejected crystal (via cryo-volcanism) can hardly escape to space. Comets are a possible and more plausible source

Early comets have been hypothesised since the 1980 to have liquid interiors, on the basis that radiogenic heating potentially caused the interior of snowballs >10km radius to reach 273K and melt. Distillation of the volatile components diffusing through the porous comet tends to concentrate gases in the outer regions, with slow reactions forming more complex molecules there. If micro-organisms are active, one would expect the suite of complex molecules to show this in highly complex compounds. Alternatively, the early surface of a snowball comet – prior to development of a quasi-stable coherent dark crust as observed on current epoch comets [5,6] – would be an environment where micro-organisms and/or biomolecules concentrate out of the sublimating aqueous phase [2]. Crystallisation processes would form patches of gas hydrates (clathrates), rather than simple distillation supposed to create pockets of volatiles CO, NH_3, CH_4, CH_3OH etc.

As shown by the comet Halley spaceprobes and Rosetta recently to comet 67P, 'dust' and micro-crystals are blown out by cometary gas jets. Large quantities are simply released on disintegration of

comets. Such crystals would have impacted asteroid regoliths during their accretion stage, eg. the asteroids Ceres or Hebe suggested as parent body of Zag and Monahans.

3. Comets as a source of organic-rich brines within halite crystals

Astronomical arguments in favour of complex organics in comets, summarised recently in Steele et al [4], go back to 1975. Interstellar organics from the pre-solar nebula together with any debris from living matter, spores etc. would be accreted on the early comets. Space probes to Halley's comet in 1986 established its dust as high in carbonaceous compounds and its surface as very dark, challenging Whipple's 'dirty snowball' comet model that was the reigning paradigm at the time. Imaging of comet nuclei on fly-by missions and the recent landing on 67P by Philae in the Rosetta mission have established comets to have coherent crusts, processed by insolation, micro-impacts and outgassing [6]. Beneath the crust, we infer temporary gassy regions, even pools [5] which, as they freeze and gradually lose H_2O, concentrate the biotic and pre-biotic organics in brines. We suggest this as a source of micron-scale halite crystals in current-day comets, but they would not survive long in free space.

4. Summary

We argue that the organics in the Zag and Monahans halite inclusions reveal biotic or pre-biotic chemicals in the first 100Myr of comets. The analyses are compatible with previous studies of cometary organics, but in the meteorite case shows a more complex suite of compounds, indicative of biotic organics. The ^{13}C depletion is particularly indicative of biotic rather than pre-biotic chemistry; if confirmed, it would be highly significant, implying comets were endowed from birth with micro-organisms able to colonise the icy cometary environment, as they colonise terrestrial antarctic snows. The comet timescales were of course far longer, ~10-100 Myr after the initial radiogenic heating decayed away.

Where are the halite crystals from more recent evolving comets? Comet formation and disintegration was of course more vigorous in the first 100 Myr. But the late bombardment and accretion of planetary oceans is put at ~500Myr. Do relatively few halite crystals survive from asteroids in this period? More intensive searches of other meteorites are eagerly awaited.

5. Figure

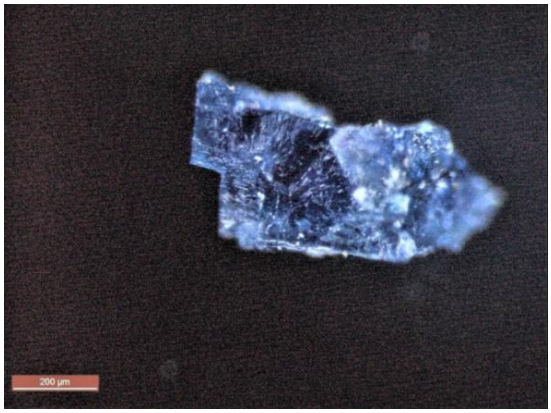

Blue halite crystal from Monahan [1]

References

[1] Queenie H.S. Chan *et al*. 2018. Organic matter in extraterrestrial water-bearing salt crystals. *Science Advances* 4 (1): eaao3521; doi: 10.1126/sciadv.aao3521

[2] L. J. Rothschild, R. L. Mancinelli, Life in extreme environments. *Nature* 409, 1092–1101, 2001

[3] Alan E. Rubin, Michael E. Zolensky and Robert J. Bodnar, Meteoritics Planet. Sci. 37(1) 2010 https://doi.org/10.1111/j.1945-5100.2002.tb00799.x

[4] Steele, E.J., et al., Cause of Cambrian Explosion - Terrestrial or Cosmic? Progress in Biophysics and Molecular Biology (2018), https://doi.org/10.1016/j.pbiomolbio.2018.03.004

[5] Max K Wallis, N C Wickramasinghe and J T Wickramasinghe, Watery Habitats in Comets: temporary sub-crustal ponds, *5th EANA Workshop on Astrobiology*, p.37, Budapest 2005

[6] M K Wallis and N C Wickramasinghe *Rosetta* images of Comet 67P/Churyumov–Gerasimenko: Inferences from its terrain and structure. *Astrobiol Outreach*, 2015 01/2015; 03(01). https://doi.org/10.4172/2332-2519.1000127

[7] M. E. Zolensky et al. The search for and analysis of direct samples of early Solar System aqueous fluids, *Philosophical Transactions of the Royal Society A: Mathematical, Physical and Engineering Sciences*, **375**, 2094, (20150386), 2017.

EPSC Abstracts
Vol. 12, EPSC2018-1072, 2018
European Planetary Science Congress 2018

The case for depth-dependent thermal properties of asteroids: evidence from Earth-based observations

Line Drube, and Alan Harris
Institute for Planetary Research, German Aerospace Center (Line.Drube@dlr.de)

Abstract

We investigate the thermal inertia of a large number of asteroids and find significant evidence for depth-dependence of thermal properties, such as density and thermal conductivity.

1. Introduction

For all types of lander missions to asteroids some prior knowledge of the surface properties of the target is important for success. Observing the thermal emission from asteroids with thermal-infrared telescopes enables predictions of surface structural properties, such as the presence of fine regolith, rubble-like regolith or low-porosity rock/metal. This difference can be seen in the thermal inertia values:

$$\Gamma=(\kappa\rho C)^{0.5} \quad (1)$$

(κ: thermal conductivity, ρ: density, C: heat capacity). The thermal emission signature depends on the material properties down to the depth to which the diurnal heat wave penetrates. A measure of this is the skin depth, d_s, which is the depth at which the amplitude of the heat wave is reduced to 1/e of its value at the surface:

$$d_s = (2/\omega)^{0.5}\,\Gamma/\rho C\,, \quad (2)$$

where ω is the angular spin rate.

2. Thermal inertia estimator

The calculation of thermal inertia using thermophysical models requires high quality thermal-infrared observations taken at different times, a shape model and spin state information. These demanding requirements have limited the number of asteroids with measured thermal inertia. In previous work [1] we presented a novel means to estimate the thermal inertia of any asteroid based on knowledge of its astrometric geometry, spin axis and thermal-infrared emission, which we refer to as the "NEATM Thermal-Inertia Estimator". With currently available archival thermal-infrared data this technique can be used to we estimate thermal-inertia values for some 1000 asteroids, depending on spin-vector availability.

Since then the number of asteroids with thermophysically modeled thermal inertia have gone from around 60 to almost 300, e.g. [2]. We compare results from our thermal-inertia estimator with newly available results from thermophysical modelling and discuss possible improvements to the estimator.

3. Thermal inertia deduced from Earth-based observations

We review results, including observations of eclipses/occulations of binary asteroids, variability of thermal inertia with temperature, and further analysis of the results of Harris and Drube, 2016, which suggest that asteroid thermal inertia is in general strongly depth dependent. While, the interpretation of such results is still in progress, we note that depth-dependence of thermal inertia would have important implications for scientific lander missions to asteroids, future in-situ asteroid resource utilization, and planetary defence, including calculations of Yarkovsky orbital drift.

4. Summary and Conclusions

We use our NEATM-based thermal-inertia estimator results, together with other observational results, to investigate the thermal properties of asteroid near-surface structure. Evidence is growing for significant depth-dependence of thermal properties, such as density and thermal conductivity.

Acknowledgements

The research leading to these results has received funding from the European Union's Horizon 2020 Programme under grant agreement no. 640351 (NEOShield-2 Project).

References

1. Harris, A.W. and L. Drube, *Thermal tomography of asteroid surface structure.* The Astrophysical Journal, 2016. **832**(2): p. 127.
2. Hanuš, J., et al., *Thermophysical modeling of main-belt asteroids from WISE thermal data.* Icarus, 2018. **309**: p. 297-337.

EPSC Abstracts
Vol. 12, EPSC2018-1084, 2018
European Planetary Science Congress 2018

Asteroid Phase Curves Seen by Pan-STARRS 1

Michele T. Bannister, Alan Fitzsimmons and David Young
(1) Astrophysics Research Centre, Queen's University Belfast, Belfast BT7 1NN, United Kingdom (m.bannister@qub.ac.uk)

Abstract

The Pan-STARRS survey made 19 million optical observations of more than half a million main-belt asteroids in 2010–2016. We use the phase curves of the $H_r > 13$ sample to derive the absolute magnitudes and slope parameters of more than half a million asteroids, and map these to the dynamical populations of the main belt.

Introduction

Phase curves provide critical information about the surface reflectance properties, shapes, and sizes of minor planets (Bowell et al., 1989; Oszkiewicz et al., 2012), which are typically unresolved in observations. Two parameters defining the physical properties of a minor planet can be derived from a phase curve. The absolute magnitude H_{filter}, as measured within a given wavelength range, provides a luminosity, often used as an albedo-independent proxy for size. The slope parameter, G, does not necessarily imply a specific lithology or morphology, but encodes bulk information about an unresolved minor planet's reflectivity. On the scale of populations, the relationships between H_{filter}, G and orbital parameters can provide insight into the formation and evolution of minor planet populations (Oszkiewicz et al., 2012).

1 Pan-STARRS1 observations

Obtaining H and G measurements for a large sample of asteroids has only been possible with the advent of systematic wide-field surveys. The Panoramic Survey Telescope and Rapid Response System 1 Survey (PS1) has created an exceptionally rich imaging dataset. PS1 has made two wide-field Northern sky surveys: the 3π survey (Chambers et al., 2016) and the ongoing Solar System survey (hereafter, S3). The PS1 imager is equipped with six filters: a Sloan-like $grizy$ set and a wide-band w filter, which approximates the gri passband (Tonry et al., 2012). The photometry from the first fifteen months of the 3π survey was considered by Vereš et al. (2015), who obtained H and G parameters for 250,000 asteroids.

We consider the asteroid photometry from both the 3π and the S3 datasets of PS1. The 3π observations we use were acquired after the telescope was refit and the software overhauled, from 2010 through to its end in mid-2014. The S3 observations were made between 2012 June and 2016 October.

We provide phase curve information sampled over this seven-year span for more than half a million asteroids, double that of the Vereš et al. (2015) set. We derive H and G parameters for all available asteroids with well-determined orbits, and map these against the precisely-known dynamical populations of the main belt.

Asteroids with $m_r < 16$ will saturate in the imaging of the upcoming LSST survey; thus, this dataset of physical parameters will remain useful in that era, complementing the phase curves that will be measured with *Gaia* (Oszkiewicz et al., 2017).

Acknowledgements

We thank Serge Chastel for assistance with the MOPS databases.

M.T.B. and A.F. appreciate support from UK STFC grant ST/P0003094/1, and M.T.B. also from STFC grant ST/L000709/1.

The authors acknowledge the sacred nature of Haleakala, and appreciate the opportunity to use observations from the mountain. The Pan-STARRS1 Surveys have been made possible through contributions of the Institute for Astronomy, the University of Hawaii, the Pan-STARRS Project Office, the Max-Planck Society and its participating institutes, the Max Planck Institute for Astronomy, Heidelberg and the Max Planck Institute for Extraterrestrial Physics, Garching, The Johns Hopkins University, Durham University, the University of Edinburgh, Queen's University Belfast, the Harvard-Smithsonian Center for As-

trophysics, and the Las Cumbres Observatory Global Telescope Network, Incorporated, the National Central University of Taiwan, and the National Aeronautics and Space Administration – United States under Grant Nos. NNX08AR22G and NNX12AR65G, issued through the Planetary Science Division of the NASA Science Mission Directorate.

References

Bowell, E., Hapke, B., Domingue, D., et al. 1989, in Asteroids II, ed. R. P. Binzel, T. Gehrels, & M. S. Matthews, 524–556

Chambers, K. C., Magnier, E. A., Metcalfe, N., et al. 2016

Oszkiewicz, D., Skiff, B., Warner, B., et al. 2017, European Planetary Science Congress, 11, EPSC2017

Oszkiewicz, D. A., Bowell, E., Wasserman, L. H., et al. 2012, Icarus, 219, 283

Tonry, J. L., Stubbs, C. W., Lykke, K. R., et al. 2012, ApJ, 750, 99

Vereš, P., Jedicke, R., Fitzsimmons, A., et al. 2015, Icarus, 261, 34.

EPSC Abstracts
Vol. 12, EPSC2018-1157, 2018
European Planetary Science Congress 2018

Retrograde 1:1 mean motion resonance: a perturbative treatment

V.V. Sidorenko
Keldysh Institute of Applied Mathematics, Moscow, Russia (vvsidorenko@list.ru)

Abstract

In the framework of restricted spatial circular three-body problem “Sun+planet+asteroid” we study the dynamics at retrograde 1:1 mean motion resonance. Retrograde motion appears clockwise when viewed from above the north ecliptic pole of the Solar System. With the use of double numerical averaging we construct evolutionary equations that describe the long-term behavior of asteroid's orbital elements. Special attention is paid to possible transitions between different types of orbits existing at retrograde 1:1 resonance.

1. Introduction

Most of objects in the Solar system move around the Sun in the anticlockwise manner when seen from above the north ecliptic pole. And only a small number of celestial bodies move in opposite direction [1,2]. Recent theoretical studies demonstrated that retrograde 1:1 MMR can predict collision of asteroid and planet in the case of co-orbital motion [3,4]. The aim of our investigation is to obtain more information about properties of this resonance.

2. Double averaged equations describing the dynamics at retrograde 1:1 mean-motion resonance

In the case of mean-motion resonance three dynamical processes can be distinguished: "fast" process corresponds to planet and asteroid motions in orbit, "semi-fast" process is variation of the resonance argument (which describes the relative position of the planet and the asteroid in their orbital motions), and, finally, "slow" process is the secular evolution of the orbit shape (characterized by the eccentricity) and orientation (it depends on the ascending node longitude, inclination and argument of pericenter).

To study the "slow" process we constructed the evolutionary equations by means of numerical averaging over the "fast" and "semi-fast" motions. As a specific feature of these evolutionary equations we should mention that their right hand sides are not uniquely defined by values of the "slow" variables in some domains of these variables. The ambiguity appears since the averaging can be done over "semi-fast" processes with different qualitative properties - in other words, it can be done over different types of resonance orbits. The consideration of this ambiguity provides us an opportunity to predict the possibility of transitions between different resonance orbits.

Acknowledgements

The author acknowledges the financial support from the Presidium of the Russian Academy of Sciences under the scope of the Program 28 "Space: investigations of the fundamental processes and their interrelationships”

References

[1]Wiegert, P., Connors, M., Veillet, C.: A retrograde co-orbital asteroid of Jupiter. Nature, Vol. 543, pp. 687-689, 2017.

[2]Kankiewicz, P., Wlodarczyk, I.: How long will asteroids on retrograde orbits survive? Planet. Space Sci., Vol. 154, pp. 72-76, 2018.

[3] Morais, M.H.M., Namouni, F.: A numerical investigation of coorbital stability and libration in three dimensions. CMDA, Vol. 125, 91-106, 2016.

[4] Huang, Y., Li, M., Li, J., Gong, S.: Dynamic portrait of the retrograde 1:1 mean motion resonance. ArXiv1804.10893, 2018.

EPSC Abstracts
Vol. 12, EPSC2018-1173, 2018
European Planetary Science Congress 2018

A Framework for Spectral Reflectance Analysis of Carbonaceous Chondrite Meteorites (and Asteroids)

Edward Cloutis – Department of Geography, University of Winnipeg, Winnipeg, MB, Canada R3B 2E9 (e.cloutis@uwinnipeg.ca)

Abstract

Determining the mineralogy of dark (presumably carbonaceous chondrite-like) asteroids using 0.3-2.5 µm reflectance spectroscopy has been hampered by a lack of knowledge of the spectral reflectance properties of these meteorites, and a general assumption that they are generally spectrally featureless. Here we show that most carbonaceous chondrite meteorites (CCs) do exhibit spectral properties that can be related to specific mineral components, and that different CCs often exhibit unique and mineralogically-diagnostic spectral features.

1. Introduction

The scientific importance of CCs includes the fact that they represent the least altered remnants of the early solar system that are delivered and available on Earth in appreciable quantities for study and analysis and because they can provide insights into solar system history and evolution, and prebiotic organic chemistry [e.g., 1, 2].

A number of studies exist that have systematically examined the spectral reflectance properties of different CCs in the 0.3-2.5 µm region [e.g., 3-11]. By determining the range and diversity of spectral reflectance properties of different CC groups and comparing between groups, we have determined that most CC groups exhibit unique ranges of spectral reflectance properties that allows them to be discriminated. Here we focus on reflectance spectra of powdered CCs, as they are expected to be most representative of regolith-bearing asteroid surfaces.

2. Results

The most diagnostic spectral reflectance properties of CCs that can be used to discriminate them include absolute reflectance, spectral slope, and the position and shape of absorption features in the 0.7, 0.9-1.3, and 2 µm regions. Using various combinations of these metrics allows us to discriminate different CC groups with varying levels of confidence.

Figure 1 shows the range of slopes (as measured by the 2.5 µm/visible region peak reflectance ratio) for different CCs and ureilites. It can be seen that there is significant overlap between groups but the aqueously-altered CCs are almost uniformly red sloped and show a wider range of slopes than unaltered CCs.

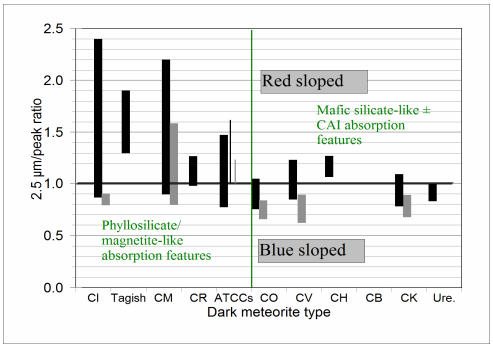

Figure 1. Spectral slope ranges for different CCs and ureilites. The black bars denote the range for powders, while the gray bars are for slabs or powders in which the finest powder fraction has been removed.

The 1 µm region of CC reflectance spectra can be quite variable. Absorption bands in this region are nearly ubiquitous and are of two main types: (1) aqueously-altered CCs commonly exhibit absorption bands near 0.75, 0.9, and 1.1 µm due to Fe-bearing phyllosilicates, while unaltered or thermally metamorphosed CCs show absorption bands near 1.05 and 1.25 µm or near 0.95 µm, due to olivine or pyroxene, respectively (Figure 2).

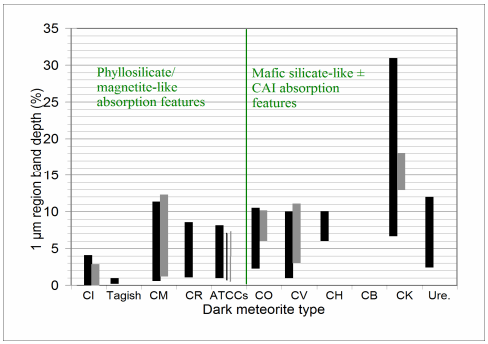

Figure 2. Same as Figure 1 for 1 µm region maximum absorption feature depth.

Finally, when peak reflectance is used as a metric (Figure 3), there is a gradual positive correlation between reflectance and degree of thermal metamorphism, and a negative correlation with aqueous alteration. In other words, increasing aqueous alteration leads to generally lower reflectance, while increasing thermal metamorphism leads to generally higher reflectance.

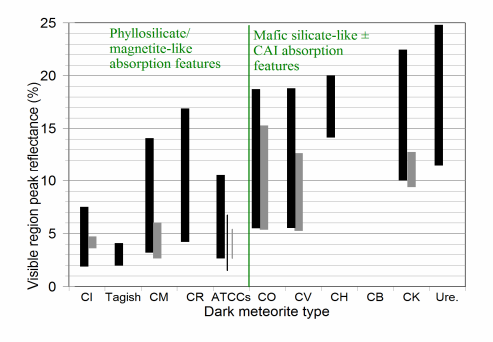

Figure 3. Same as Figure 1 for reflectance at the visible region reflectance peak.

3. Discussion

These simple spectral metrics can be combined with other parameters for CC discrimination. These include: (1) determining whether absorption features in the 1 µm region are phyllosilicate-like, olivine-like, magnetite-like, or pyroxene-line; (2) the presence or absence of absorption features in the 2 µm region that are attributable to pyroxene or Fe-bearing spinels in calcium aluminum inclusions (CAIs), and presence or absence of phyllosilicate absorption features in the 2.3 µm region.

Acknowledgements

EAC thanks the NASA-supported RELAB spectrometer facility at Brown University for acquiring many of the spectra referred to in this work and maintaining a publicly-accessible archive of this data, and the Natural Sciences and Engineering Research Council of Canada, the Canada Foundation for Innovation, the Manitoba Research Innovation Fund, the Canadian Space Agency, and the University of Winnipeg for supporting the establishment and continuing operation of UWinnipeg's Planetary Spectrophotometer Facility.

References

[1] Morbidelli, A et al., Meteorit. Planet. Sci. 35, 1309-1320, 2000.

[2] Nagy, B., 1975. Carbonaceous Meteorites. Elsevier, Amsterdam, 747 pp.

[3] Cloutis, E.A., et al., Meteorit. Planet. Sci., 45, 1668-1694, 2010.

[4] Cloutis, E.A., et al., Icarus, 212, 180-209, 2011.

[5] Cloutis, E.A., et al., Icarus, 216, 309-346, 2011.

[6] Cloutis, E.A., et al., Icarus, 217, 389-407, 2012.

[7] Cloutis, E.A., et al., Icarus, 220, 586-617, 2012.

[8] Cloutis, E.A., et al., Icarus, 220, 466-486, 2012.

[9] Cloutis, E.A., et al., Icarus, 221, 328-358, 2012.

[10] Cloutis, E.A., et al., Icarus, 221, 911-924, 2012.

[11] Cloutis, E.A., et al., Icarus, 221, 984-1001, 2012.

EPSC Abstracts
Vol. 12, EPSC2018-1205, 2018
European Planetary Science Congress 2018

The chronology of formation of solids and meteorite parent bodies in the early solar system

Mario Trieloff
Klaus-Tschira-Labor für Kosmochemie, Institut für Geowissenschaften, Universität Heidelberg (Mario.trieloff@geow.uni-heidelberg.de)

Abstract

Meteorites are fragments from small bodies (mostly asteroids) in the early solar system. These planetesimals formed within a few Ma, before the solar nebula was dissipated. Radioisotope dating allows to infer a detailed insight into the chronology of formation of the first solids, meteorite parent body formation and their thermal evolution. While differentiation was completed within a few Ma, cooling of both undifferentiated chondrites and differentiated parent bodies took place over tens of Ma.

1. Introduction

Meteorites contain both decay products of long-lived nuclides (^{238,235}U-^{206,207}Pb, ^{40}K-^{40}Ar [1,2]) and also short-lived radionuclides (^{129}Xe from ^{129}I; $T_{1/2}$=16 Myr [3], excess ^{26}Mg from ^{26}Al; $T_{1/2}$=0.73 Myr [4], ^{53}Cr from ^{53}Mn; $T_{1/2}$=3.7 Myr [5], ^{182}Hf from ^{182}W; $T_{1/2}$=9 Myr [6,7]). Radioisotope dating based on these nuclides provide a framework for the formation of solids in the early solar system. Particular short-lived nuclides can provide a high resolution early solar system chronology, if short-lived isotope chronometries are calibrated against each other using several tie points (e.g., CAIs, some H chondrites, Acapulco). Moreover, it is possible to derive planetesimal formation timescales by constraints derived from ^{26}Al heating of meteorite parent bodies [2,8]. Conditions of formation of the first solids in the solar nebula varied - most probably due to p,T differences imposed by the early sun - with radial distance and/or time, and caused the compositional variety of planetesimals concerning refractory and volatile elements, metals, and Mg-rich silicates [8,9].

2. Chronology of formation of solids and planetesimals

The oldest solids in the early solar system (c. 4567 Ma old) are cm-sized refractory Ca,Al rich inclusions (CAIs) in meteorites. Abundant spherical chondrules are about 2-4 Ma younger. Radiometric dating of chondrules from different meteorite classes and formation time scales inferred by ^{26}Al heating (Figure 1) define a sequence of formation of ordinary chondrites (L and LL type), and carbonaceous CO and CR chondrites about 2-4 Ma after CAIs. These data and chemical composition - particular chondrule-matrix complementarity – suggest that individual planetesimals grew rapidly in the asteroid belt (within < 1 Ma), but different planetesimals formed over a time interval of 4 million years [2,7,8], well within the lifetime of protoplanetary dust disks inferred from extrasolar systems [10,11]. Planetesimals forming earlier than undifferentiated chondrites were even more strongly heated by decay heat of short-lived nuclides, primarily ^{26}Al [2]. This caused melting and differentiation in planetesimals that formed within < 2 Ma after CAIs and led to the formation of iron cores and basaltic rocks, while chondritic planetesimals that accreted later remained undifferentiated [2,7,8]. As most chondrules were immediately consumed in accreting planetesimals, they were only preserved in unmelted chondritic parent bodies and their age distribution is biased to the formation time interval of chondrites 2-4 Ma after CAIs [8].

3. Conclusions and open questions

The formation of solids in the early solar system (CAIs, chondrules, planetesimals and terrestrial planets) are still insufficiently linked to astrophysically constrained processes like early protostellar activity, disk dissipation, formation and

migration of gas planets interacting with young disks [10,11]. Models of Earth and Mars formation based on $^{182}Hf-^{182}W$ core formation ages infer the presence of planetary embryos of 60% the size of Mars after 2-4 Ma. This indicates the early presence of Jupiter to effectively prevent the formation of a proto-planet in the asteroid belt. Planetesimal formation in the asteroid belt and the terrestrial planet formation zone at <3 Ma after CAIs was likely accompanied by inner disk clearing accompanied by solar wind irradiation and likely volatile element depletion of terrestrial – and partly asteroidal - precursor planetesimals [12].

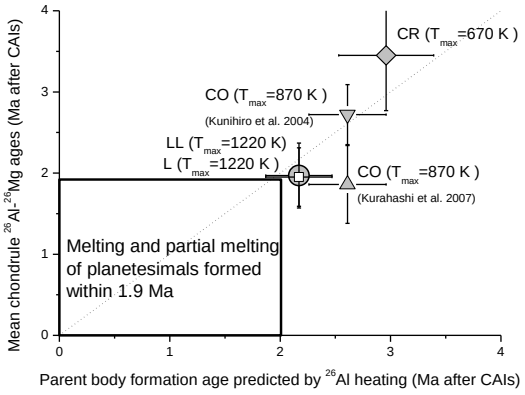

Acknowledgements

Support by Klaus Tschira Stiftung gGmbH and Deutsche Forschungsgemeinschaft (DFG) is acknowledged.

References

[1] Amelin, Y., Krot, A.N., Hutcheon, I.D., Ulyanov, A.A.: Lead Isotopic Ages of Chondrules and Calcium-Aluminum-Rich Inclusions. Science 1678, 2002.

[2] Trieloff, M., Jessberger, E.K., Herrwerth, I., Hopp, J., Fieni, C., Ghelis, M., Bourot-Denise, M., Pellas, P.: Structure and thermal history of the H-chondrite parent asteroid revealed by thermochronometry Nature 422, 502, 2003.

[3] Gilmour J. D., Pravdivtseva O. V., Busfield A., and Hohenberg C. M.: The I-Xe chronometer and the early solar system. Meteoritics & Planetary Science 41:19–31, 2006.

[4] Bizzarro, M., Baker, J.A., Haack, H.: Mg isotope evidence for contemporaneous formation of chondrules and refractory inclusions. Nature 431, 275, 2004.

[5] Lugmair, G.W., Shukolyukov, A.: Early Solar System Timescales According to Mn-Cr Systematics. Geochim. Cosmochim. Acta 62, 2863, 1998.

[6] Kleine, T., Münker, C., Mezger, K., Palme, H.: Rapid accretion and early core formation on asteroids and the terrestrial planets from Hf-W chronometry. Nature 418, 952, 2002

[7] Kleine T., Mezger, K, Münker, C., Palme, H., Bischoff A.: $^{182}Hf-^{182}W$ isotope systematics of chondrites, eucrites, and martian meteorites: Chronology of core formation and early mantle differentiation in Vesta and Mars. Geochim. Cosmochim. Acta 68, 2935, 2004.

[8] Trieloff M. in: Chronology of the solar system. In: Landolt-Börnstein, Numerical data and functional relationships, New Series Vol. VI/4 Astronomy, Astrophysics, Cosmology, (ed. J. Trümper), pp. 599-612. Springer, Berlin-Heidelberg, 2009.

[9] Palme, H.: Chemical and isotopic heterogeneity in protosolar matter. Phil. Trans. R. Soc. Lond. A 359, 2061, 2001.

[10] Haisch, K.E. Jr., Lada, E.A., Lada, C.J.: Disk Frequencies and Lifetimes in Young Clusters. Astrophys. J. 553, L153, 2001.

[11] Briceno, C. et al.: The CIDA-QUEST Large-Scale Survey of Orion OB1: Evidence for Rapid Disk Dissipation in a Dispersed Stellar Population Science 291, 93, 2001.

[12] Trieloff, M., Kunz, J., Clague, D.A., Harrison, D., Allègre, C.J.: The nature of pristine noble gases in mantle plumes. Science 288, 1036, 2000.